AN ABSTRACT OF THE DISSERTATION OF

Malwina Gradecka for the degree of Doctor of Philosophy in Nuclear Engineering presented on June 17, 2015.

Title: Modification of Lower Plenum Structure for Mixing Promotion during Normal Operation of the High Temperature Gas Cooled Reactor

Abstract approved: _____

Brian G. Woods Piotr Furmański

Since High Temperature Gas-cooled Reactors are being considered as most promising design of upcoming IV Gen reactors, thus key research areas were identified to address safety aspects of this design. Number of simulations and experiments need to be conducted in this field. In this study thermal-hydraulics aspects of coolant flow through Lower Plenum (LP) of HTGR were considered. In specific: flow characteristics, risk of temperature stratification in LP and hot streaking. As power profile is non-uniform across the core, jets of coolant exit the core region at different temperatures and enter the LP impinging on LP floor creating possibility of hot spots at LP structure and temperature stratification in the plenum itself. Large local temperature gradients can cause material degradation effects. To address those issues

numerical simulation and an experiment were developed. The numerical simulation provides coolant flow velocity and temperature fields. The purpose of this study is developing a method for gas mixing promotion in the Lower Plenum of HTTF to reduce risk of the hot streaking and thermal stratification phenomena during normal operation. Following aspect are being examined: identification of gas flow behavior in lower plenum of HTTF based on CFD simulations, identification of hot streaking issue in the HTTF lower plenum using CFD tools, scooping study for available methods for mixing promotion and computational investigation of efficiency of selected method. Study includes description of experimental setup of HTTF, guidance for LP CFD modeling, results and analysis of CFD simulations and proposition of thermal mixing enhancement using available methods.

Modification of Lower Plenum Structure for Mixing Promotion during Normal Operation of the High Temperature Gas Cooled Reactor

by
Malwina Gradecka

A DISSERTATION

submitted to

Oregon State University

in partial fulfillment of
the requirements for the
degree of

Doctor of Philosophy

Presented June 17, 2015
Commencement June 2016

Doctor of Philosophy dissertation of Malwina Gradecka presented on June 17, 2015

APPROVED:

Major Professor, representing Nuclear Engineering

Head of the Department of Nuclear Engineering and Radiation Health Physics

Dean of the Graduate School

I understand that my dissertation will become part of the permanent collection of Oregon State University libraries. My signature below authorizes release of my dissertation to any reader upon request.

Malwina Gradecka, Author

ACKNOWLEDGEMENTS

I would like to express my deepest appreciation to both of my PhD advisers, Dr. Brian Woods and Prof. Piotr Furmański, without your guidance this dissertation would not have been possible.

Special thanks to Dr Kathryn Higley, who was always offering support and always making sure, that all I need to complete this dissertation, and more, is always in my reach.

I would like to thank to all of my PhD Committee members, for many constructive advices and your patience during meetings hold via internet.

I wish to express my sincere thanks to Prof. Tom Giebułtowicz, Prof. Roman Domański and Prof. Konrad Świrski who facilitated cooperation between Warsaw University of Technology and Oregon State University.

During the period of studies in Poland and US I was repeatedly supported by many Faculty Members of both universities, for what I am deeply thankful.

Finally, I would like to direct great amount of appreciation to my family, my partner and friends, who were full of understanding through the whole process of my PhD studies, providing me with encouragement and help whenever I needed it.

Modification of lower plenum structure for mixing promotion during normal operation of the High Temperature Gas Cooled Reactor

PhD candidate: Malwina Gradecka

OSU Adviser: Dr Brian Woods

WUT Adviser: Prof. Piotr Furmański

TABLE OF CONTENTS

TABLE OF CONTENTS (CONTINUED)

TABLE OF CONTENTS (CONTINUED)

LIST OF FIGURES

LIST OF FIGURES (Continued)

LIST OF FIGURES (Continued)

LIST OF FIGURES (Continued)

LIST OF TABLES

Nomenclature

μ_t – turbulent "viscosity" (also called the eddy viscosity)

C – constant

k - mean turbulent kinetic energy

l – length scale

S_{ij} – mean strain rate

U - characteristic velocity

Γ - characteristic diffusivity

Δx - mean mesh dimension,

ε – dissipation rate of turbulent kinetic energy

ϑ – velocity length scale

ϱ - density,

m – mass

T – temperature

c_p – specific heat

f_s – Strouhal frequency , vortex shedding frequency

Abbreviations

HTTF – High Temperature Test Facility

LP – Lower Plenum

MHTGR – Modular High Temperature Gas-cooled Reactor

NRC – Nuclear Regulatory Commission

NGNP – Next Generation Nuclear Plant

1 Introduction

Nowadays Generation II and III nuclear power plant designs offer a secure and stable-cost electricity supply in many markets. However, further advances in the nuclear industry have broadened the prospects of nuclear energy use. Thus to explore new opportunities, the U.S. Department of Energy's Office of Nuclear Energy has engaged governments, industry, and the research community worldwide in a comprehensive discussion on the development of next generation nuclear energy systems known as Generation IV. ("Review of DOE's Nuclear Energy Research and Development Program" n.d.)

1.1 High Temperature Gas-cooled Reactor for non-electric heat application

The VHTR (Very High Temperature Reactor) is a GEN IV reactor considered as a prime candidate for future deployment mainly because of its advantageous characteristics for non-electric applications. It is anticipated that it will be deployed mostly for process heat applications coupling the nuclear unit by an intermediate heat exchanger to large, energy intensive industrial complexes which could benefit from cogeneration of high temperature steam and electricity. In the short term, the sector interested in this kind of energy source could be the petroleum and petrochemical industry, and in the long term when, temperatures of 1000^0C and higher will be technically achievable, then nuclear heat application would expand to other processes like those used in the metallurgical industry.

The high temperature of the coolant at the reactor's outlet can be also used for the production of synthetic fuels. To satisfy future demand for transportation fuel, nuclear process heat may assist in the production of methanol, ethanol, coal gasification, oil extraction and provide CO_2 free hydrogen production.

The crucial issue for deployment of nuclear power for non-electric applications is cost effectiveness. In addition, close proximity between an industrial site and the nuclear unit is

limiting as transporting steam large distances can cause energy and/or product transmission losses. (IAEA-TECDOC, May 2014)

1.1.1 Worldwide HTGR's development

Due to the attractive features of this reactor concept, several countries are involved in developing this technology. However at the moment there is no vendor offering this design licensed and commercially available. Around the world there are a few R&D projects dedicated to HTR's at different levels of development. The most advanced one is in China but the US and Europe are also pursuing development of this technology on a somewhat slower pace. Many years of operational experience has been collected, mainly in US and Germany - Figure 1. The first built and operated prismatic core HTR was the Dragon Reactor. This 20 MW_{th} reactor located in the UK, was constructed strictly as a fuel and materials test facility. Produced heat was rejected to the environment via secondary water – steam circuit and tertiary water circuit.

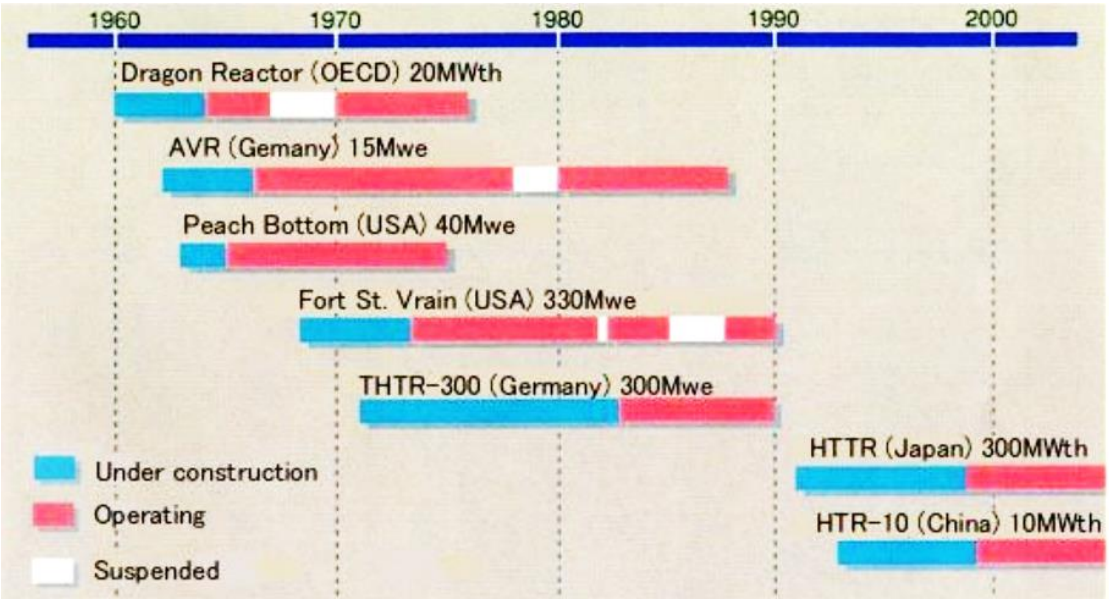

Figure 1 Schedule of the HTR projects ("High Temperature Gas Reactors: Assessment of Applicable Codes and Standards" n.d.)

The next prismatic HTR was Peach Bottom constructed in Pennsylvania US which become the first HTR to produce electricity. It was operated for seven years and after a successful demonstration mission it was decommissioned as the plant was too small to be commercially

viable. While Peach Bottom was in operation another HTR project was launched in the US – 330 MW_e Fort St. Vrain. FSV was the only commercial HTR to operate in the US. The FSV core featured 37 flow regions regulated by the operators to equalize temperature in the core. More on this subject is presented in section 2.3.1. The plant was shut down due to operational problems by June 1990. The most recent prismatic HTR project is located in Japan. The HTTR is a 30 MWth test reactor, it was first critical in November 1998. At the moment it is not operational for political reasons.

1.1.1.1 USA

> *"The mission of the Energy Department is to ensure America's security and prosperity by addressing its energy, environmental and nuclear challenges through transformative science and technology solutions."* (US Department of Energy, 2014)

In 2002 the DOE published its Generation IV Technology Roadmap concerning the future of nuclear power generation in United States of America. There are three major objectives imposed on Generation IV nuclear power plants:

- Electricity generation at economically beneficial cost in small and large units,
- High temperature process heat for industrial applications and hydrogen production,
- Sustainable use of fuel resources by used-fuel recycle and actinide burning to reduce the waste production.

Minor goals are also enhancing reliability and safety as well as increasing proliferation resistance and physical security. The DOE Nuclear Energy Research Advisory Committee (NERAC) reviewed the Generation IV Roadmap and recommended a faster schedule for the NGNP[1] project with a reduced technologically aggressive approach for the VHTR design. The main changes

[1] The NGNP Industrial Alliance is a focused effort to deploy a Very High Temperature Reactor under Generation IV project.

NERAC proposed were: reduced coolant temperature on the core outlet, usage of more traditional materials and core fueling with proven and validated UO_2 particle fuel. ("Review of DOE's Nuclear Energy Research and Development Program" n.d.)

The process from conceptual design to commercialization was divided into three stages by NERAC :

1. *Viability assessment phase R&D* – Viability assessment involves examination of the feasibility of the key technologies. The aim of this phase is to prove a laboratory scale, the basic concepts, technologies, and processes under relevant conditions to identify potential issues.
2. *Performance assessment phase R&D* – the performance assessment objective is to develop performance data and optimization of the design on an engineering basis. This stage should provide data about verification and optimization of the engineering scale process, physical phenomena, and material performance under relevant conditions.
3. *Demonstration phase R&D* – The demonstration phase shall carry out licensing, construction, and operation of a prototype or demonstration system in cooperation with a third party (industry, other countries). This stage prepares the final version of the detailed design and licensing documentation to deliver the new product for wide-scale commercial deployment.

Each of these phases generates extensive costs and requires advanced facilities. An additional nine criteria were developed to step through the process in the most reasonable path. In order to advance to the next stage in R&D each criteria listed in literature source ("Review of DOE's Nuclear Energy Research and Development Program" n.d.) must be met. Since these end points establish reasonable criteria for Generation IV R&D for evaluating technologies they have been used also as a basis for evaluating the readiness of the NGNP.

The NGNP program is a focused effort to deploy a Very High Temperature Reactor under the Generation IV project. The NGNP design can be characterized by the following description:

- Commercial scale modular gas-cooled thermal reactor operating at 600 MW_{th}.
- Reactor will be cooled with helium at core exit temperature of ~850 to 950^0 C for generation of electricity and/or hydrogen production.
- Both, pebble bed and prismatic fuel are currently being considered. For both core types the elementary fuel particle is the TRISO (tristructural isotropic) coated particle. TRISO fuel will maintain integrity at high burnup levels and retain fission products for steady state conditions as well as for transients and accident conditions.

The NGNP design will aim to satisfy as many objectives of Generation IV as possible:

- high reliability,
- enhanced safety,
- proliferation resistance,
- low waste generation,
- Improved economic factors.

The first version of the Roadmap (2002) assumed a coolant outlet temperature of approximately 1000^0 C, which requires extensive knowledge in the following areas:

- High-temperature helium turbine
- Reactor/hydrogen production coupling approach
- Identification of targeted operating temperature
- Fuel design material and design concept
- Adequacy of fuel performance potential
- Reactor structure material selection

In order to decrease challenges due to material and fuel integrity outlet core temperature was reduced to 900^0 C by the NGNP officials.

1.1.1.2 Europe

The European Union is the leader of reducing CO_2 emissions at the moment. The amount of attention paid to the reduction of greenhouse gas emissions, promotes a search for the new, cleaner and more effective power sources. At the same time the volatile prices for fossil fuels caused by unstable political events is a clear signal to search for power sources which will secure the supply and provide energy at economically beneficial prices independent form the oil, gas and coal market.

Nuclear power, proven in many countries around the world, can be solution to those issues if properly developed. Gen II and III reactors are supplying the world with 5.6 % (in 2010) of annual energy production. Over 438 nuclear reactors work mostly as base load in electricity production in power plants around the world providing 374.3 GWe of total capacity (as of January 2014). (IAEA-TECDOC, May 2014)(European Commission 2013)

This deployment of nuclear reactors is dominated by electric applications, but other non-electric deployment options have been considered and even applied in a few cases. For example cogeneration of electricity and heat (Hungry, Japan). As reactors of Gen IV are being developed other possible applications are considered and researched.

1.1.1.2.1 **Nuclear Cogeneration Industrial Initiative – NC2I**

The Nuclear Cogeneration Industrial Initiative was created as a continuation of previous efforts to deploy HTR's in the EU. The Task Force of the project consists of research units, engineering companies as well as industry representatives.

The NC2I-R project aims at creating a deployment strategy for HTR's for non-electric applications. In the near term horizon, which is about ten years, it postulates commissioning a demonstrator for cogeneration of electricity and heat (temperature at the core outlet no more than 750^0C). The nuclear cogeneration units would be located in the vicinity of the heat-intensive industrial sites providing technological steam as a priority and converting leftover load to electricity, which can be sold to the site or to the grid. The industrial sectors of interest are mainly chemical clusters and petrochemical sites. (NC2I, 2014)

Medium and long term horizons include increasing the temperature at the core outlet to over 1000^0C. This increased temperature steam can be used for a larger number of industrial processes as well as hydrogen production and water distillation.

1.1.1.3 China

At the moment China is the leader in HTR demonstration as they are building an industrial demonstration nuclear power plant of the modular pebble-bed high temperature gas-cooled reactor. The HTR-PM facility consists of two units, 250 MW_{th} each. Both units are coupled to separate steam generators and a common steam-turbine generator set of 200 MW_e. The main design parameters of the HTR-PM are listed in Table 1. Construction began in December 2012. HTR-PM is a continuation of the national long-term science & technology development program of China. Previous efforts to develop HTGR's in China was centered on the HTR-10 project which proved the technology as successful tests demonstrated robust safety features of this design. (HTR2014 Conference, 2014)

Table 1 Main design parameters of the HTR-PM (HTR2014 Conference, 2014)

Parameter	Unit	Value
Rated electrical power	MW_e	210
Reactor total thermal power	MW_{th}	2 × 250
Designed life time	a	40
Average core power density	MW/m^3	3.22
Electrical efficiency	%	42
Primary helium pressure	MPa	7
Helium temperature at reactor inlet/outlet	°C	250/750
Fuel type		TRISO (UO_2)
Heavy metal loading per fuel element	g	7
Enrichment of fresh fuel element	%	8.9
Active core diameter	m	3
Equivalent active core height	m	11
Number of fuel elements in one reactor core		420,000
Average burn-up	GWd/tU	90
Type of steam generator		Once through helical coil
Main steam pressure	MPa	13.24
Main steam temperature	°C	566
Main feed-water temperature	°C	205
Main steam flow rate at the inlet of turbine	t/h	673
Type of steam turbine		Super high-pressure condensing bleeder turbine

1.1.1.4 Japan

The Japanese project HTTR, High Temperature Test Reactor, is another input into the world knowledge and experience on HTGR's. As previous designs, it is a graphite-moderated, gas-cooled research reactor. However, the reactor core is made of prismatic blocks with uranium oxide fuel (enriched to 6%) unlike the Chinese pebble bed design. The main design parameters of the HTTR are listed in Table 2. The project is managed and operated by the Japan Atomic Energy Agency.

The reactor was started up for the first time in 1999 to a full power of 30 MW_{th}. Tests conducted at the facility confirmed the ability to achieve temperature sufficient for hydrogen production. The operational conditions of this reactor are pressure of about 4 MPa and inlet/outlet temperatures of 395^0C/850-950^0C. (JAEA, 2014) (Lebenhaft, 2001)

Table 2 Specification of HTTR

Reactor Thermal Power	**30MW**
Rector Coolant	**Helium Gas**
Reactor Outlet Coolant Temperature	**850 ℃/950℃**
Reactor Inlet Coolant Temperature	**395 ℃**
Primary Coolant Pressure	**4MPa**
Core Material	**Graphite**
Core Diameter	**290cm**
Average Power Density	**2.5W/cm^3**
Fuel	**Low Enriched UO**
Fuel Element Type	**Prismatic Block**
Uranium Enrichment	**3～10%**
Average	**6%**
Reactor Pressure Vessel	**Steel(21/4Cr-Mo)**
Number of Main Cooling Loop	**1**

1.1.1.5 South Africa

Project PBMR which is Pebble bed Modular Reactor was located in South Africa. The pebble core consists of 360 thousand pebbles, cooled by helium. Moderation is implemented using graphite. This unit was rated at 400 MW_{th} or 165 MW_e of nominal power. This design was developed by South African company PBMR (Pty) Ltd. The project envisaged construction of a demonstration plant and a fuel plant for this reactor. However, the project was closed in 2012. (Lebenhaft, 2001)

1.1.2 Advantages of high temperature reactor deployment

In 2010 nuclear power plants were providing about 20% of US electricity production. Nuclear power is also considered as a low greenhouse gas emission supply and represents 70% of this group. HTGR's can be substituted for fossil fuel power plants such as natural gas and provide high temperature and pressure process steam to industry. In comparison to a natural gas plant, every 750 MW_{th} of installed power in HTGR technology would prevent at least 1 million tons of CO_2 emission every year. HTGR technology can be easily used in co-generation mode and provide stable cost energy, a good buffer for constantly changing prices of natural gas. HTGR can

be coupled also with petro-chemical processes in order to produce ammonium, hydrogen and extract unconventional crude. (*Next Generation Nuclear Plant:A Report to Congress* 2010)

1.1.3 HTGR/NGNP challenges and development needs [DOE]

In the past, several gas-cooled reactors has been built and operated. The operational reliability of this type of reactor has been proven. However, gas reactors operating at significantly higher temperatures introduce new and unique challenges to be solved. The R&D needs were identified by DOE and classified into six groups. ("Review of DOE's Nuclear Energy Research and Development Program" n.d.)

1. *Material Development and Improvements* –VHTR design challenges are based on material strength and stability at high temperatures for the transport of corrosion products from metal and graphite in the presence of possibly impure helium. A number of materials are being used in high temperature applications in industry but at present none of them is qualified by ASME. That is why the following areas need to be subjected to R&D:
    a. Material property changes induced by irradiation and high temperature of nuclear graphite and carbon fiber matrix composites,
    b. Professional codes and standard development for very high-temperature design methodologies,
    c. Better understanding of environmental impacts on metallic alloys, thermal aging, as well as improved models for studying them, and
    d. Improved understanding of radiation cooling of the pressure vessel and core barrel for passive cooling optimization.
2. *Fuels development and requirements* – fueling systems in high-temperature gas-cooled reactors are based on TRISO fuel particles. Still there is number of challenges which need to be coped with. The main issues to deal with are: anisotropic shrinkage, swelling of the pyrolytic carbon, mechanical stability at high pressure, kernel migration, palladium attack on the silicon carbide layer, and selective diffusion of certain fission products.

3. *Primary to secondary heat transfer* – The main requirements in a heat transport fluid are:
    a. Be chemically indifferent with surrounding structural materials,
    b. Distinguish with superior fluid-mechanical and heat-transfer properties ,
    c. Have adequate safety characteristics for normal, as well as transient and accident conditions.
4. *Plant operation* – For NGNP two complicated processes need to be coordinated: electricity production and hydrogen production. In order to achieve reliable configurations and control schemes, design and analytical studies need to be done.

1.1.4 Modular High Temperature Gas-cooled Reactor

The Modular High Temperature Gas-cooled Reactor (MHTGR) was introduced by General Atomics in the '80s. However because of material concern due to high operational temperature it was not constructed. Currently more advanced structural materials technology is available and the MHTGR design can be used as a template in the process of designing a Generation IV reactor.

The MHTGR (Figure 2, Table 3) is an existing design considered as an accurate template for developing the New Generation of Nuclear Plant (NGNP) (*Next Generation Nuclear Plant:A Report to Congress* 2010). This design is very attractive from a safety and operational perspective. One of the important properties of this design is a working fluid at very high temperatures which can be extremely beneficial for industry (hydrogen production, high temperature and pressure technology steam production). This also presents a challenge from engineering perspective. Before commercial usage of this technology a comprehensive process of licensing must be performed.

A comprehensive description of this project was presented in the publications of the US Nuclear Regulatory Commission (Mccreery, Condie, and Schultz 2007). Key design parameters of the MHTGR are listed in Table 3.

Table 3 NOMINAL REACTOR DESIGN PARAMETERS

NOMINAL REACTOR DESIGN PARAMETERS	
Core power	350.0 MW(t)
Core power density	5.9 MW/m^3
Inlet helium flow	157.05 kg/s
Inlet helium temp.	258.6 ^{0}C
Inlet helium pressure	6.38 MPa
Core outlet helium temp.	687 ^{0}C (960K)
Average reactor pressure drop	31.4 kPa
Core average outlet helium temp.	716 ^{0}C

The other commercial design ANTARES, is also a block type HTR reactor by Areva. However, this project has been stopped due to lack of potential buyer at this time.

1.1.5 High Temperature Test Facility – HTTF

The HTTF is one of the facilities related to HTGR development. It will support regulatory R&D needs for the NGNP project. The HTTF will be used for, analysis and validation of the reference design with the numerical tools which will be at the heart of the licensing process for performance prediction at normal and accident conditions. (*Next Generation Nuclear Plant:A Report to Congress* 2010)

The High Temperature Test Facility was designed to simulate scaled coolant flow and heat transfer of the MHTGR during the depressurized cooling conduction event, the pressurized cooling conduction event and normal operations. The HTTF design (Figure 3) proposed by OSU is a quarter height, 1/8 pressure, full temperature model of the MHTGR.

There are two major differences between the HTTF project proposed by OSU and MHTGR design. To prevent the significant heat loss to environment prismatic graphite blocks are replaced with ceramic core base. Also nuclear fuel is substituted with electric graphite heaters.

1.1.6 HTGR's and challenges associated with coolant flow in Lower Plenum (LP)

The Next Generation Nuclear Plant design is being considered as a prismatic/pebble bed, cooled with helium, moderated with graphite consisting of an annular fuel region surrounded by inner and outer graphite reflectors. The core design is based on the GT-MHR, which is the General Atomics Gas Turbine Modular Helium Reactor. The core exit temperature range varies from 973 to 1273 K. Helium in the core flows with velocity of about 70 m/s in the vertical cooling channels. The hot helium jets exit the core and impinge on the lower insulated plate in the LP chamber after partial mixing. The gas then exits the LP through the outlet duct. The flow is mostly turbulent with limited cross flow due to gas density stratification and obstruction by support posts. The gas in the lower part of the plenum on the surface of lower plate may approach stagnation. For some cases due to the annular core geometry and the fuel loading configuration it is anticipated that temperature of some of the cooling channels may be 300 K hotter than average helium temperature at the core exit. (S. B. Rodriguez and El-Genk 2010)

The potential operational issues within the lower plenum are *hot streaking/hot spots* (the hot helium jets impinge onto bottom plate in LP causing local temperature peak on the structural material surface).

During normal operation the Reynolds Number in the LP at the core outlet (LP inlet) varies around 10^5 while in the LP, the range of Re is $2.4 \cdot 10^4$ to $3 \cdot 10^6$ depending on the location. The highest Re are located at the LP junction with the outlet duct. The lowest are located at the outer sides of the plenum. Flow can be characterized as highly anisotropic, turbulent due to post obstruction and multiple jets interactions.

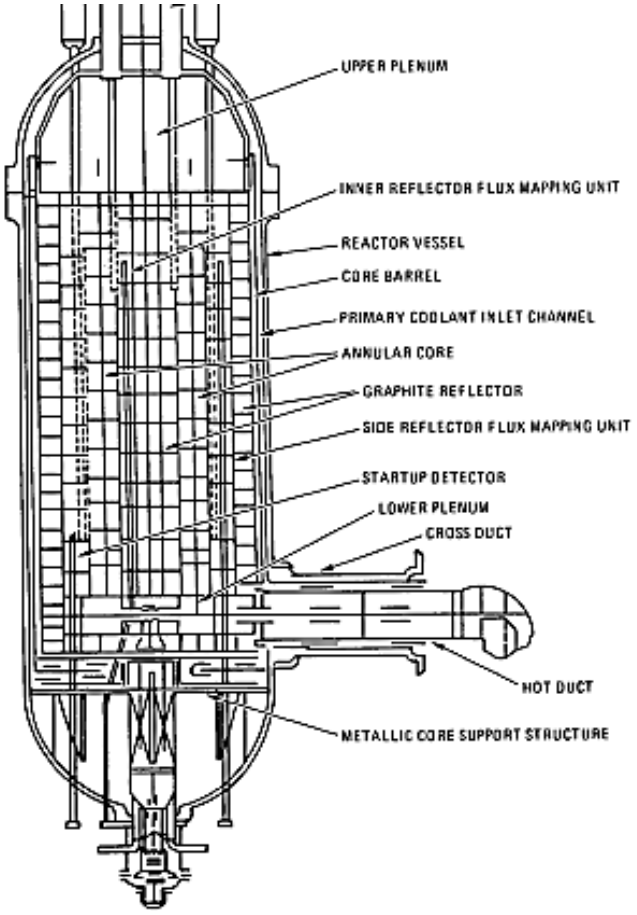

Figure 2 MHTGR

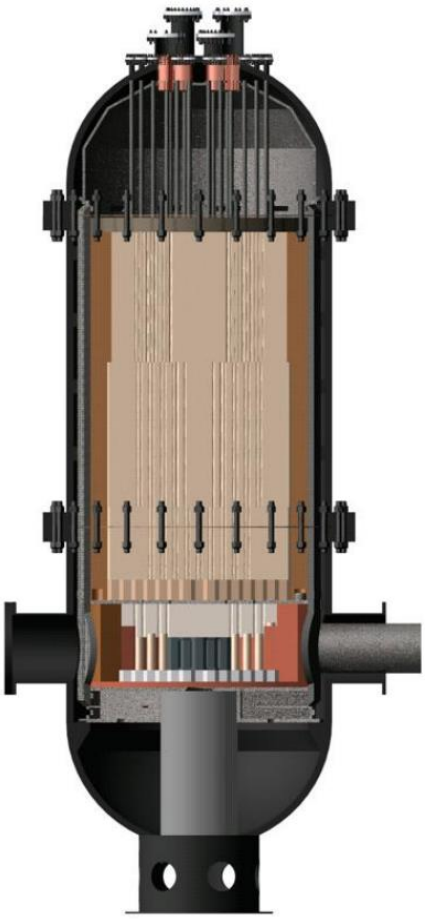

Figure 3 HTTF

1.2 Problem formulation

The working fluid in the MHTGR reaches very high temperatures on the hot side of the loop. Helium has good chemical properties for this type of application. However, it can cause structural problems if the power distribution across the core is not uniform. While cooling core sections with higher power density (hot channels), the helium achieves significantly higher temperatures then in other channels. Flow is a function of dynamic viscosity, which increases with temperature causing Reynolds number the decrease. Thus for the same axial location in the core, the hot

channel flow will have lower Re number than an average channel. Additionally flow with lower Re number will characterize higher friction factor further slowing down the flow. Decreased mass flow will be heated to higher temperature enlarging the temperature gradient between hot channel and average coolant temperature (R. W. Johnson and Schultz 2004). Hot helium jets at different temperatures are supposed to uniformly mix in the Lower Plenum chamber. However, it is anticipated that the level of mixing might not be sufficient to reduce the temperature peak before the hot jet impinges the LP structure which can cause issues with structural materials of the MHTGR.

There is a need for assuring that HTR will maintain its integrity, function safely and remain intact during normal operation conditions for various levels of power generation. In previous research it was shown that hot helium jets entering the LP (VHTR) strike in lower plate (LP bottom structure element) causing local increase in temperature of material causing "hot spots". By enhancement of thermal mixing hot jets can be dissolved before reaching bottom part of LP. (S. B. Rodriguez and El-Genk 2010)

1.3 Goals and outline

To safely operate the MHTGR-like reactor, the issue of hot streaking in the LP must be examined and if needed, resolved. The geometry of the HTTF facility allows for the enhancement of mixing through a few different mechanisms.

Promotion of thermal mixing can be introduced by various methods. For example, in previous work by Rodriguez and El-Genk (2010), it was shown that hot helium jets entering the LP (VHTR) strike the lower plate (LP bottom structure element) causing local increases in temperature of the material (hot spots). By enhancement of thermal mixing, hot jets can get dissolved before reaching bottom part of LP. Available methods for thermal mixing enhancement will be reviewed and analyzed from the perspective of usage in HTGR's reactors. The main objective is:

The purpose of this study is to develop a method for gas mixing promotion in the Lower Plenum of an HTR to reduce the risk of the hot streaking and thermal stratification phenomena during normal operation.

To achieve this goal, following steps must be taken:

1. Identification of gas flow behavior in lower plenum of the HTTF based on CFD simulations.
2. Identification of hot streaking issue in the HTTF lower plenum using CFD tools.
3. Examination of available methods for mixing promotion and computational investigation of efficiency of selected methods.

The study will be introduced in three stages described in next section.

1.4 Scope of study

1.4.1 Part 1 – Identification

This part of the research contains preliminary calculations for the lower plenum mixing in the HTTF. These calculations were prepared using a best estimate methodology to obtain simulations as close to the reality as possible considering available computational resources. Cases described in section 3.1.3 were developed and analyzed to quantify characteristics of the coolant flow, thermal mixing, and detect and confirm the existence of the potential operational issues.

The *Base case* scenario simulation will be the foundation for the analysis, displaying flow and temperature fields across the LP and LP outlet. This case will be compared to other postulated scenarios with various modifications (geometrical/conditional) to evaluate proposed methods for enhancement in mixing effect in the LP coolant flow.

A CFD model of the LP and part of the outlet duct was built in order to obtain temperature and velocity fields to be analyzed in terms of hot streaking and temperature stratification. This stage predicts flow characteristics and preliminarily addresses the main objective.

1.4.2 Part 2 – Mixing enhancement methods

During this stage mixing enhancment methods are proposed and examined to obtain an accurate and efficient way of eliminating potential issues with coolant jet mixing. The HTTF located at Oregon State University was used as a reference design for the investigation of the mixing enhancement methods in the LP of the typical HTR. The description of the test facility and experimental setup can be found in Chapter 3 in section 3.1.

The applied method should result in enhanced mixing of the coolant which can be quantified by the temperature gradient at the LP exit or at the end of cross duct/ outlet duct. The mixing enhancement methods are described in the section 2.2.2.

The bulk part of these CFD calculations is performed using a reduced LP geometry like a LP section or a single channel. The computational domains developed for this study are described in chapter 3.

1.4.3 Part 3 – Modified outlet plenum geometry

This is the last part of the study, summarizing CFD simulation of the flow in the LP. The results from Part 1 and Part 2 are merged in this part, culminating with CFD analysis of the full LP geometry with Part 2's best mixing enhancement method. Part 3 concludes the research with the solution for the problem stated in section 1.2.

2 State of knowledge

Fluid dynamics of coolant flow in the prismatic HTR's has been studied intensively for decades. Since various physical phenomena often overlap with each other, the conditions are generally difficult to describe using analytical tools. Study of separate phenomena that occur in the flow can improve our understanding of the overall physical situation.

2.1 Fluid flow characteristics in Lower Plenum

The flow in the lower plenum is a highly complicated phenomena. Hot gas injected from the core has mostly vertical momentum when entering the LP. Because of multiple post located within the LP flow can be characterized as flow in a staggered tube bank/bundle. Although the phenomena occurring in the LP are much more complicated since the flow is inclined not parallel to the LP floor. The gas flow is constantly obstructed by support posts, consequently the maximum velocity can be found between posts near to the exit of the LP. The anticipated flow sequence is following: Inlet gas jets are initially injected in vertical direction, subsequently some of the jets hit the bottom plate and disperse. Rest of the gas is entrained with other jets in direction of plenum outlet in horizontal direction.

The anticipated Reynolds Numbers in the LP varies with the location, for instance at the inlet Re=5'000 but at the outlet it is Re=90'000. The value of the Reynolds number within post area depends strongly on the definition of the characteristic length. If one selects the distance between the posts as the characteristic dimension the predicted Re=7'000. This range is called subcritical and the vortex shedding is a strong periodic. Figure 4 displays fluid flow regimes across a single, smooth tube. The regime shown second from the top in Figure 4 should therefore be a representative of the flow in the LP. It indicates fully turbulent vortex street. However, regime shown in that figure illustrates flow across a single cylinder not a tube bank. In case of the LP flow will be disturbed with almost 200 posts and number of coolant jets coming down from the inlets located on the LP roof.

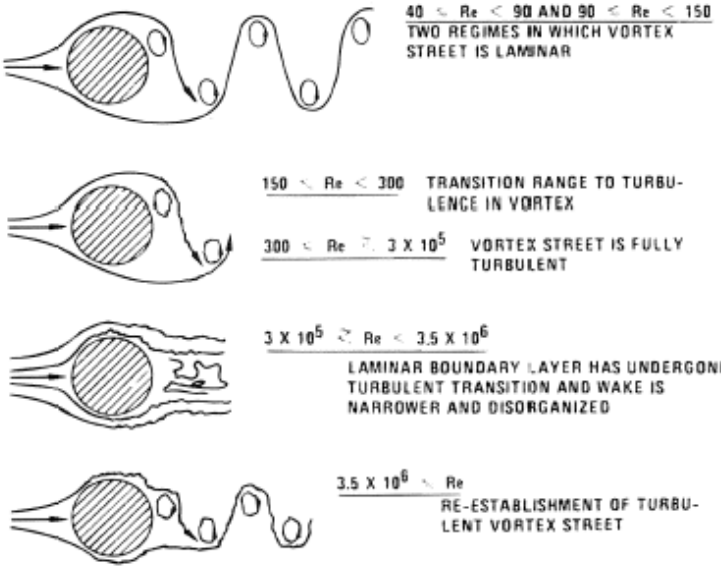

Figure 4 Flow regimes across smooth tube. From (Blevins, 1990)

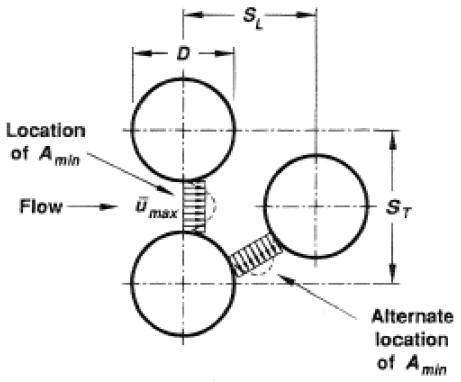

Figure 5 Equilateral triangle tube bank

2.1.1 Vortex shedding in tube bundle

Cross flow characteristics in tube bundles are influenced by many factors like periodic fluid forces, frequency linearly dependent on flow velocity which cause periodic excitation – vortex shedding. It can be described as narrow peak in turbulence and pressure spectra. The vortex shedding peak is dependent on gap velocity. Vortexes are formed near to the surface of cylinders alternately from one side and then the other and shed along with fluid flow. Thus, due to alternately created vortexes and consequently created forces this process has a major influence from engineering perspective and needs to be considered especially for flows with high velocity. For vortex shedding frequencies close to the structural vibration frequency of the body resonance may occur. This phenomenon can be dangerous and cause structural damage of the tube bundle. To describe the phenomena of vortex shedding, the dimensionless number, Strouhal number, can be used. The definition of this number is following:

$$St = \frac{f_s \cdot L}{U_\infty}$$

Where L is a characteristic length (equal to the diameter D in case of a circular cylinder or tube in cross flow), f_s is vortex shedding frequency and U_∞ the free-stream velocity. For a stationary tube, Strouhal number, is mainly function of the Reynolds number, surface roughness, and free-stream turbulence. For large Reynolds numbers, it has been shown that the St number is in range of 0.2, regardless of the body shape.

The phenomenon of vortex shedding occurs also for multiple tubes. However, the ratio between cylinders distance and cylinder diameter is significant. In closely packed tube bundles vortex shedding frequency is not distinct but appears as wider spectrum of frequencies possibly causing flow-induced vibrations. (Williamson 1988) (Ziada 2006)

2.1.2 Pressure drop calculations in tube bundle

The pressure drop in tube bundle can be described using the Euler number. It is a dimensionless number used in fluid flow calculations to express ratio between local pressure drop and kinetic energy per volume. The definition of this number is following:

$$Eu \stackrel{\text{def}}{=} \frac{\Delta \bar{p}_{row}}{\frac{1}{2}\rho \cdot \bar{u}_{max}^2}$$

Various correlations of pressure drop in tube bank were developed and published. For example The Heat Exchanger Design Handbook (Schlünder, 1983) contains analytical expressions approximating curves of Re vs. Eu which are displayed at Figure 6. They are if form of power series:

$$Eu = \sum_{i=0}^{4} \frac{c_i}{Re^i}$$

for all in-line and rotated square banks, except in-line banks with b=2.5, for which

$$Eu = \sum_{i=0}^{4} c_i \cdot Re^i$$

For equilateral triangle tube banks coefficients c_i are listed in Table 4.

Inclined cross-flow is additional factor which enhance pressure drop in the tube bundle. However in case of flow in LP it is extremely difficult to assess angle of incline since "new" jets join the flow along the LP. (Schlünder, 1983)

Table 4 C_i coefficients for generation of pressure drop coefficients for equilateral triangle bundle. From Heat Exchanger Design Handbook (1983)

b	Re Range	c_0	c_1	c_2	c_3	c_4
1.25	$3–10^3$	0.795	0.247×10^3	0.335×10^3	-0.155×10^4	0.241×10^4
1.25	$10^3–2 \times 10^6$	0.245	0.339×10^4	-0.984×10^7	0.132×10^{11}	-0.599×10^{13}
1.5	$3–10^3$	0.683	0.111×10^3	-0.973×10^2	-0.426×10^3	0.574×10^3
1.5	$10^3–2 \times 10^6$	0.203	0.248×10^4	-0.758×10^7	0.104×10^{11}	-0.482×10^{13}
2	$7–10^2$	0.713	0.448×10^2	-0.126×10^3	-0.582×10^3	–
2	$10^2–10^4$	0.343	0.303×10^3	-0.717×10^5	0.88×10^7	-0.38×10^9
2	$10^4–10^6$	0.162	0.181×10^4	0.792×10^8	-0.165×10^{13}	0.872×10^{16}
2.5	$10^2–5 \times 10^3$	0.33	0.989×10^2	-0.148×10^5	0.192×10^7	-0.862×10^8
2.5	$5 \times 10^3–2 \times 10^6$	0.119	0.498×10^4	-0.507×10^8	0.251×10^{12}	-0.463×10^{15}

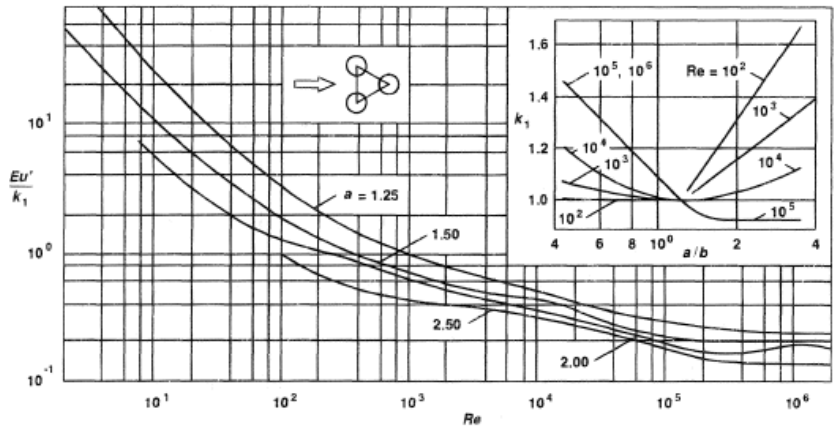

Figure 6 Pressure drop coefficients vs. Reynolds number for staggered tube bundle. From (Schlünder, 1983)

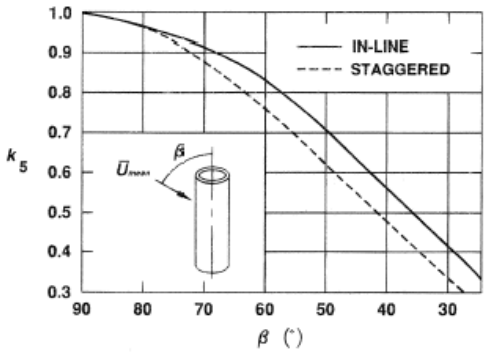

Figure 7 Effect of angle of flow on overall pressure drop for inclined crossflow in tube banks. From (Zukauskas 1987)

2.2 State of research on typical VHTGR's LP

The High Temperature Gas-cooled Reactors have been the subject of research for decades. However due to pressure in connection to NGNP initiative development, the last few years were

essential for overall progress in that manner. Various experiments and CFD simulations were conducted and analyzed for better understanding of the processes occurring in the HTGR's.

CFD is a suitable tool for simulating gas mixing in three dimensional flow, however, it needs to be done using an "accurate" methodology to obtain the mixing behavior in a lower plenum for steady boundary conditions. R. R. Shultz (H. McIlroy and McEligot 2006) prepared a methodology and analysis technique for the evaluation of a plant behavior for a Generation IV Very High Temperature Gas-cooled Reactor (VHTR) using coupled thermal-hydraulics and neutronics computational codes such as FLUENT or STAR ccm+ and RELAP. The thermal-hydraulic analysis of following phenomena is required:

- Core hot channel characterization
- Bypass – bypass flow in reflector region and between prismatic block
- Mixing
- Transition between turbulent and laminar flow as well as forced-natural mixed convection flow
- Air and water ingress
- RCCS – reactor cavity cooling system

Coolant mixing is a three dimensional phenomenon in the inlet and outlet plenums and it depends on number of variables. During normal operation coolant mixing takes place in the LP between bottom of the core and intermediate heat exchanger or turbine. It has been shown that for VHTR variations of coolant temperature could exceed 300 ^{0}C. This value is significantly higher than acceptable temperature variation which is ±20 ^{0}C. Moreover it has been presented (R. Johnson and Schultz 2009) that helium as a coolant is resistible to precise thermal mixing what results in temperature variations on the lower plenum outlet. Special design features may be needed to enhance good mixing and reduce thermal streaking in lower plenum. (H. McIlroy and McEligot 2006)

Several cases of the flow in typical HTR's LP have been reported using CFD tools. Each approach to the subject of study varies by assumptions, boundary conditions and methods of modeling. One of the early works of Johnson and Schultz (R. W. Johnson and Schultz 2004) concerns temperature bounding estimate at the hot channel exit and preliminary calculations of the LP mixing. It was indicated that maximum radial power variation across the core will be 1.25 times the average. Maximum hot channel temperature is strongly dependent on the coolant flow rate which is not yet a fixed value for NGNP. The temperature in the hot channel will be increased due to two phenomena, higher power density and higher wall friction of hotter fluid which will cause decrease in coolant flow velocity. To estimate the flow rate in the hot channel, a CFD tool – Fluent ANSYS was used. For needs of the CFD simulation the axial peaking factor was assumed 1.3 and the radial peaking factor 1.25. The value of the wall friction was the critical aspect of the calculations. Standard k-ϵ turbulence model with enhanced wall treatment was used to compute the value of the wall friction coefficient. In this simulation it was assumed (wrongly, as authors point out) that for both hot and average channel pressure drop to be the same. It has been shown, using the dimensionless ratio Grashoff Number, that the buoyancy effects are negligible for hot channel calculations. Heat transfer between the cooling channels is not accounted, in reality temperature in the hot channel would be lower due to heat transfer in direction of lower power densities. Hence the temperature of the hot channel can be considered as bounded. Coolant mixing in the lower plenum depends on turbulence intensity and on overall flow regime including vortices behind support posts. It was shown that hot gas is more concentrated in the back side of the LP and more mixing effects are notable as coolant approach the outlet duct.

R. W. Johnson (R. Johnson 2005) performed a validation study for numerical simulation of flow phenomena expected in the VHTR. In his research, the following elements were in the focus, as general flow characteristic of the flow in LP and several RANS turbulence models available in Fluent ANSYS software (which were employed to simulate staggered tube bundle flow data of (O. Simonin, 1988)). Simulations resulted with converged solution and few significant observations have been made. The standard and realizable k~ϵ models with applied enhanced

wall treatment provided the best results for the k~ϵ models. The realizable model results were somewhat better than for the standard model. The k~ω model along with shear stress transport feature shows generally better agreement with the data than the realizable k~ϵ model. The Reynolds stress model using standard wall functions yield the best agreement overall than any of the other results presented. However, neither of models showed results completely congruent to the data of Simonin and Barcouda. DES (detached eddy simulation) simulation was recommended for production of more promising results.

The next study of R. W. Johnson and others (R. Johnson, Guillen, and Gallaway 2006) investigated the application of CFD tools to simulate the flow expected in the LP of the prismatic VHTR. The investigation performed using subsection of the LP geometry, reports progress of turbulent CFD predictions using NPHASE and FLUENT software. The conducted research concluded with following statements. 2D URANS model showed satisfactory agreement with the Simonin and Barcouda data as well as presented correct trends due to computing the flow as a non-stationary. The shear Reynolds stress results were also agreeable and display correct trends. Simulation of the normal stresses did not always lead to satisfactory results, however, they seem to not have significant effect on the mean velocities. Nevertheless, connection between accurate prediction of the Reynolds stresses and obtaining accurate results for hot jet mixing in the lower plenum in not clear yet.

In 2006 (H. McIlroy and McEligot 2006) in Idaho National Laboratory experiment concerning flow in a scaled model of a VHTR LP was presented. Experimental data from Matched-Index-Refraction (MIR) Laboratory – measurements of the flow in the LP of prismatic VHTR concept reactor were used for assessment of CFD codes. Background of the experimental setup, procedures and sample sets of data along with uncertainty assessment were published. Three dimensional velocity field description of the flow data were collected for Reynolds Numbers of approximately 4300 and 12400. PIV system consists of two ImagePro Plus digital CCD cameras

and a double-pulsed Nd:YAG laser from Big Sky Laser. Data extraction was done using DaVis 7.1 software in a LaVision dual-processor Programmable Timing Unit (PTU).

The model design and flow facility were proven by previous scaling studies to produce satisfactory flow conditions. Objectives for CFD solutions of the momentum equations, scalar mixing and adequate turbulence models in case of negligible buoyancy and constant fluid properties have been met. Hence benchmark databases for CFD solutions assessment were developed. Obtained data additionally meets requirements of a standard problem. The uncertainty study of measurements has been conducted and documented.

Another work of Johnson and Schultz (R. Johnson and Schultz 2009) concerns CFD analysis of the VHTR LP standard problem. Computational model of scaled section of LP was build and calculated using Star-ccm+ software. The results were compared to the experimental data previously collected form MIR facility. This study presents results of CFD simulations to investigate usage of the data as validation data set or standard problem. Several variations of initial conditions were computed, overall it had little effect on final results. Four turbulence models were applied and examined: standard k~ϵ two-layer model, AKN low Re k~ϵ model, and Menter SST k~ω model, all with all y+ wall treatments, and RSM with linear pressure strain and high y+ wall treatment. The standard k~ϵ model and the RSM showed the greatest turbulent viscosity, the k~ω model the least, and the AKN model somewhat more than the k~ω model. The RSM results appeared to be diminishing in their unsteadiness toward a steady state condition, which is inconsistent with vortex-shedding.

Yizhou Yan and Rizwan-uddin (2011) (Yan and Rizwan-uddin 2011) conducted coupled CFD-system code simulation of a gas cooled reactor. Their simulation approach was based on FLUENT and RELAP-3D and applied for Gas Turbine-Modular Helium Reactor (GT-MHR) which is considered as a IV generation reactor design. Helium features such as significant thermal expansion and buoyancy resistance results in power variations in hot channels. Performance of the modern gas turbines is strictly bounded to thermal uniformity and flow swirl. Consequently

the most significant thermal-hydraulics challenges are variation of coolant temperature – the peak coolant temperature at the core outlet can be 200 ^{0}C above the average coolant temperature in the GT-MHR also the flow velocities demonstrate a significant differences in various coolant channels across the reactor core.

Scaling studies were carried by D. M. McEligot and G. E. McCreery (Mceligot and Mccreery 2004). The objective of their work was documenting scaling studies and conceptual designs for heat transfer and flow experiments proposed to assess data derived by CFD codes and applied turbulence models proposed for application to prismatic NGNP concepts. There are two major research questions regarding complex flow in a typical prismatic HTR:

- flow and thermal mixing in the lower plenum ("hot streaking" issue)
- turbulence and resulting temperature distributions in reactor cooling channels ("hot channel" issue)

It has been indicated that during normal operation on full power, buoyancy impact should be insignificant in the LP coolant flow. Benchmark experiments were performed for normal operation and reduced power or accident scenarios. The aim of study was developing analytical tool essential for NGNP design works, safety studies, and eventually licensing process.

E. Karaismail and I. Celik (2010)(Karaismail and Celik 2010) performed CFD calculations for turbulent isothermal flow inside a plenum model that resembles a segment of the LP of a typical Very High Temperature Reactor. The plenum was reduced to a small subsection, but even then accurate prediction of the flow filed was still highly advanced task due to unsteadiness, flow regime transition, formation of vortices and strong stream line curvature. Due to extensive computational cost needed for LES simulation, URANS turbulence modeling was applied. It was demonstrated that the flow regime can be strongly influenced by different turbulence models, grid type and size and value of Reynolds number. Strong non-linear interaction between the turbulent eddy viscosity and numerical viscosity can result in local changes of flow regimes especially around supporting posts in the LP. It has been shown that Shared Stress Transport

(SST) k-ω results with smaller turbulent eddy viscosity in comparison to the Renormalization-group (RNG) k-ε model. However, RNG k-ε model can be used to obtain mean flow behavior while grid convergence study is verified. Validation process, uncertainty study as well as Richardson Extrapolation were applied to the long-term averaged velocity and wall shear stress data. Nevertheless, for highly unsteady flows those methods have not been studied thoroughly.

2.3 Theory of mixing

Turbulent mixing is a complex phenomenon and has been researched extensively mainly for industrial purposes (industrial mixing, chemical reactions etc.). There has been many theories (Kresta and Brodkey 2004) developed to describe process and outcome of mixing. In this section this matter is broke down to explain the principles without going into complicated mathematical formulas.

The understanding of mixing process requires to break it down to basic phenomena. Mixing can be occurs via several different mechanisms:

- Dispersion or diffusion – using nozzles for example to disperse fluid B in A
- Molecular diffusion – molecular motion, governed by molecular diffusivity, property of fluids A and B
- Eddy diffusion – migration of molecule formation called eddy, governed by turbulent diffusivity which is property of the local flow
- Convection – bulk diffusion of the fluid,
- Taylor dispersion – special case of convection when mean velocity gradient cause dispersion

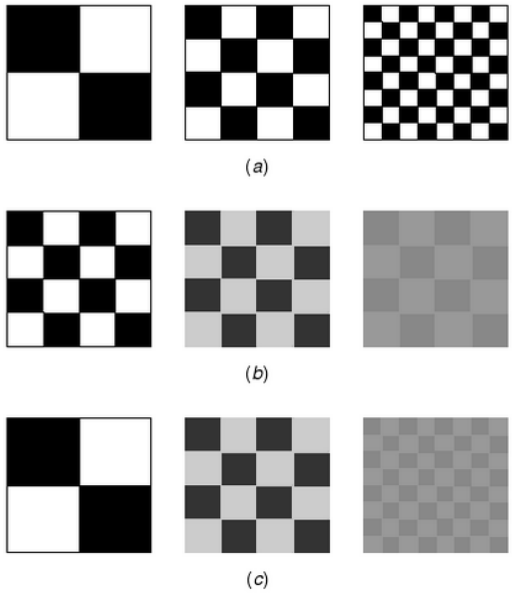

Figure 8 Schematic presentation of mixing mechanisms (a) turbulent dispersion only (b) molecular diffusion only (c) molecular diffusion and turbulent dispersion (Paul, Atiemo-Obeng, and Kresta 2004)

Understanding of the turbulent mixing is limited to the transition region and few simplest cases of turbulent flow. Figure 8 a presents schematically how (bulk) convection and eddy diffusivity impact the mixture. The main result of these mechanisms is reduction of the segregation scales. On another hand molecular diffusion presented in Figure 8 b results in reduction of the segregation intensity. The later mechanism would eventually reduce the segregation intensity to zero, however this process can be carried out much faster if turbulent motion enlarge the interfacial are between the fluids.

If those effects were possible to be separated the mixing outcome from ether of them would not be satisfactory. If the molecular diffusion present alone, the dispersion of fluid A in fluid B would be a very slow process, which in case of large mixing chambers would require substantial amounts of time. On another hand if only turbulent dispersion would take place in the mixing chamber, depending on size of the (stationary) eddies, the mixed layer would only be present on the eddies surface. This mixing layer would be only 1Å wide, however the bulk of fluids would not interact in any other way resulting in extremely low mixing efficiency. Even for very large

reduction of the segregation the interaction layer between fluids A and B is extremely limited. Only coexistence of bulk mixing, turbulent scale reduction and molecular diffusion enables reaching efficient mixing within practical timescales. (Paul, Atiemo-Obeng, and Kresta 2004)

The Prandtl number for low in the LP is estimated at 0.66 which indicates that in viscous sublayer the molecular diffusion dominates but turbulent core is governed by turbulent mixing.(Shah and Sekulic 2003)

2.4 Thermal mixing promotion methods

Thermal mixing promotion can be executed by few mechanisms. Heat transport by thermal conduction is phenomena carried out through molecular motion of the particles. In case of fluids, considering relatively low density of media, conduction is a slow process. Thermal mixing can be performed much more efficiently by forced convection. The most efficient mechanism is turbulent convection, due to eddy formation. Mixing is introduced by vortex formation which transports momentum and heat by local three-dimensional advection in fluid.

Usually convective heat transfer is referred as phenomenon of heat exchange between fluid and solid. In this study surface of the LP is poor thermal conductor and is not significant thermal storage. The most important phenomena is heat exchange fluid to fluid, and solid component can be used as geometrical obstacle for turbulence promotion. Selected mixing methods summarized in this section can be classified as passive, structural methods for mixing enhancement. They can be introduced by modifying LP geometry and they do not require further control during normal operation of the plant.

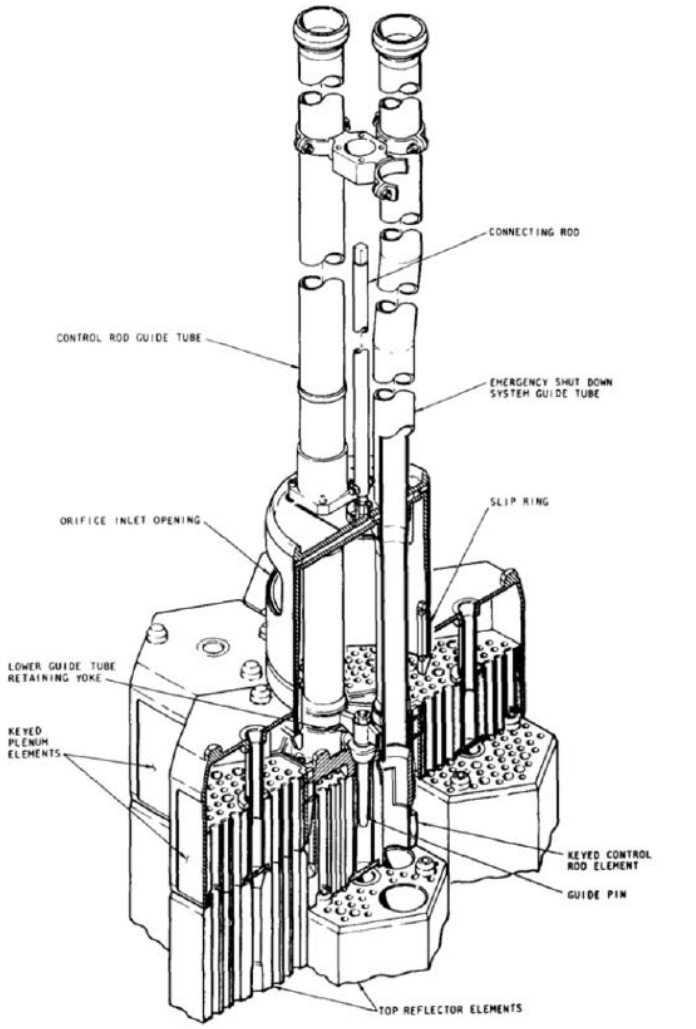

Figure 9 Adjustable orifice device from St Vrain reactor (Paul D. D. 1976)

2.4.1 Past solution "adjustable orifice inlet device installed" - Fort St Vrain

One of the past solutions for the LP mixing problem was application of the adjustable orifice inlet device installed at the Fort St- Vrain reactor (Paul D. D. 1976). The 96.5% of the total coolant flow was distributed between the 37 refueling regions. Coolant was entering the refueling region from the upper plenum by an adjustable orifice valve shown in Figure 9. The orifice was responsible for regulation of the mass flow in every refueling region. The regulation was executed by adjustment of the inlet area in the upper plenum. In practice the orifice was constructed of two concentric cylinders with overlapping slots. To reduce the flow outer cylinder was shifted upwards while the inner cylinder remained in previous location. The imperfect overlap of the

slots resulted in reduced "window" area available for gas flow. Orifice devises were adjusted by a step motor over a range of 17 positions.

This solution as any automated mechanism is vulnerable for mechanical failure and the operation of such complicated mechanism (37 orifices with 17 possible positions) was introducing some difficulties to the operators. This solution must be replaced with passive system which will satisfy expected safety level for IV GEN reactors.

2.4.2 Flow swirling adds

S. B. Rodriguez from Sandia National Laboratories, was studying issues of hot streaking and stratification in LP (S. B. Rodriguez and El-Genk 2010; S. B. Rodriguez and El-genk 2011; S. Rodriguez and El-Genk 2011; S. Rodriguez 2011), which introduce unique operation and safety challenges. This effort leaded to publishing few papers investigating flow characteristics of free conventional and swirling jets, and a conventional jet with cross flow. CFD analysis was summarized with few significant conclusions. The most substantial is the temperature range of hot jet exiting from the hot channel. Rodriguez showed that without additional jet entraining, hot gas will reach the bottom plate of plenum before mixing with cooler jets from other inlets. Helical swirl initiating device was proposed to increase azimuthal and decrease axial velocity. Inserts are designed to redistribute the principally axial momentum of the exiting hot helium gas into axial radial and azimuthal momentum components with extensive mixing and entrainment of the surrounding gas in LP. The resulting swirling gas flow minimizes the impingement onto bottom plate and hence the formation of the hot spots. Usage of those devices resulted in negligible pressure loses.

High turbulent viscosity of the helium strongly affects not only entrainment but also the mixing of the surrounding gas by the jets. Analysis was performed with Fuego CFD code (with LES turbulence model) coupled with Calore heat transfer code. To identify swirling adds effect on the flow, the hot jets were applied to the model (as boundary condition), at the same velocity but 200 degrees hotter than representative jets. The LP flow field was identified as very complex and

consist several phenomena as cross flow, flow stagnation zones, vortex interactions, multiple jet flow interaction, vortex shedding, entrainment, large variation of Re, recirculation and suppression regions. The CFD study showed that usage of this type of device will result with increased temperature uniformity and decrease probability of hot streaking.

2.4.3 Jet mixing actuators - vortex generators

The mixing may be introduced by decay of vertical velocity component and cause vertical jet entrainment promoting turbulence and as a result mixing of the jest with higher temperatures (coolant jest from the "hot channel"). The jet nozzle modification is another opportunity to control and enhance jet mixing. D. E. Parekh (M. Carletti, Rogers, and Parekh 1996) performed a study on a passive mixing enhancement techniques for axisymmetric jet. Varying types of vortex generators are illustrated in Figure 10 Vortex generators configuration and geomtery. **(M. Carletti, Rogers, and Parekh 1996)**. For delta tabs and half delta-wing vortex generator blockage, velocity and average vorticity were examined. Flow tabs have been a subject for extensive research which resulted with following conclusions (Ahuja and Brown 1989; Bradbury and Khadem 2006; Samimy, Reeder, and Zaman 1991; K. B. M. . Zaman 1993; K. B. M. Q. Zaman, Reeder, and Samimy 1994):

- Appreciably faster decay of the centerline velocity for 1, 2, 4, and 6 tab cases, relative to the reference case.
- Mixing enhancement greater for supersonic cases than subsonic cases.
- Heating the jet provides no significant change in the effectiveness of the tabs.
- Smaller tabs have less effect in distorting the jet. Tab width is more critical than tab height.
- A tab height greater than the boundary layer thickness is required to be effective.
- Tab shape (rectangular vs. triangular) has little effect on tab performance.
- Orientation or angle of the tab is more critical than shape; triangular tab leaning 45° downstream, referred to as a "delta" tab, has the greatest effect.

Similar research was conducted for half delta-wing vortex generators, which are similarly effective in jet mixing enhancement (M. J. Carletti and Rogers 1994; Surks, Rogers, and Parekh 1994) follows:

- Half delta-wing vortex generators allow for more flexibility in nozzle design in that they only produce a single vortex. Counter-rotating pairs may be produced by having two adjacent generators of opposing sign.
- Generator orientations producing co-rotating vortices show increased mixing relative to counter-rotating configurations.
- Improved mixing is achieved for increased generator height and angle of attack to the oncoming flow.
- Generators smaller than the boundary layer thickness were found to have essentially no effect on the mass entrainment of an axisymmetric jet, at low speeds (Re=50,000).

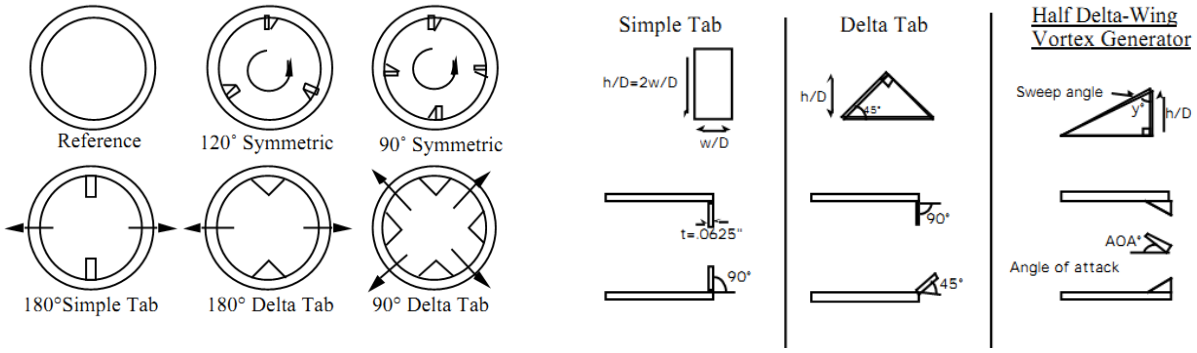

Figure 10 Vortex generators configuration and geomtery. (M. Carletti, Rogers, and Parekh 1996)

The key results of work Carletti showed that actual blockage of the half delta-wing vortex generator is reduced about approximately to one third of the blockage in case of delta tab of equivalent projected frontal blockage. Maximum values of average vorticity, measured at a distance of two jet diameters downstream, generated by both type of tabs are higher nearly 25% than for reference nozzle without tabs. Further analysis of half delta-wing vortex generator parameters showed that axial velocity decay is strongly dependent on height and incline. Whereas sweep angle and tab shape variation are less influential.

This passive technique can be easily applied for HTGR's in the jet inlets to LP to enhance decay of axial velocity component and that way promote jet mixing.

2.4.4 Surface roughness

It is well known that in case of fluid flow in contact with solids surface roughness will increase turbulent heat transfer coefficient. However, form LP appliance perspective effect which may be interesting is change in velocity components and turbulence promotion.

Study done by Lyles (Lyles, Disrud, and Krauss 1971) concerned effects of surface roughness and mean wind-speed on the fluctuations of velocity components in the boundary layer of a low-velocity wind tunnel. It was shown that for rough surface, both longitudinal and vertical turbulence intensity increased with surface roughness.

This method may not achieve sufficient level of effectiveness needed for promotion of turbulence and following mixing enhancement.

2.4.5 Boundary layer displacement

This effect is particularly important for mixing of the fluid adjacent to solid surface. It can be introduced by placing ribs transverse to the flow which results in creation of the small recirculation zone in front of the rib, formation of recirculation zone behind the rib, flow reattachment on the base wall and flow over the next rib. Above ribs line recirculation eddies are created. Rabas and Arman summarized effects, listed elsewhere (Thome 2004), caused by heat transfer process. The flow pattern is shown in Figure 11.

This effect may be used in HTR LP through placement of ribs on supporting posts surface. Ribs can be horizontal, vertical or in shape of twisted tape wrapped around the posts as shown in Figure 12. Detached boundary layer and additional recirculation zones can have beneficial influence on the final mixing effect and temperature distribution at the LP outlet.

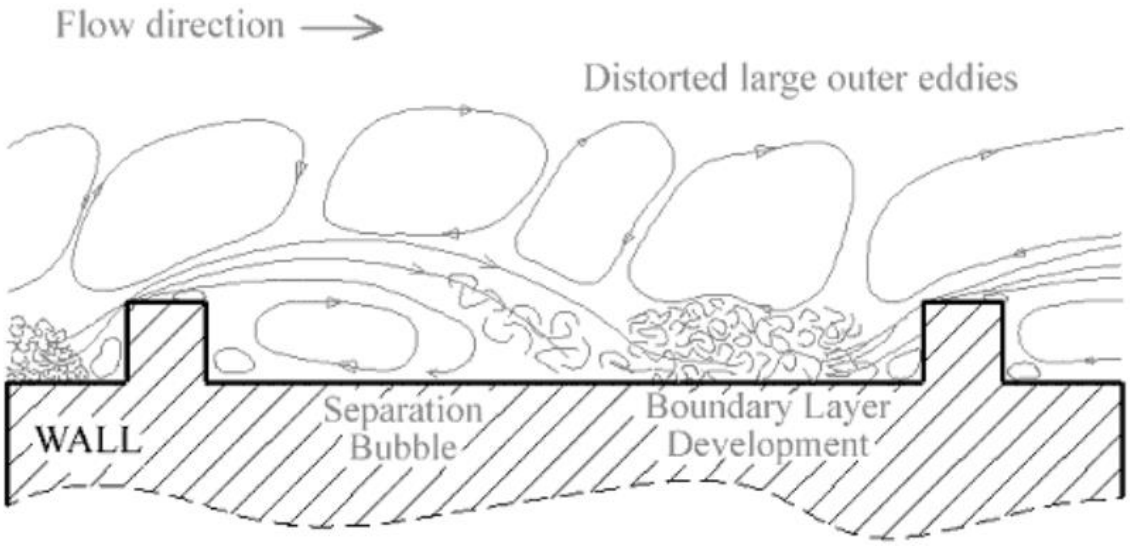

Figure 11 Turbulent flow structure over a two-dimensional rib from (Thome 2004)

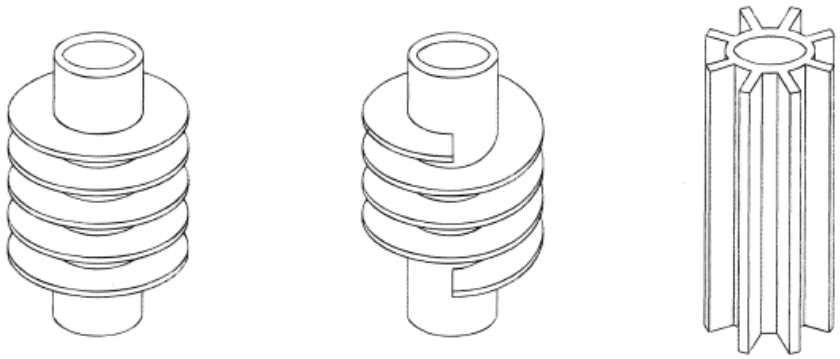

Figure 12 Examples of finned posts (Beale, 2011)

2.4.6 Other types of post arrangement arrays

Support posts in LP of HTGR are arranged in staggered array. There are other common tube bank arrangements, for instance – in-line. Iwaki (Iwaki et al. 2004) introduced PIV measurement of the vertical crossflow structure over both of them. However, it has been proven that staggered array in comparison to in-line array is more beneficial from mixing perspective and to become fully developed at a shorter distance from the inlet than in-line array. Other significant conclusions regarding flow structure in staggered array:

- Three kinds of flow region were identified: vortex region, branching region, meeting region.
- Only symmetric vortices formed behind all of the posts.
- Wake was closed at the midpoint behind the tubes.

In general flow in staggered array can be characterized as more homogenous and isotropic due to turbulence than in case of the in-line array. Thus, changes in post arrangements would not result in turbulence enhancement and will not be taken in further consideration.

2.4.7 Mesh inserts

The study performed by Naga Sarada (S, Radha, and Raju 2009) related to augmentation of turbulent heat transfer in a horizontal tube by means of mesh inserts, may be beneficial for HTGR's applications. The study presents experimental investigation of mesh inserts of varying diameters to promote heat transfer between fluid flow and heated surface of the pipe. Hydraulic diameter reduced by mesh inserts and thereby increased velocity in the pipe causes enhanced heat dissipation from the heating section. A careful analyze of various cases with and without mesh insets shows that increase in mesh diameter cause increase in turbulence and following decrease in pipe surface temperature. For all values of examined porosity higher heat transfer rates are observed as Reynolds number increases. As expected the highest thermal performance mesh insert causes the highest pressure drop. However, penalty of the pressure drop is not as significant as increase in Nusselt number with ratio of porous material.

Although surface of LP is to be isolated and not conduct any significant heat fluxes mesh inserts could yield to interesting effects in turbulence promotion in outlet duct of the LP, especially for GT-HTR design with extremely sensitive gas turbine.

2.4.8 Screen

The other approach to ensure thermal mixing in the LP is installation of the screen or perforated baffler at LP exit. This solution introduces additional benefit which is including bypass flow into mixing activities. Bypass flow is defined as the gas passing between the prismatic blocs in the core and reflector area. Since it does not enter the coolant channels it is anticipated to be significantly colder than gas flowing through average channel and thus introduce even larger temperature gradient than hot channel-to-average channel.

This solution was applied in similar context for HTR-PM by J. H. Ha (Ha et al. 2014). To ensure uniform distribution of the helium flow into the steam generator several screen designs and placements were examined. It was stated that for this application screen presented in Figure 13 provided the best coolant distribution.

Similar screen could be redesigned for HTR and installed in the LP outlet of the prismatic HTR or at the inlet to the hot leg of the cross duct. This type of modification would cover optimization of not only hot-to-average channel gas mixing but also bypass flow-to-average channel mixing issue.

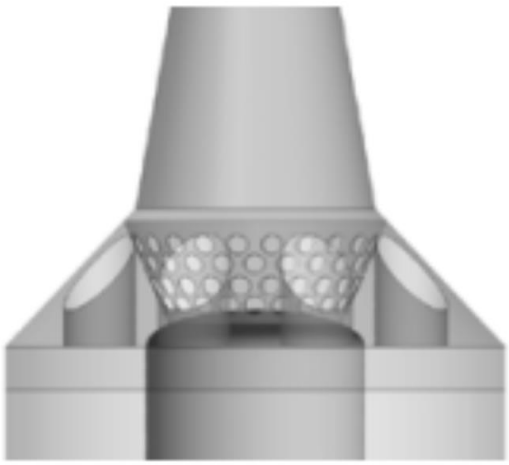

Figure 13 Proposed screen in the steam generator of the HTR-PM with opening ratio 0.4 (Ha et al. 2014)

2.5 Summary and recommendations

Much work is needed to advance the design of HTR-like reactors in order to go through with strenuous certification process in US and European countries. Extrapolation of the data gained from simplified experiments to full scale is not entirely unambiguous. In this circumstance, it is necessary to employ computational tools to perform simulations helpful during the process of design, testing and certification of NGNP. CFD tools can be very useful providing temperature and velocity values locally as well as comprehensively to identify possible issues with hot spots or large temperature gradients.(Karaismail and Celik 2010)

In the literature many modeling approaches concerning HTGR's have been confronted. Flow phenomenon in the LP was investigated in numerous scientific publications. Also experiments concerning LP subsection flow have been developed, conducted and analyzed. Boundary conditions for experimental or computational studies are approximate due to lack of operational data in this matter (for particular modern HTR design). In spite of variety modeling approaches for LP flow investigation hot streaking issue was examined in few sources. Rodriguez, investigated the issue along with solution for this problem. However, just one method was examined. Jet mixing enhancement subject was extensively subjected to research in other areas of science and engineering. Methods used for other applications can be modified and redesigned to be used for application in HTGR's LP.

The past solution from St Vrain in US - adjustable orifice inlet device introduced high level of complexity in terms of operation and automated mechanism is vulnerable for mechanical failure. This solution shall be replaced with passive system which will satisfy expected safety level for IV GEN reactors. The solution presented by Rodriguez – flow swirling adds, seem to provide satisfactory results. However non other methods has been presented to confront the effectiveness and feasibility of this option. To thoroughly examine possibilities of optimizing mixing in the LP of the prismatic HTR other possible methods should be investigated, for instance:

- Vortex generators - This passive technique can be easily applied for HTGR's in the jet inlets to LP to enhance decay of axial velocity component and that way promote jet mixing.
- Surface roughness – This method may not achieve sufficient level of effectiveness needed for promotion of turbulence and following mixing enhancement.
- Boundary layer displacement – This effect may be used in HTR LP through placement of ribs on supporting posts surface. Ribs can be horizontal, vertical or in shape of twisted tape wrapped around the posts. Detached boundary layer and additional recirculation zones can have beneficial influence on the final mixing effect and temperature distribution at the LP outlet.
- Mesh inserts – Although surface of LP is to be isolated and not conduct any significant heat fluxes mesh inserts could yield to interesting effects in turbulence promotion in outlet duct of the LP, especially for GT-HTR design with extremely sensitive gas turbine.
- Screen – screen-like insert could be designed for HTR and installed in the LP outlet of the prismatic HTR or at the inlet to the hot leg of the cross duct. This type of modification would cover optimization of not only hot-to-average channel gas mixing but also bypass flow-to-average channel mixing issue. Additional study should be performed regarding shape, placement and opening ratio of the screen.

Listed methods may represent various range of effectiveness feasibility for application in modern prismatic HTR. Thus they should be fatherly analyzed to select method or combination of methods which will provide sufficient mixing level of coolant in the LP or at the entrance to the next component of the primary loop like steam turbine, gas turbine or IHX.

3 Materials and Methods

This study was conducted using numerical tools namely CFD code – STAR-CCM+ from CD ADAPCO. It was based on the experimental facility for the MHTGR located at Oregon State University (HTTF). The study was designed in a way so that future experimental data from HTTF can be used for validation of the STAR-CCM+ code and applied model for HTR's. Since results obtained from experiments and CFD simulations are subject to some level of error, an uncertainty analysis needs to be applied. Section 3.1 describes the HTTF facility in order to justify the choice of geometry, boundary conditions and models to the reader. Section 3.2 describes the computational study.

3.1 HTTF - facility and experimental set up

The High Temperature Test Facility is a scaled – one quarter, test installation model of Modular High Temperature Gas-cooled Reactor. The HTTF is a full temperature facility operating at maximum temperature 850°C (for well mixed gas) and operating pressure 0.8 MPa. The facility, equipped with a heater power approximately 2.2 MW, is cooled with helium. However, other gases can be used.

The HTTF was designed to simulate a variety of accident conditions, transients and normal operation conditions. Main elements of the facility are:

- Vessel with 2.2 MW electrically heated prismatic block core simulator
- Ceramic reflector and core regions
- Gas circulator
- Forced flow cavity cooling system
- Break valves
- Confinement simulation tank
- Instrumentation package
- Complete data acquisition system

The HTTF pressure vessel is constructed form stainless steel (SS304) which is the choice recommended by American Society of Mechanical Engineers (ASME) for operational conditions up to 0.965 MPa at 550^0C. The vessel outside diameter and height are respectively 1.663 m and 6.1 m. The vessel is combined with elliptical upper head, LP and inner ceramic liner. The lower head includes instrument taps and penetration of the electric heater rods. The core structure is supported by ceramic posts that rest on the bottom of the LP.

3.1.1 Internals of the High Temperature Test Facility Reactor Pressure Vessel

The structural internals in the HTTF pressure vessel are formed as a stack of ceramic blocks. Starting from the top of the pressure vessel, the first internal section is the upper plenum. Next there are three levels of reflector under the fuel region. Following layers are respectively the LP roof, LP chamber with support posts and LP floor. These blocks are surrounded by outer reflectors (also constructed of ceramic blocks). All mentioned elements are composed of ceramic material – Greencast-94F Plus with following properties:

- *Composition* – Alumina (Al_2O_3) – 96.5%, Lime (CaO) – 3% remaining 0.5% is Silica, Iron Oxide, Magnesia and Alkalies
- *Maximum service temperature* – 1870^0C
- *Density* – at temperature 816^0C is 2.92 g/cm^3 (no significant change for higher temperatures)
- *Thermal conductivity* – at temperatures 650^0C and 870^0C respectively 2.83 and 2.49 W/m^{0}C.

3.1.2 Experiment Instrumentation located in the LP

To collect all data necessary for investigation of mixing occurring in the LP of the HTTF experimental instrumentation was placed not only in the LP area but also in the outlet duct of the HTTF. The following elements are employed in data extraction: temperature readings in the LP interior, surfaces, reflector area and the outlet duct. In sections 3.1.2.1 and 3.1.2.2 all experimental instrumentation from the area of the LP and the outlet duct is described.

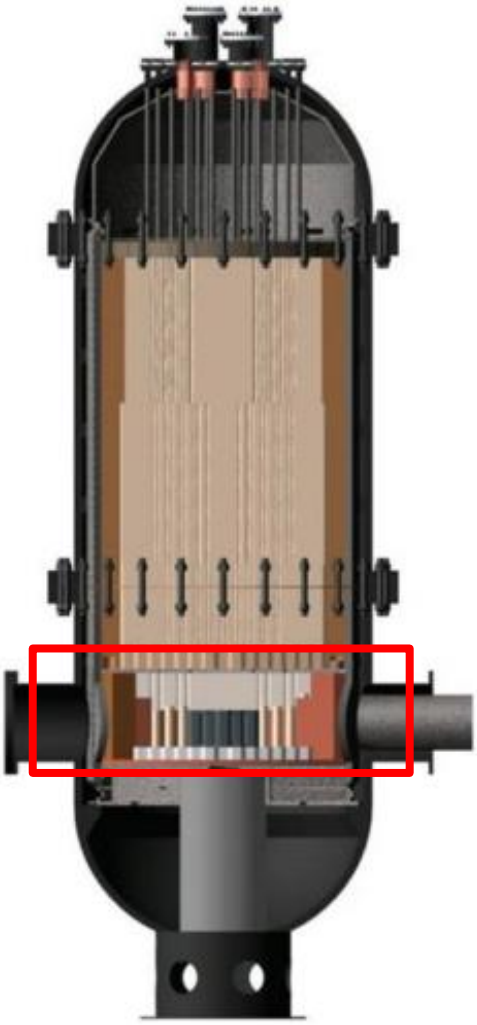

Figure 14 Vertical section through solid model of the High Temperature Test Facility Reactor Pressure Vessel. Red rectangle contains the area of LP

Table 5 Temperature measurement instrumentation in the LP

Location	Number
Lower Plenum Gas TCs	32
Lower Plenum Inlet Gas TCs	12
Lower Plenum Floor TCs	12
Lower Plenum Side Reflector TCs	2
Total TCs in lower plenum	58

3.1.2.1 LP's instrumentation

The jet mixing behavior in the HTTF's LP is examined using data collected from a number of strategically placed thermocouples and one pressure sensor. The static pressure sensor, marked with a green circle at Figure 16, is placed opposite the plenum exit, near to the side reflector of the LP. Reference line for this pressure tap is the vessel inlet pressure.

Coolant temperature data is collected using a total of 62 K-type thermocouples located within the LP structure as shown in Figure 16. TC's can be divided into three types: gas thermocouples located at certain height of the support posts, ceramic temperature thermocouples placed on the surface of the LP floor and gas thermocouples positioned at the exit of the transition blocks as shown in Figure 15. Two primary phenomena are to be characterized by TC's located in LP: air ingress and jet mixing along with impingement behavior. First 32 TC's, marked by black lines at Figure 16 are placed at the surface of support posts in the 16 locations at 25% and 75% of the plenum height as shown at Figure 15. The jet characterization is obtained using supplementary TC's. Additionally in 12 of these locations there are LP's inlet gas temperature thermocouples and a LP floor thermocouples. Their primary aim is to characterize air ingress, stratified flow and gas temperature. The remaining 2 TC's are located in rear part of LP reflector (purple circles) to measure temperature of the structural elements which are not in direct contact with the gas flow.

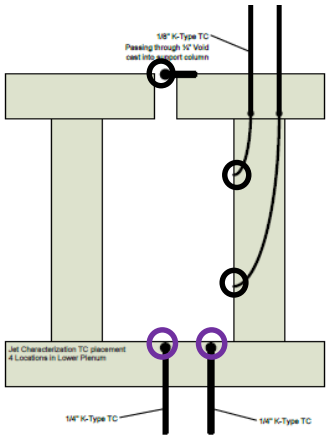

Figure 15 TC's layout for investigation of the single gas jet; purple circle – LP floor TC's; black circle – jet characterization TC's

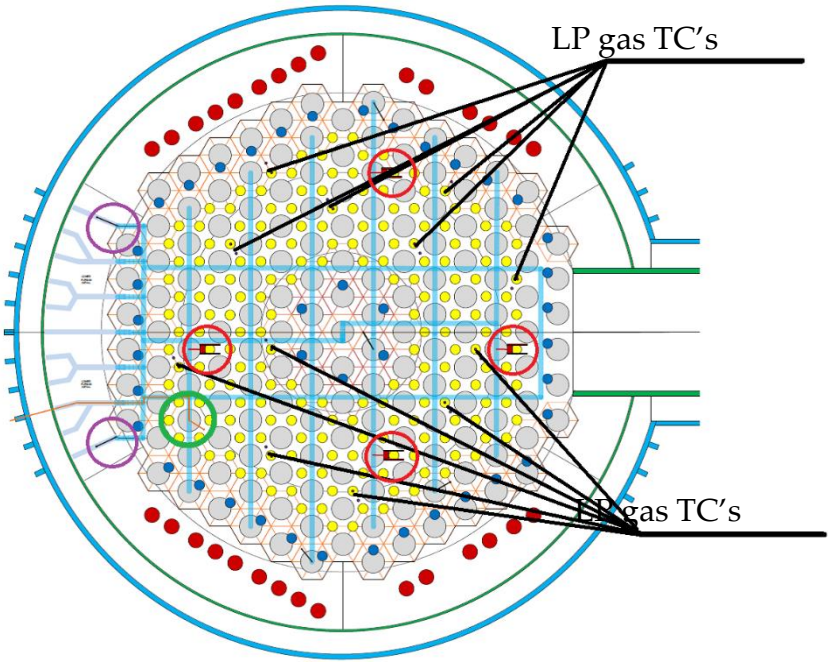

Figure 16 Instrumentation locations in LP; red arrow – pressure tap; purple circle – reflector TC's; black circle – gas coolant channel TC's; blue circle – jet characterization and LP floor TC's

3.1.2.2 Instrumentation in the outlet duct

The outlet duct is equipped with pressure tap and several K-type thermocouples through the crossover duct rakes. Rake 1 is located near to the pressure vessel. It has instrumentation ports for the thermocouples and the pressure instruments. Three thermocouples are aligned vertically. Rake 2 is located on the hot leg prior RCST (Reactor Cavity Simulation Tank) and it is also equipped with thermocouples and pressure instruments. Thermocouples are located in the same way as in Rake 1. There is also one pressure tap located at Rake 1. The reference line for this instrument is pressure in the cold leg.

3.2 CFD tool - Model Equations

This study was carried out using computational fluid dynamics software – STAR-CCM+ ADAPCO. The simulation of the coolant flow through the LP (or its section) structure was conducted in accordance with best practice rules for this software and CFD simulations in general.

The following sections describe tools, options and models applied to obtain the most physically realistic solution for turbulent, compressible gas flow through the typical HTGR's LP geometry.

STAR-CCM+ software use finite volume domain discretization. In this method the solution domain is subdivided into a finite number of control volumes – mesh cells. Integral forms of continuum transport equations are discretized and assigned to every mesh cell to obtain a system of linear algebraic equations with the number of unknowns in each equation system corresponding to quantity of control volumes in the computational grid. An algebraic multigrid solver is applied to obtain a system of linear equations. STAR-CCM+ has implemented the following integral form of the transport equation for the scalar quantity φ in the continuous medium:

$$\frac{d}{dx}\int_V \rho\,\chi\phi dV + \oint_A \rho + \phi(\mathbf{v}-\mathbf{v}_\mathrm{g})\cdot d\boldsymbol{a} = \oint_A \Gamma\nabla\phi\cdot d\boldsymbol{a} + \int_V S_\phi dV$$

From the left side: transient term, convective flux, diffusive flux and volumetric source term. (CD-Adapco, 2012)

3.2.1 Turbulence modeling

Despite the rapidly progressing development of computational power in the recent years direct simulation of large domains of a turbulent flow is still too expensive for most industrial applications. Due to this fact major simplifications are still needed in CFD simulations for practical applications. A Direct Numerical Simulation of the Navier-Stokes equation is still off the table for complicated simulations as too computationally intensive. Numerical power to simulate flow with this method grows a the cube of the Re number so it cannot be used for application of coolant flow in a domain the size of a nuclear reactor.

The simplified version of this approach is a Large Eddy Simulation. LES also solves the Navier-Stokes equations but just for accordingly large scale of length and time. Small scale events are calculated using a turbulence modeling approach. This method is still very expensive and

requires great mesh resolution, especially near to the wall regions to obtain sufficient resolution of the boundary layer.

The most popular and widely used method in turbulence modeling is based on Reynolds Averaged Navier-Stokes equation. In comparison to the previous methods it is computationally cheap since it eliminates turbulence fluctuations through averaging process to obtain locally averaged flow. In this method an additional variable is created – Reynolds Stress. However, the process of the averaging of the nonlinear terms in N-S equation is the main source of problems with this method.

Detached Eddy Simulation is other option to calculate a turbulent flow. This method is a hybrid build of RANS model near wall and LES far from wall region.

RANS based turbulence are the most frequently used models for industrial applications, however, this type of modeling can be still time consuming. In commercial codes there is a variety of turbulence models built based on various assumptions. Most models are based on linear eddy viscosity assumption. In these models Reynolds stresses are modeled by a linear constitutive relationship with the mean flow straining field, as obtained from a Reynolds averaging of Navier-Stokes equations (CFD Online, 2014):

$$-\rho\langle u_i u_j\rangle = 2\mu_t S_{ij} - \frac{2}{3}\rho k\delta_{ij}$$

$$k = \frac{1}{2}(\langle u_1 u_1\rangle + \langle u_2 u_2\rangle + \langle u_3 u_3\rangle)$$

$$S_{ij} = \frac{1}{2}\left[\frac{\partial U_i}{\partial x_j} + \frac{\partial U_j}{\partial x_i}\right] - \frac{1}{3}\frac{\partial U_k}{\partial x_k}\delta_{ij}$$

Depending on the number of equations solved to compute eddy viscosity coefficient, turbulence models (in category of RANS) can be classified as:

- **Algebraic models** – those models will not solve any additional equations but compute solution using only flow variables (thus often will not account properly on

history of the flow and convection and diffusion of turbulent energy). Those models can be used just for very simple geometries or start-up simulations.

- **One-equation models** – this model solves one transport equation, usually turbulent kinetic energy equation. One of the examples is Prandtl's one equation model. This kind of method was found to be very useful in simple two dimensional flows with slow changes in the direction of the flow.
- **Two-equation models** – those models are the most commonly used, especially for industrial applications. As the name suggests in this method two additional transport equations are solved to account for past effects like convection and diffusion of the turbulent energy. The most common choice for the first variable is turbulent kinetic energy. This equation is responsible for determining energy of the turbulence. The second variable responsible for quantifying the scale of turbulence (length or time scale) is usually turbulent dissipation ε or specific dissipation ω. This approach is based on Boussinesq assumption which is strength and the weakness of the model. On one hand it allows us to introduce very useful scalar values describing the flow like turbulent energy and dissipation. On the other hand it is vast simplification to assume that the Reynolds stress tensor is proportional to the strain rate tensor. This is true for simple flows in not complicated geometries but for complex flows with stagnation zones, rapid acceleration effects and where curvature effects are significant this assumption may not be valid. (CFD Online, 2014)

$$\tau_{ij} = 2\mu_t S_{ij} - \frac{2}{3}\rho k \delta_{ij}$$

Usually additional near wall treatment is applied to resolve the field in the vicinity of the wall were flow variables gradients are large. Two approaches can be distinguished:

- Low Reynolds number treatment (LRN) – right Figure 17

- High Reynolds number treatment (HRN) – left Figure 17

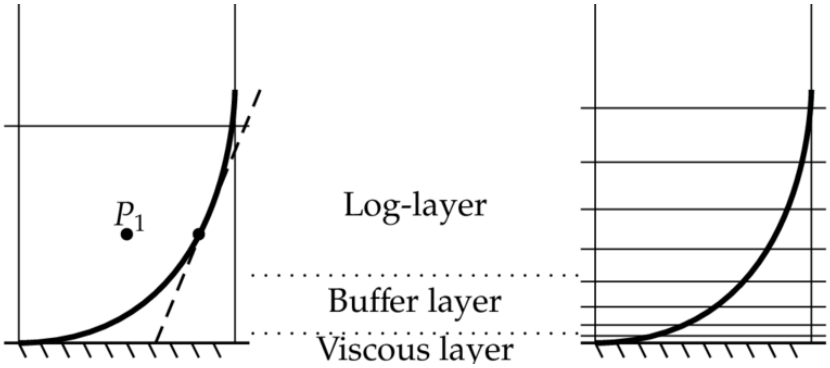

Figure 17 Illustration of the near wall treatment for RANS models (CFD Online, 2014)

3.2.1.1 K-ε turbulence model

RANS based turbulence model. This model solves two additional transport equations for turbulent kinetic energy k and dissipation of turbulent kinetic energy ε. (Versteeg and Malalasekera 2007)

$$\frac{\partial(\rho k)}{\partial t} + div(\rho k \boldsymbol{U}) = div\left[\frac{\mu_t}{\sigma_k} grad\ k\right] + 2\mu_t S_{ij} \cdot S_{ij} - \rho\varepsilon$$

$$\frac{\partial(\rho \varepsilon)}{\partial t} + div(\rho \varepsilon \boldsymbol{U}) = div\left[\frac{\mu_t}{\sigma_\varepsilon} grad\ \varepsilon\right] + C_{1\varepsilon}\frac{\varepsilon}{k} 2\mu_t S_{ij} \cdot S_{ij} - C_{2\varepsilon}\frac{\varepsilon^2}{k}$$

Thus in words:

Rate of change of k and ε	+	Transport of k and ε by convection	=	Transport of k and ε by diffusion	+	Rate of production of k and ε	-	Rate of destruction of k and ε

Where constants vales are (Versteeg and Malalasekera 2007):

$$C_\mu = 0.09;\ \sigma_k = 1;\ \sigma_\varepsilon = 1.3;\ C_{1\varepsilon} = 1.44;\ C_{2\varepsilon} = 1.92$$

These variables can be used to define velocity length scale ϑ and length scale l, which represent large scale turbulence:

$$\vartheta = k^{1/2}$$

$$l = \frac{k^{3/2}}{\varepsilon}$$

Those definitions can be introduced into eddy viscosity formula as follows:

$$\mu_t = C\rho\vartheta l = \rho C_\mu \frac{k^2}{\varepsilon}$$

To compute Reynolds stresses, Boussinesq relationship is used. (Versteeg and Malalasekera 2007)

$$-\rho\overline{u_i' u_j'} = \mu_t\left(\frac{\partial U_i}{\partial x_j} + \frac{\partial U_j}{\partial x_i}\right) - \frac{2}{3}\rho k\delta_{ij} = 2\mu_t S_{ij} - \frac{2}{3}\rho k\delta_{ij}$$

K-ϵ model assumes turbulent viscosity is isotropic, which is inaccurate for many complex flows. Thus this widely used and well established model can be used to simulate number of simple flows, but it has poor performance on swirling, rotating flows in non-circular ducts.

3.2.1.2 Reynolds stress equation model

Reynolds stress model is seven-equation models – not as widely used due to extensive computational cost of solving seven additional PDE's. Reynolds stress model is the most complex model in RANS approximation which accounts for anisotropic effects of the Reynolds stress field. (Versteeg and Malalasekera 2007)

$$R_{ij} = -\frac{\tau_{ij}}{\rho} = \overline{u_i' u_j'}$$

$$\frac{DR_{ij}}{Dt} = P_{ij} + D_{ij} - \varepsilon_{ij} + \Pi_{ij} + \Omega_{ij}$$

Rate of change of $R_{ij} = \overline{u_i' u_j'}$	+	Transport of R_{ij} by convection	=	Rate of production R_{ij}	+	Transport of R_{ij} by diffusion	-	Rate of dissipation of R_{ij}	+	Transport of R_{ij} due to turbulent pressure-strain interactions	+	Transport of R_{ij} due to rotation

Equation above describes six independent partial differential equations for the Reynolds stresses: $\overline{u_1'^2}$, $\overline{u_2'^2}$, $\overline{u_3'^2}$, $\overline{u_1'^2 u_2'^2}$, $\overline{u_1'^2 u_3'^2}$, $\overline{u_2'^2 u_3'^2}$. When comparing this equation to the exact transport

equation, two new processes are found and Reynolds stress equations. It is pressure strain correlation term Πij and rotation term Ωij. The pressure strain term is the most difficult and most important to be modeled accurately as it influences Reynolds stresses by two means: pressure fluctuations due to two eddies interactions and pressure fluctuations due to eddy interaction with flow region of different mean velocity. Thus the pressure strain term aims into restructuring energy location between making normal Reynolds stresses (i=j) more isotropic and reducing Reynolds shear stresses (i≠j). For this model six Reynolds stress equation are solved plus additional equation for the scalar dissipation rate ε. In total seven equations are being solved.

Although RSM is computationally more expensive than two-equation models it is potential the most general of all classical turbulence models. It provides accurate calculation of the mean flow for jets, non-circular and axisymmetric channel flows and curved flows. The disadvantage of this model is much smaller validation documentation than for the k-ε model.

3.3 Limitations

This work was conducted with the following limitations:

1. Work presented in this document concerns the HTTF, a scaled test facility of the MHTGR. However, as in the case of every scaled model not every phenomenon can be reflected accurately and results presented within this dissertation need to be considered with caution.
2. This study does not contain a validation of the numerical model of coolant flow in the LP of the HTTF against experimental data from the HTTF since, there are no experiments in this study. In the CFD model, only selected geometrical elements of the HTTF are included, not the entire facility. LP (void filled with gas) and outlet duct are included in the modeled geometry. The geometry is not a closed loop as it is in the case of the real facility. Instead the numerical model is limited to the LP chamber and the outlet duct where the inlet and the outlet boundary conditions are applied to simulate hot helium flow in LP geometry.

Other limitations:

- The boundary and initial conditions are approximated and not exact values. Boundary conditions for CFD models are presumed for probable operational conditions
- Ideal gas assumption
- Not calculating nuclear chain reactions in the core (core not present in the model)
- Simplified fluid flow approach is used (turbulence modeling, not DNS)

4 CFD models description and results

The computational simulation was modeled using STAR-CCM+ software. In each case, the model was build using a best estimate policy. Therefore the LP flow is modeled as closely to reality as possible taking into account the limited computational time and capacity of the computer cluster available for this research.

To avoid confusing the reader due to multiple CFD simulations with varying geometries, assumptions and boundary conditions the methodology and setup of each simulation is summarized in Table 6. The following subsections present descriptions of the simulation setup, results and analysis of each studied case.

4.1 Part 1 – identification

A number of simulations and experiments need to be conducted in this field. In this section, the thermal-hydraulics aspects of coolant flow through LP of HTGR were considered, specifically flow characteristics to identify the risk of temperature stratification in LP and hot spotting on LP floor. Local temperature gradients can cause material degradation. As the power profile is non-uniform across the core, jets of coolant exit the core region at different temperatures and enter the LP impinging on LP floor causing hot spots at LP structure and temperature stratification. To address those issues numerical simulation were developed. The numerical simulation provides coolant flow velocity and temperature fields. The purpose of this study is to investigate the mixing phenomenon in the LP due to risk of the hot streaking and thermal stratification phenomena during normal operation of HTGR. The following aspects are being examined: identification of gas flow behavior in LP of HTTF based on CFD simulations, identification of hot streaking issue in the HTTF LP using CFD tools, and computational investigation of gas mixing efficiency. This section includes guidance for LP CFD modeling, the results and analysis of the CFD simulation.

Table 6 STAR-CCM+ run schedule (without sensitivity studies)

PART	case no	Case name	geometry	mesh [mln]	turbulence model	time	BC
1	P1.1a	"hot channel" / ΔT=50 K	whole LP + part of outlet duct	2.4/5.5	realizable k-ε(Two layer, all y+), v2f k-ε (all y+), k-ω SST, RSM	steady	v=20.8 [m/s]; T=950/1000 [K] + passive scalar
	P1.1b	ΔT=100 K		5.5/8.4			
	P1.1c	ΔT=150 K		5.5	k-ε, Two layer, All y+		v= 20.8 [m/s]; T=950/T=950+ΔT [K] + pasisve scalar
	P1.1d	ΔT=200 K		5.5			
	P1.1e	ΔT=250 K		5.5			
	P1.1f	ΔT=300 K		5.5			
	P1.2.1	Approx. temp. profile B		5.5	k-ε, Two layer, All y+		separate doc
	P1.2.2	Approx. temp. profile A		5.5	k-ε, Two layer, All y+		
2	P2.1.1	reference	single channel	6	standard k-ε (low Re, low y+)	steady	v=20.8 [m/s]; T=960 [K]
	P2.1.2	delta tab					
	P2.1.3	delta 45					
	P2.1.4	delta swirl					
	P2.2.1	MIR	MIR	2.5	realizable k-ε(Two layer, all y+), k-ω SST	Implicit unsteady	mass flow; T=950/1000 [K] + passive scalar
	P2.2.2	MIR delta					
	P2.2.3	MIR oil					mass flow; T=295 [K] + passive scalar
	P2.2.4	MIR delta oil					
	P2.3.1	Reference	outlet duct	0.25	realizable k-ε(Two layer, all y+)	steady	extracted from P1.2.2
	P2.3.2	Kwiat					
	P2.3.3	Motionless mixer					
3	P3.1	LP + MM	whole LP + MM + outlet duct	6	realizable k-ε(Two layer, all y+)	steady	separate doc

4.1.1 RANS simulation of the thermal mixing in HTTF LP during normal operation conditions

4.1.1.1 Materials and Methods

This work is the first out of three stages of study concerning the optimization of the flow mixing in the LP of the HTTF during normal operation conditions. The first stage of research contains preliminary calculations for the LP mixing in the HTTF. Pretest calculations were prepared using a best estimate methodology to obtain simulation as close to the reality as possible considering available computational resources. Cases described in Table 7 were applied and analyzed to quantify characteristics of the coolant flow, thermal mixing and detect/confirm existence of the potential exploitation issues. STAR-CCM+ software was used for the computational fluid dynamics part of the research.

Table 7 Test cases boundary condition description (variation of the P1 cases, not included in Table 6)

Case name	Description	
	inlet velocity	temperature
Base case	20.8 m/s	950 K
Hot channel	20.8 m/s ; 950 K + section of 6 channels has increased inlet temperature to 1000 K	
Variation 1	as *Base case* + reduced mass flow by ~5%	
Variation 2	as *Hot channel* case + reduced mass flow by ~5%	

4.1.1.2 CFD Simulation

The CFD simulation was modeled so it resembles the HTTF as closely as possible considering the limited computational resources. The simulation was conducted for turbulent, compressible gas flow through a HTTF's LP geometry. The geometry (Figure 18) of the model built in NX 7 consists of the LP roof, the LP floor, inlet channels, the outer reflector, support posts and the outlet duct (hot duct). Gas is delivered to the LP by 234 inlet channels. Approximately 520 cooling channels of various diameters from the core area are merged in reflector number 1 into 234 channels of constant diameter.

Inlet channels can be divided in two categories due to their function. The majority of the channels (main channels - 192) cool the core, removing produced heat. Those channels are

distributed by triangular array through the core. However, they are placed just in the heated area so they create an annular shape. The remaining 42 channels (bypass channels) are distributed along the inner (6 channels) and the outer boundary (36 channels) of the fueled area in the reflector. Those channels transport up to 11% of the flow rate and at the temperature of the coolant. In addition, the velocity in the bypass channels will be substantially lower than for regular channels.

The outlet duct (ID 0.298 m) transports hot mixed helium out of the reactor vessel. The reactor core weight rests on 163 cylindrical posts of diameter 0.057 m. The posts obstruct the flow creating stagnation, recirculation and high turbulence zones. All structural elements in the LP are made of ceramic material (Greencast 94-F). The surface of all elements is not perfectly smooth and may introduce considerable friction effects.

The computational mesh was created using unstructured polyhedral cells with prism layer applied to the wall vicinity resulting in approximate number of 650 thousand, 2 million and 2.5 million cells. The physical interior was established using the following models and assumptions:

- Ideal gas
- 3 dimensional mesh
- Turbulent flow regime
- Adiabatic walls
- Reynolds-Averaged Navier-Stokes turbulence model

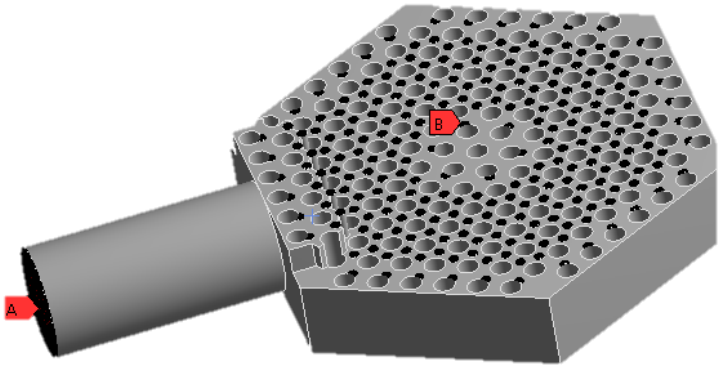

Figure 18 Computational domain with outlet duct, support posts and inlets.

The boundary conditions for the LP model were implemented in the following manner. Inlet channels were divided into subsections/ zones which are controlled from the HTTF operating panel. Thus there are 10 different inlet zones of inlet channels and for every zone is capable of delivering different gas properties. These 10 zones contain 234 channels in total, providing in total flow rate of 0.9874 kg/s. About 11% of the flow is bypassed, gas which flow through the outer and central reflector, that is several degrees colder than gas in the other channels entering the LP. Flow rates, jet temperatures and velocities are summarized in Table 7. The interior walls were modeled with no-slip condition, wall boundary as smooth surfaces.

4.1.1.3 Test cases description for CFD simulation

Several cases of operational conditions will be tested and analyzed, however the first two cases, Base case and Hot channel case, are more vital for the study results. Base case was used to obtain flow characteristics in the LP as well as validate data obtained in the first stage of research from computational analysis.

Table 8 Test description

Case table	Time dependence	Turbulence model	Mesh	Boundary conditions
PHASE 1 STAR-CCM+	Steady state	K-epsilon Realizable two layer All y+	2.5 mln 2 mln 650 k	*Base case* *Hot channel* *Variation 1* *Variation 2*

The second test – Hot channel indicates mixing characteristics in case of uneven power distribution and consequences of this operational condition, as well as provides answers for questions about the need for preventing hot spotting/thermal stratification. The two following tests (Variation 1 and 2) are designed to examine the influence of reduced coolant flow rate at temperature distribution on lower plate surface and temperature variations of the gas at the LP outlet.

4.1.1.4 Preliminary results

A number of simulations were conducted as described in Table 7 and Table 8. Preliminary calculations – Base case was calculated to obtain a generic profile of the flow in order to address requirements for definition of next more advanced simulations. The temperature and velocity profiles were obtained using the RANS k-ε model. Since it is a two equation model, complex flow occurring in the LP may have poor performance on swirling flows in non-circular ducts, but for the purpose of this preliminary analysis it is sufficient.

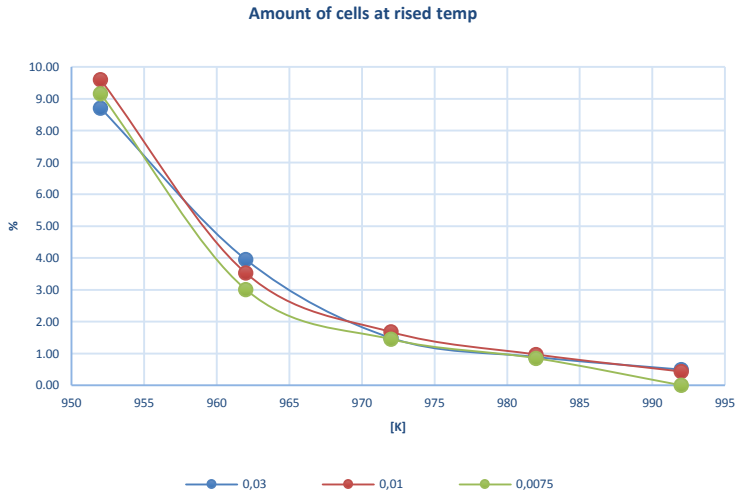

Figure 19 Percent amount of cells at selected temperatures in LP for different meshes

To examine the solution independence of the numerical grid, three mesh sizes were generated and solved. In Figure 19, the percentage of cells under a certain temperature threshold is presented for all calculated meshes. The amounts of cells at selected temperatures were varying by less than 1%. On average, the finest mesh contained the least amount of cells falling into the temperature threshold.

From a perspective of mixing, the hot channel case is the most interesting thus its results are described in detail. In Figure 21, the progress of gas mixing can be seen for the medium mesh consisting of 5.5 million cells. For the lowest value of the threshold – 952 K, just 2 degrees over temperature in rest of the plenum, we can distinguish the area where gas from the hot channel influenced temperature rise on its way to the outlet. The next threshold of 962 K represents only

fraction of cells amount from 1st threshold, indicating that the primarily distinguished area of mixing represents an insignificant level of actual thermal mixing between LP gas and hot inlet gas. The following illustrations show higher level of threshold. For the highest value containing temperatures from 992 to 1000 K, the amount of cells which is suitable for this threshold is rather low; however, gas at this temperature reaches over half of plenum height before mixing with lower temperature gases. This results in heating up the surface of LP floor along the flow path of the hot gas. The maximum value of temperature in vicinity of the LP floor caused by hot channel presence was 970.7 K. This hot spot is localized in front half of the plenum.

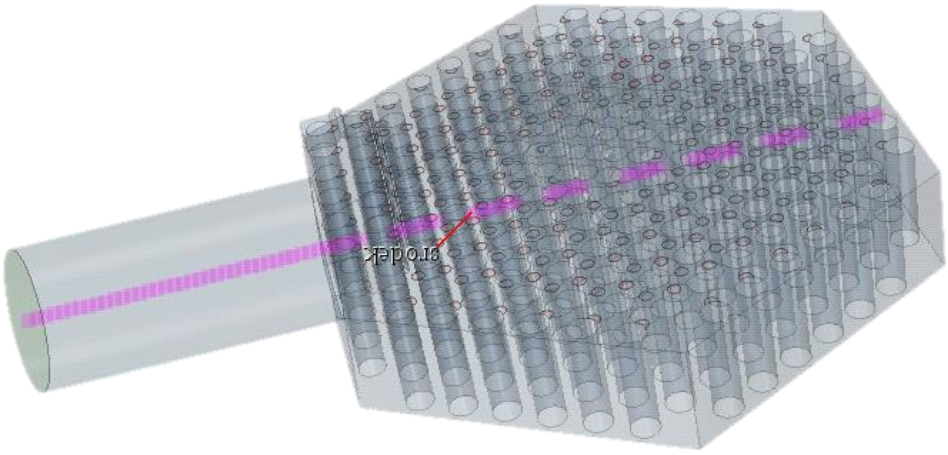

Figure 20 Location of probe line 1

Figure 22 and Figure 23 and Figure 24 display the velocity (x and z directions)and temperature profile along probe line 1, which goes from a central point on the outlet along the x axis all the way through the LP. This probe line, shown in Figure 20, passes through a few support columns, which are visible on the charts as blank gaps between data points. Since the hot section of the inlets are not located in central part of the LP, through over half length of the plenum no significant temperature increase can be seen in Figure 24. Subsequently, some variation in the temperature reading can be seen as initial hot gas mixes into the flow, then temperature increases smoothly almost until the end of the probe line which is located at LP outlet.

T< 952 K

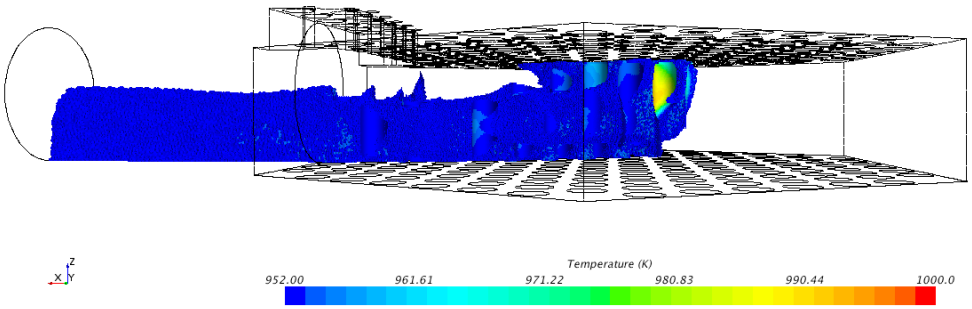

T< 962 K

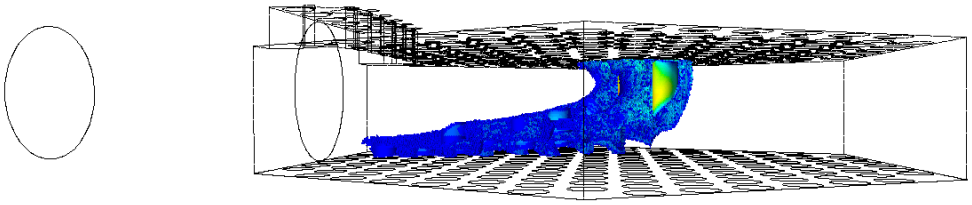

T< 972 K

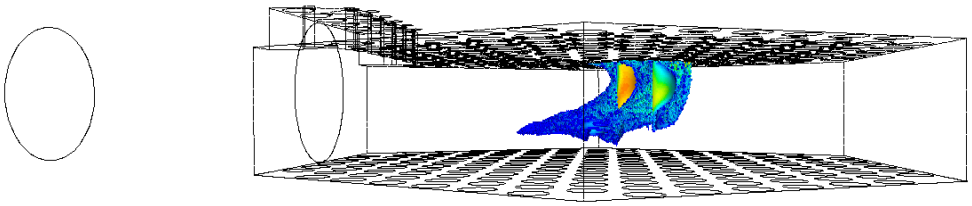

T< 982 K

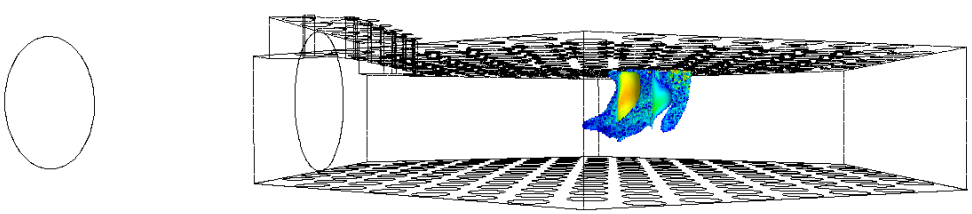

T< 992 K

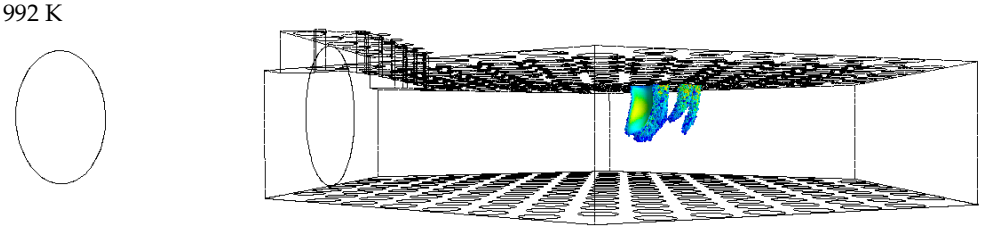

Figure 21 Temperature threshold for discretized computational domain

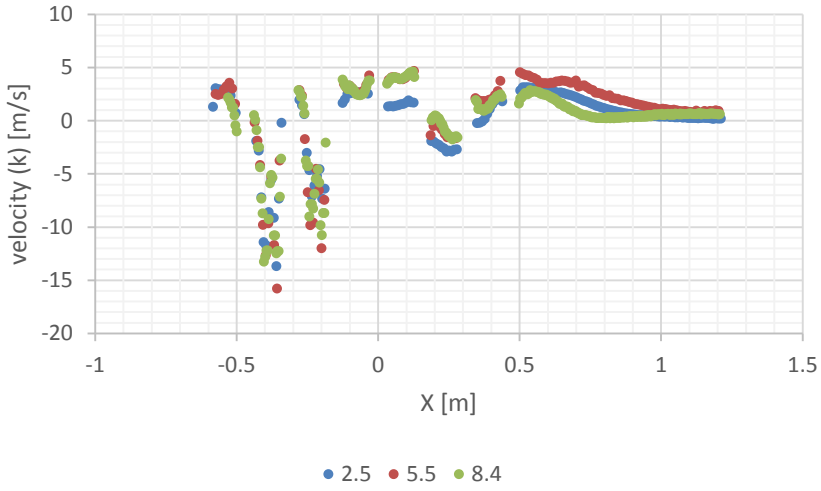

Figure 22 Velocity (k) extracted from probe line 1 for fine, medium and coarse mesh

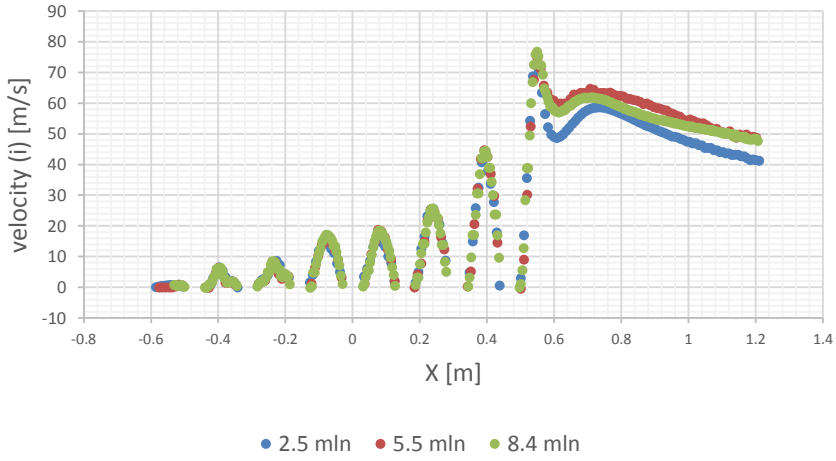

Figure 23 Velocity (i) extracted from probe line 1 for fine, medium and coarse mesh

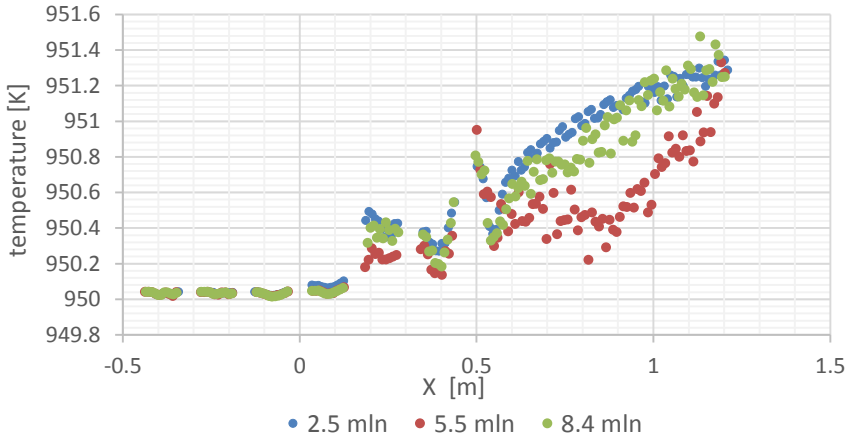

Figure 24 Temperature profile at probe line 1 for fine, medium and coarse mesh

The results extracted from all meshes seem reasonable and for the most part coincide. Some discrepancies between results can be observed especially for the coarse mesh in the outlet duct. Also the finest mesh result in a different temperature profile in the outlet duct than the medium and coarse meshs. This suggest that mesh independent solution has not been reached in the outlet duct area and further mesh refinement is advised, especially in order to achieve better agreement on flow velocity near and inside of outlet duct. The comparison of the flow and temperature fields for the remaining cases is shown in Figure 25, Figure 26, Figure 27 and Figure 28.

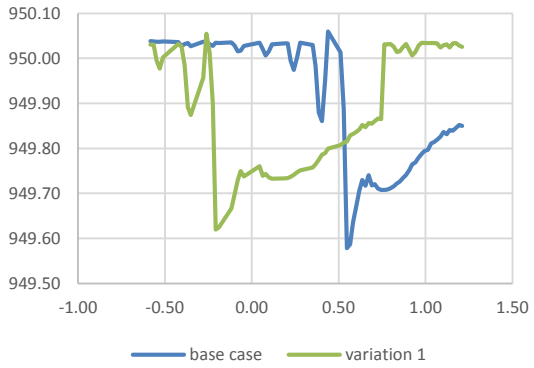

Figure 25 Temperature profile at probe line 1 for base case and variation 1

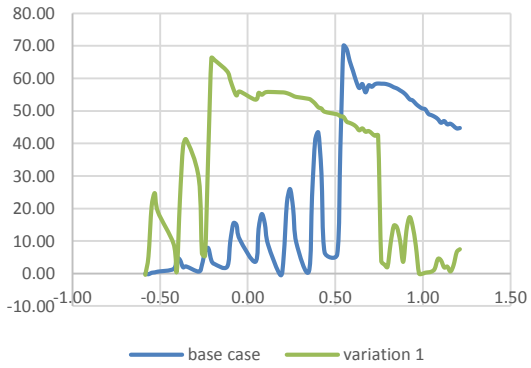

Figure 26 Velocity [i] profile at probe line 1 for base case and variation 1

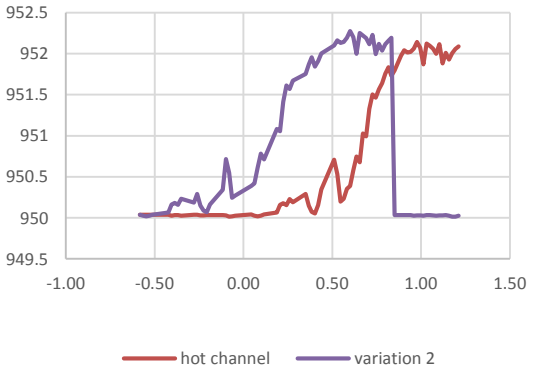

Figure 27 Temperature profile at probe line 1 for hot channel and variation 2 cases

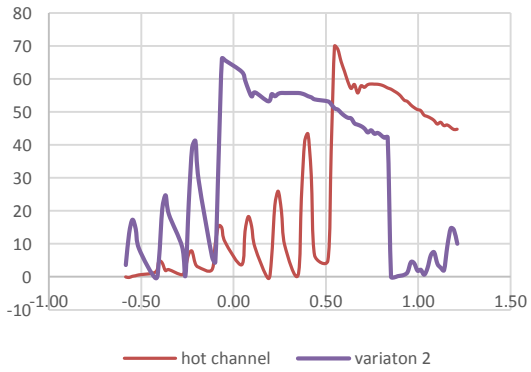

Figure 28 Velocity [i] profile at probe line 1 for hot channel and variation 2 cases

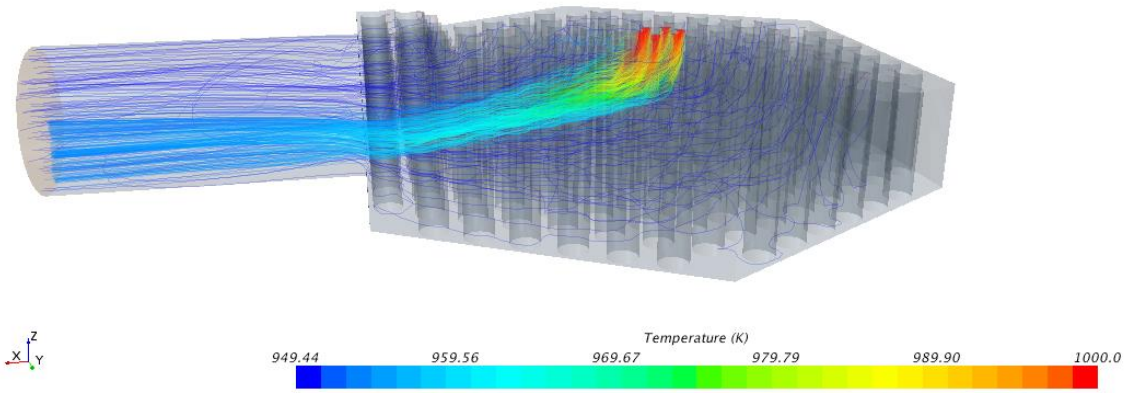

Figure 29 Streamlines seeded from hot channel section

The hot channel case enabled visualization of coolant flow paths, which is shown in Figure 29. The initial z-component of velocity from the inlet jet dominates the flow towards the LP floor. The jet reaches about half height of the plenum before momentum is entrained by flow from behind and redirected towards the outlet. Additionally, it is visible that heat exchange mechanisms reduced the temperature of hot section jets. However, visualized streamlines suggest low level of dispersion of the initial jet.

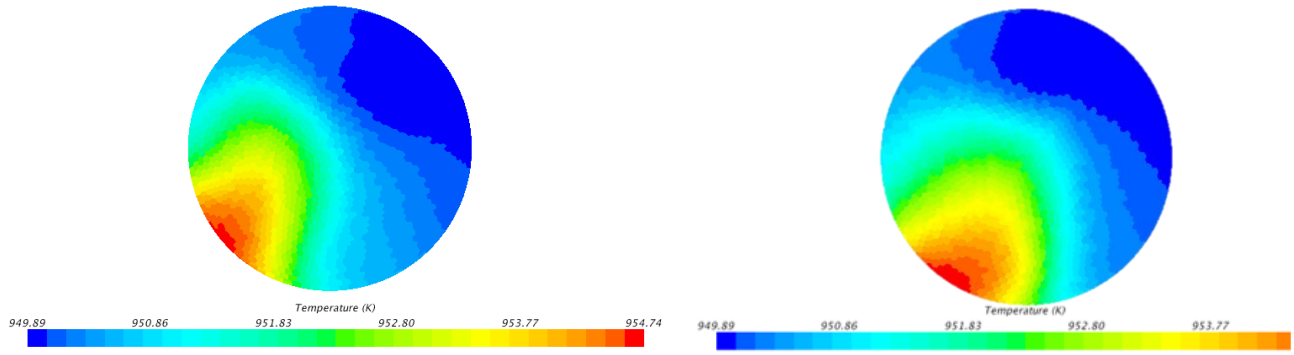

Figure 30 Temperature profile at LP outlet for hot channel and variation 2 cases

It can be seen in Figure 30 that the temperature profile for the hot channel and variation-2 cases are similar, despite the difference in applied mass flow rate. It can be assumed that mass flow rate change does not influence mixing capability in the LP.

The development of the mixing in the outlet duct can be seen in Figure 31. The left column presents the velocity magnitude extracted from four plane sections along the outlet duct. The

sections were made in the following manner: the first section is located a few millimeters down from the entrance to the outlet duct. Following three sections are placed within spacing of 20 cm. The last section is located nearby the outlet boundary. At the top section there are developed three very high velocity (up to 74 m/s) planar jets. These jets are the result of the limited flow area at the duct inlet due to direct vicinity of four support posts. The presence of the posts results with creation of stagnation zones at both sides of the high velocity jets. These areas are furtherly developed into vortexes and stagnation area, as can be seen in following images of this figure. The velocity field at the outlet is not uniform, and varies from 0 to 50 m/s. The flow is not fully developed what results in reversed flow on the outlet boundary.

The right column of Figure 31 represents temperature contours at the same locations. The gas entering the duct inlet varies between 950 K up to 960 K. The temperature field is non-uniform and the areas of higher temperature are not regular. Along the duct highly turbulent flow promotes thermal mixing however at the last cross-section temperature gradient of 5 K is still visible.

4.1.1.5 Conclusions

A numerical model of the LP was built in order to simulate and investigate gas mixing efficiency and assess probability of "hot spotting" on the LP structure. Application of one hot section with 50 K temperature rise to the model caused a LP floor temperature increase of over 20 K. A hot spot is present at the front part of the LP model, however still in area of LP. The outlet temperature gradient is approaching 5 K, with the hottest gas being in direct contact with outlet duct structure.

The selected mesh sized resulted with solutions which are somewhat grid dependent. Thus further mesh advancement is advised. Additionally applied k-ε turbulence model, as 2-equation model, doesn't reflect advanced flow features as swirl flow and recirculation zones. It is advised to investigate application of more advanced models like RSM-RANS, LES.

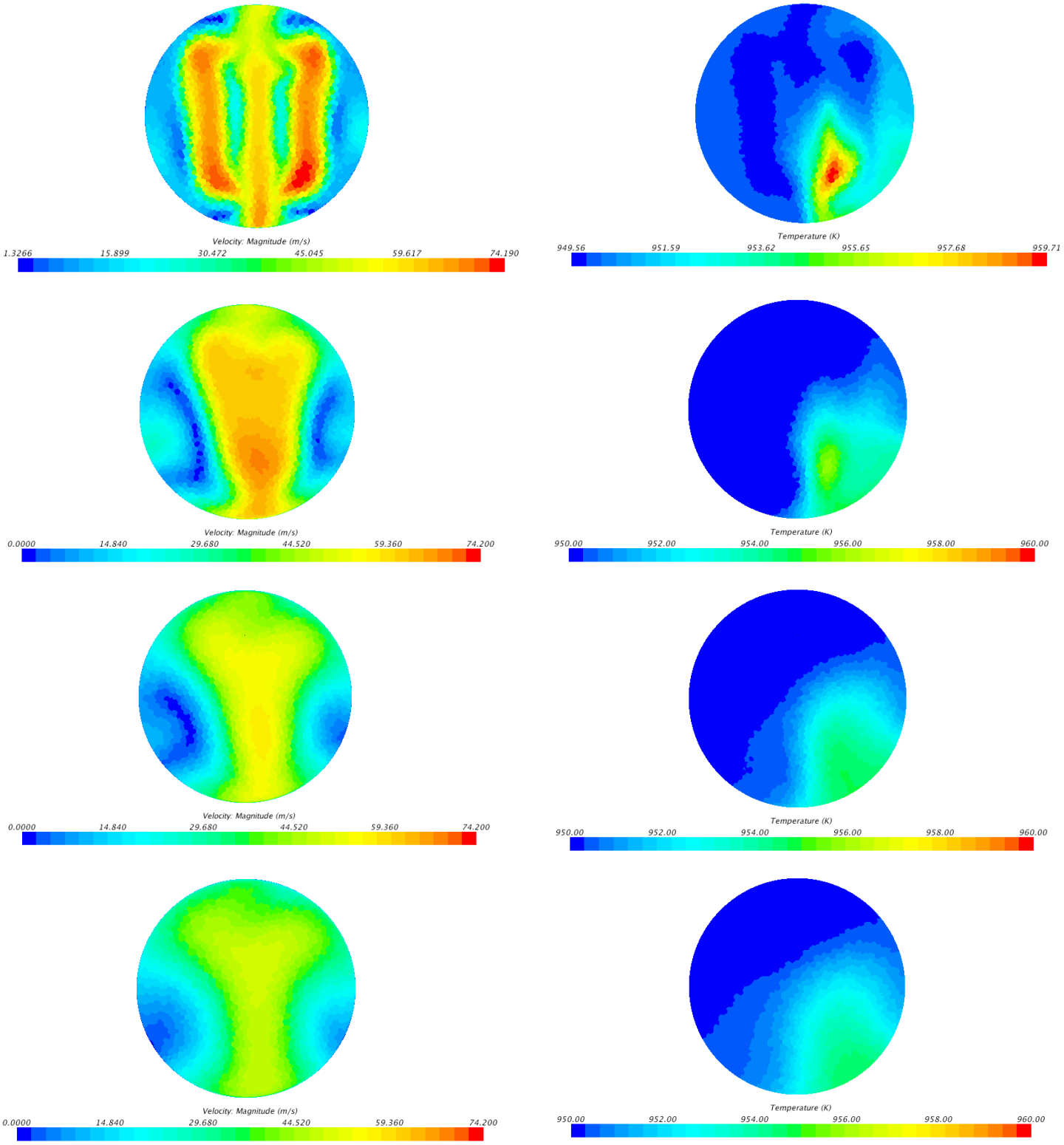

Figure 31 Left: Velocity magnitude contour at planar sections of the outlet duct, the planes located at respectively x=0.62, x=0.82, x=1.02 and x=1.2 m. Right: Temperature profile at four plane sections as in left column

4.1.2 Sensitivity study

CFD simulations enable understanding of the fluid dynamics in cases of complicated flows where analytical solutions would be very hard if not impossible to obtain. However, the solution of such problem must be considered with caution as improper use of CFD tools can lead to unphysical and unrealistic solution. The obtained solution needs to be investigated in terms of grid dependence (space and time), models sensitivity (turbulence modeling) and scheme of the solution.

4.1.2.1 Mesh independence study – Richardson Extrapolation

The rule of thumb for the computational mesh size is as follows: mesh should be fine enough so decreasing the size of the mesh cell does not influence the final solution. In practical applications this threshold may be hard to reach and some residual difference remains after comparing the solutions. In this case engineering judgement must be used to evaluate how precise a solution is required for this particular application.

The mesh sensitivity study has been performed for case P1.1a. To asses mesh adequacy Richardson's Extrapolation has been used with "halving" size of the cell size (Roache 1997). This extrapolation uses two solutions performed on a full size and a half size grid to calculate exact solution therefore value independent from the mesh size. The coarse mesh cell size was set to 0.012 m whereas the fine mesh cell size was 0.006 m. The solutions from coarse and fine mesh were combined using formula:

$$f(exact) \cong \frac{4}{3} f_1 - \frac{1}{3} f_2$$

Where f_1 and f_2 stand respectively for the solution for fine and coarse grids. The function selected for RE is velocity magnitude at probe line 1 (which goes from the back of the LP to the center of the outlet boundary). The velocity magnitude for both meshes and consequent exact solutions are plotted in Figure 32. Additionally, to exhibit the trend of velocity magnitude shift, while refining the mesh, the medium mesh results were included as well. The agreement between meshes is precise in the LP and neither the coarse nor the fine solution can be distinguished from

the exact solution. Only some slight discrepancy can be noted in the front area of the outlet duct where the velocity magnitude reaches maximum.

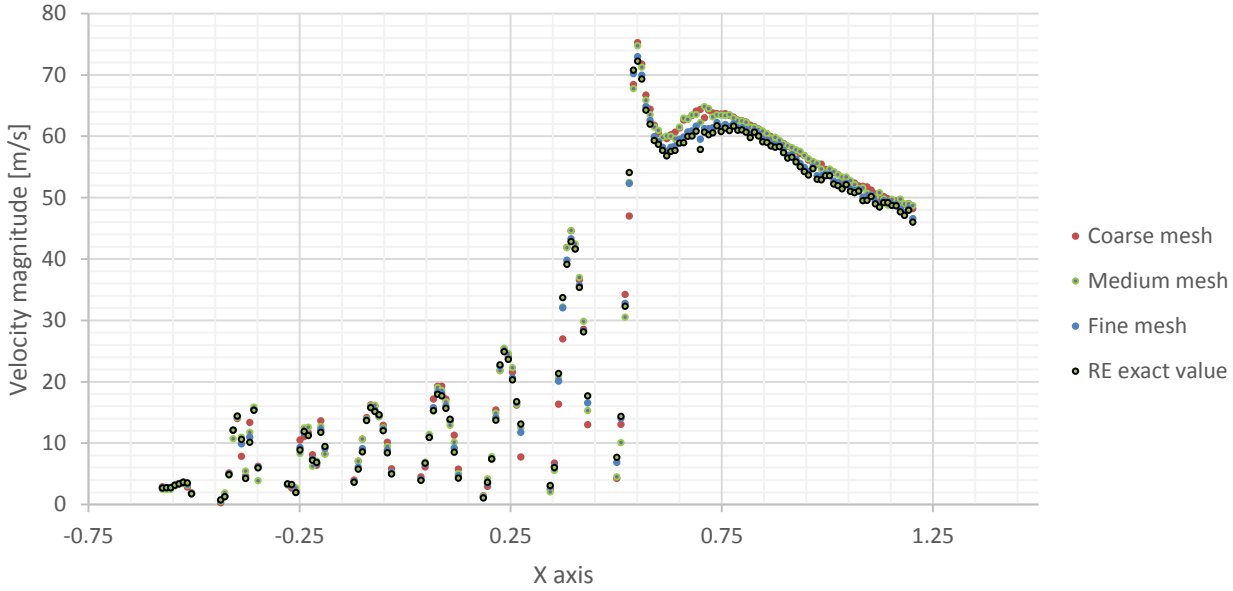

Figure 32 Solution for coarse mesh, fine mesh and resulting exact solution

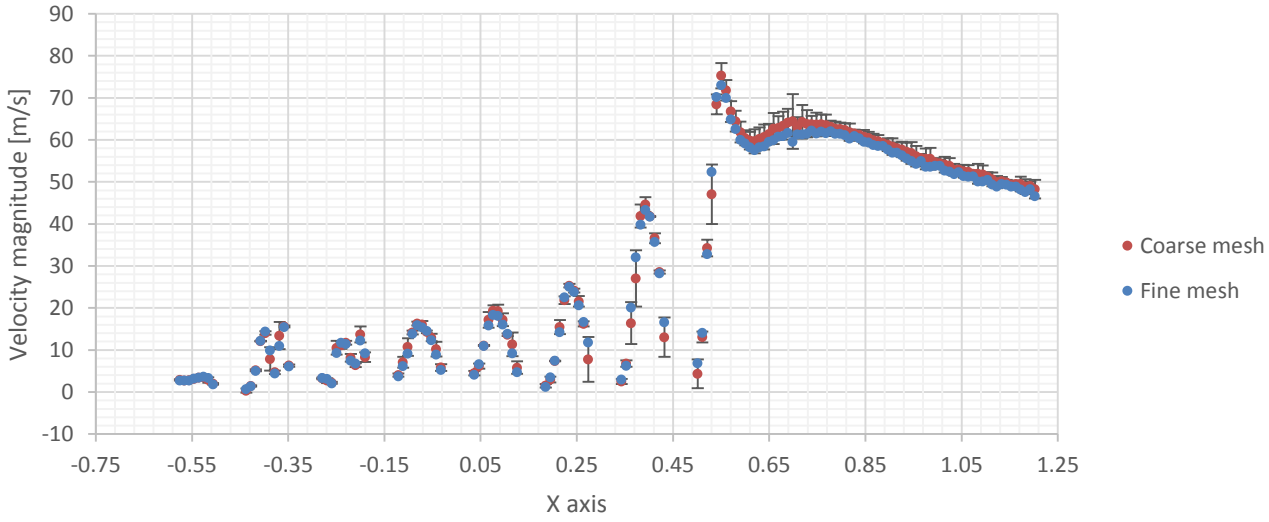

Figure 33 Error calculated for solution on coarse mesh according to (Roache 1997)

Figure 33 exhibits the same solution but with marked error bars for the coarse mesh solution. According to Roache (1997) the error for coarse mesh solution in this case can be described with the following formula:

$$E_{coarse} = \frac{r^p \varepsilon}{1 - r^p}$$

Where

r – refinement factor between the coarse and fine mesh ,
p – official order of accuracy of the algorithm,
ε – difference between coarse and fine-grid solution.

The error for the fine mesh solution was also calculated using the formula below. However, the obtained values were too small to exhibit them in the form of a plot. The maximum error value for the fine mesh solution was 1.77 m/s which cannot be effectively shown in this range of velocities (from 0 to 80 m/s).

$$E_{fine} = \frac{\varepsilon}{1 - r^p}$$

4.1.2.2 Turbulence model sensitivity

The other important aspect of the CFD solution verification is conducting a turbulence model sensitivity study. All of the cases though this research were calculated using k-epsilon realizable turbulence model, with various wall functions. To ensure that solution is not significantly dependent on the turbulence model the case P1.1a was recalculated using three additional models. The main turbulence model used for this study, realizable k-epsilon, is a widely used model especially for industrial applications with multiple recirculation zones. This solution has been compared with two two-equation models: another k-epsilon model v2f (good for cases with impingement) and k-omega SST model (used when near wall solution is of high importance) as well as with a seven-equation RSM (good performance for strongly swirling flows). The results for the mentioned turbulence models were summarized in Figure 34. It can be noted that all turbulence models result in the comparable velocity magnitude. In fact the realizable k-epsilon model is characterized by slight deviation from other models. However, all models are in general agreement within LP volume. The solution in the outlet duct introduces slight variation between models with standard deviation of 4.8 m/s.

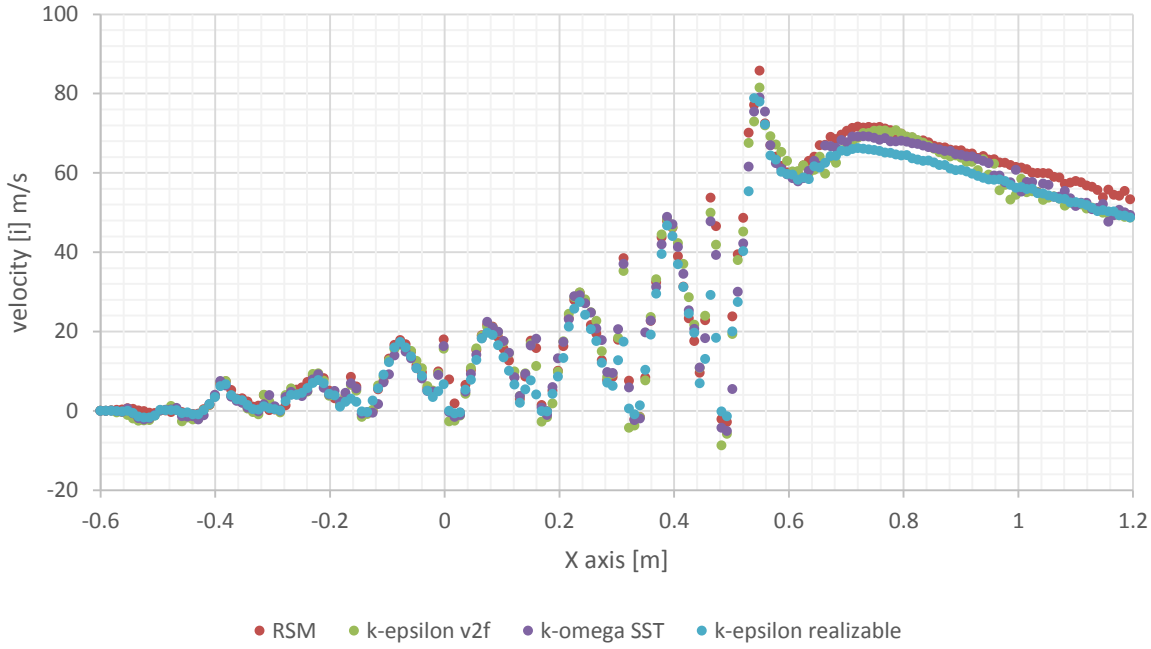

Figure 34 Comparison of solution for velocity [i] at probe line across LP using various turbulence models

4.1.3 Scalar mixing as a function of temperature

The hot gas mixing in the LP shall be considered as a function of multiple factors. In section 4.1.1 it was assumed that the hot channel's position and temperature are known and constant. However, none of this information is known at this time. The information used in this study has been drawn from analysis with simplified and averaged approaches and boundary conditions which are also approximate. Thus the mixing process should be investigated not by using a single set of boundary conditions but a span of them. In particular three variables seem the most influential in terms of mixing: temperature, position, number and distribution of the hot channels.

4.1.3.1 Temperature of the hot channel

The main function of the LP is to merge and mix all of the coolant jets coming out of the reactor core (and support the core structure). Gas should be thoroughly mixed before being transported to the energy conversion circuit (gas turbine, IHX or steam generator). The temperature of the gas is the key factor in mixing considerations. Thus influence of the temperature of the hot channel to final mix quality will be investigated and reported.

4.1.3.2 Simulation setup

To investigate foregoing matter, a set of five cases has been calculated. Geometry, mesh and solver setup remained unchanged and can be reviewed in section 4.1.1.2. The only varying boundary condition is temperature of the hot channel. Thus, five additional cases were calculated with hot channel temperature rise (the difference between hot channel and regular channel) as listed in Table 9.

Table 9 Temperature at the inlet boundary of the "hot section"

Case name	Temperature gradient at the inlets
P1.1a	"hot channel" / ΔT=50 K
P1.1b	ΔT=100 K
P1.1c	ΔT=150 K
P1.1d	ΔT=200 K
P1.1e	ΔT=250 K
P1.1f	ΔT=300 K

4.1.3.3 Results

Mixing quality is not an unequivocal term, there are many ways to display it, although the simplest way is presentation of temperature range in the gas at the LP outlet and at the hot duct structure. In Figure 35 the temperature rise at the outlet boundary of the model has been presented.

As shown in Figure 35 and Figure 36 the value of maximum temperature at the outlet of the LP model is a non-linear function. The increase in the hot channel temperature does not promote proportional increase in the maximum outlet temperature. Figure 35 exhibits that the share of the temperature rise (against hot channel temperature rise) decreases as hot channel temperature increases. For instance, the hot channel temperature rise of 50 degrees promotes maximum outlet temperature rise of 5 degrees (~11%), whereas the 250 degree increase of hot channel temperature results only with 18.8 degrees (~7.5%) maximum outlet temperature rise. The case of the highest temperature difference between hot and normal channel – 300 K results with a 21.4 degree rise (~7.12%). The clear decreasing tendency can be seen for the percentage of the

temperature gradient at the outlet with increasing temperature gradient at the model inlet, which suggests that if high temperature channel increases another 100 or 200 degrees the change in maximum outlet temperature should not be significant (if current flow field will be preserved).

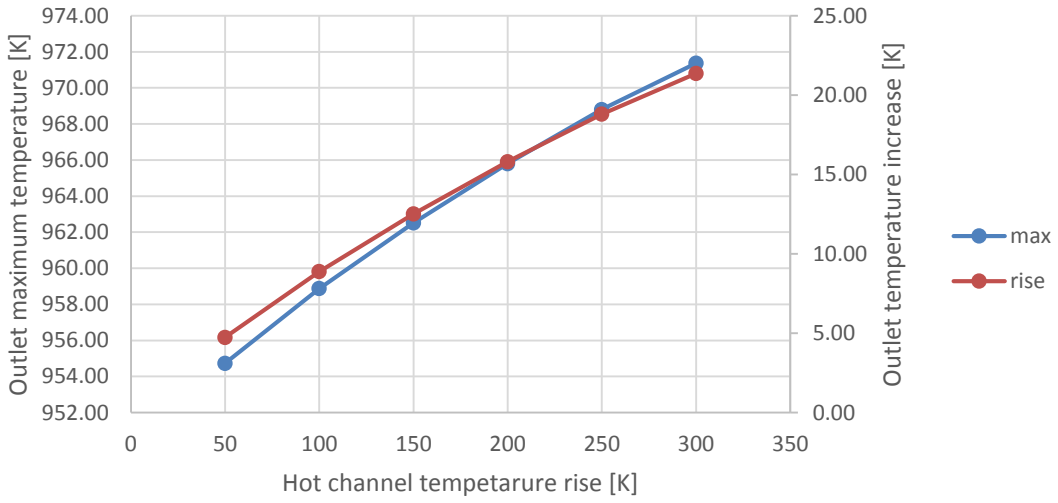

Figure 35 Outlet temperature increase vs temperature of the hot channel

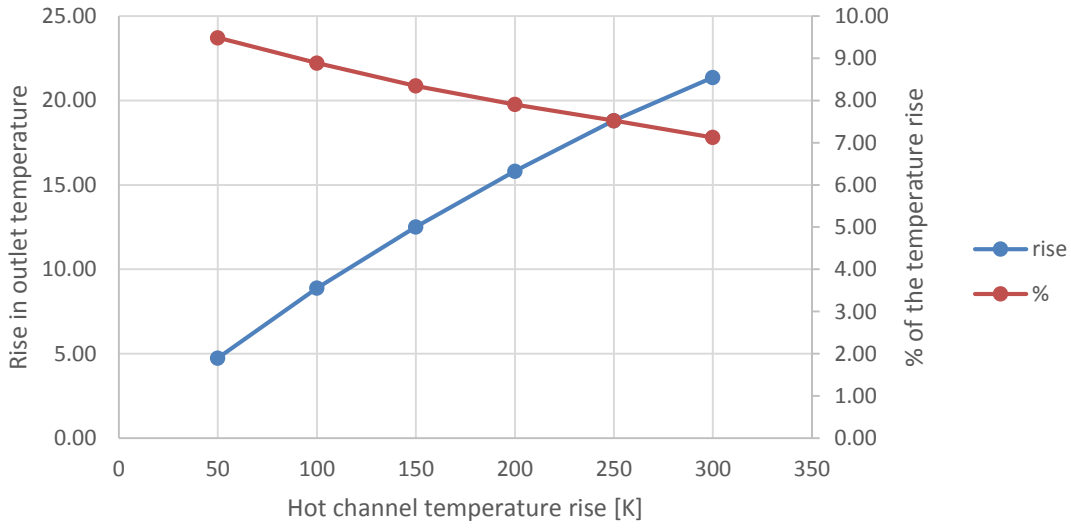

Figure 36 Rise in maximum outlet temperature vs hot channel temperature

4.1.3.4 Conclusions

The applied boundary condition set resulted in a curve of temperature change at the outlet boundary of the model as a function of the temperature. The hot section was modeled with an overall temperature rise from 50 up to 300 K. This rise resulted with maximum temperature rise from 5 to 21 K at the outlet boundary. From Figure 36 it can be concluded that a further increase of the "hot section" inlet temperature will not have a major impact on the maximum temperature at the outlet boundary. However, it should be noted that the hot section in this study consisted of only 2.6 % of inlet channels (6 out of 234). Considering this fact the impact of this limited hot section on the maximum outlet temperature is major.

This conclusion suggests that it can be beneficial to perform another study investigating the influence of the size and location of the hot section on final maximum temperature at the model outlet. Also multiple hot section investigations can result with interesting conclusions.

4.1.4 Approximate temperature profile

Two previous simulations were carried out using a simplified and non-realistic temperature profile to exhibit the influence of the hot channel effect on overall flow characteristics. This section is dedicated to a more accurate case of the temperature profile in the HTTF core; thus, this section presents a set of the boundary conditions that are the closest to the actual experimental facility.

4.1.4.1 Simulation setup

As for previous simulations the solid model was preserved, and the description of it can be found in section 4.1.1.2. The computational mesh and boundary conditions for these simulations were modified to accommodate new flow conditions. The final mesh for steady state calculations consisted of 5.5 million cells. The bulk of the model was meshed with polyhedral mesh cells, whereas the near wall boundaries were lined with prismatic cells to ensure accurate resolution of the boundary layer.

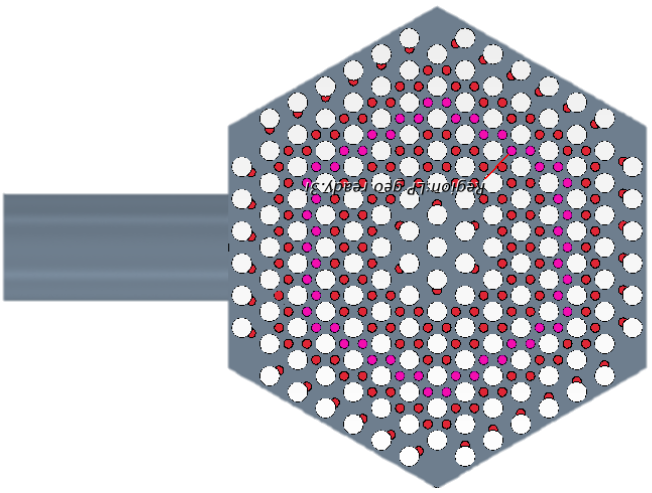

Figure 37 Inlet zone 3 – pink highlighted areas

The boundary condition arrangement differs from the previous cases. The outlet boundary and all of the model walls are setup as for previous cases. The model inlets are divided into six zones, two bypass zones and four core flow zones. All of the inlets have assigned the same velocity but the temperatures are diversified. Each of the inlet zones has a temperature assigned according to the profile described in subsequent subsections. The zones are formed as concentric circles from the center of the LP to the most outer row of inlets. The example of Zone 3 is shown in Figure 37.

4.1.4.1.1 **Case P1.2.1**

This case was based on the temperature profile calculations performed by the OSU HTTF research team. The temperature profile was calculated using a solid state CFD simulation of the core structure aimed at reproducing a normalized temperature profile in the VHTR core. After normalization of this profile it was adjusted to fit the MHTGR and the HTTF temperature range. The inlet boundaries have the following temperatures (from the inner circle out):

- Inner bypass – 1270 K
- Zone 1 – 1270 K
- Zone 2 – 1270 K
- Zone 3 – 1095 K
- Zone 4 – 900 K
- Outer bypass – 754 K

4.1.4.1.2 **Case P1.2.2**

This case was based on calculations performed by N. Anderson (2006) who performed a simplified simulation of the coolant flow in the VHTR core using the RELAP5-3D code. The reactor core was divided into eleven rings concentrically located. The core consists of nine rings in the fuel region and two rings in the reflector region. The set of results from this study included not only temperature profiles but also the mass flow for every ring. These data have been normalized and adjusted for normal operation conditions of the HTTF and approximated to use in six ring inlet zones instead of eleven. The final set of the BC's can be seen in Table 10. To match the mass flow in this case the pressure was increased to 0.869 MPa in accordance with the BC's in Anderson (2006).

Table 10 Set of boundary conditions for Case P1.2.2

Zone	Temperature [K]	Mass flow [m/s]
Inner bypass	915.4	0.0075
Zone 1	1128.3	0.0838
Zone 2	1046.9	0.1640
Zone 3	924.7	0.3754
Zone 4	938.3	0.2706
Outer bypass	769.9	0.0987

4.1.4.2 Results – Case P1.2.1

The temperature and velocity fields were calculated. Due to the selection of the temperature profile approximation the value of mass averaged temperature at the outlet was 70 degrees higher (1028 K) than the average temperature of operation of the HTTF (960 K). However after normalization the result of this simulation still represents the correct characteristics.

The temperature outline of this simulation can be seen in Figure 38. At the inner surface of the LP, only the central part of the geometry contains gas with a very high temperature whereas all peripheral areas are filled with gas at a much lower temperature. The range of the temperatures varies from 754 K up to 1270 K. In the front part (closer to the outlet) of the lower plenum roof,

the C-shaped plume of gas at the highest temperature remains unmixed. In contrast to that, the gas at peripheral areas almost never reaches the lowest temperature and some low level of thermal mixing occurs.

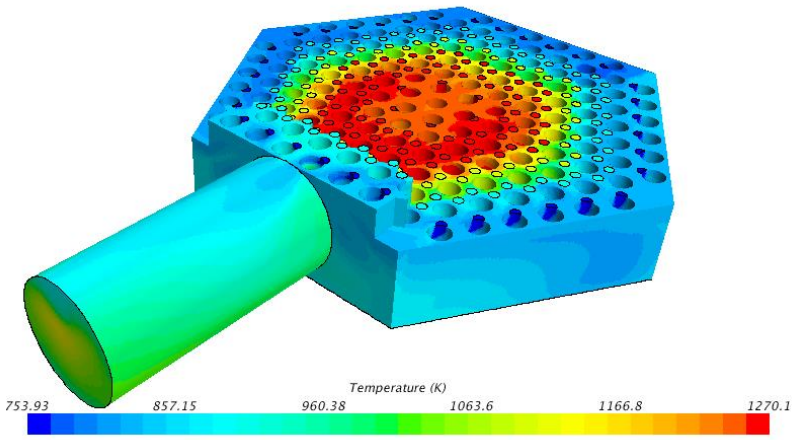

Figure 38 Temperature contours at the inner surface of the model

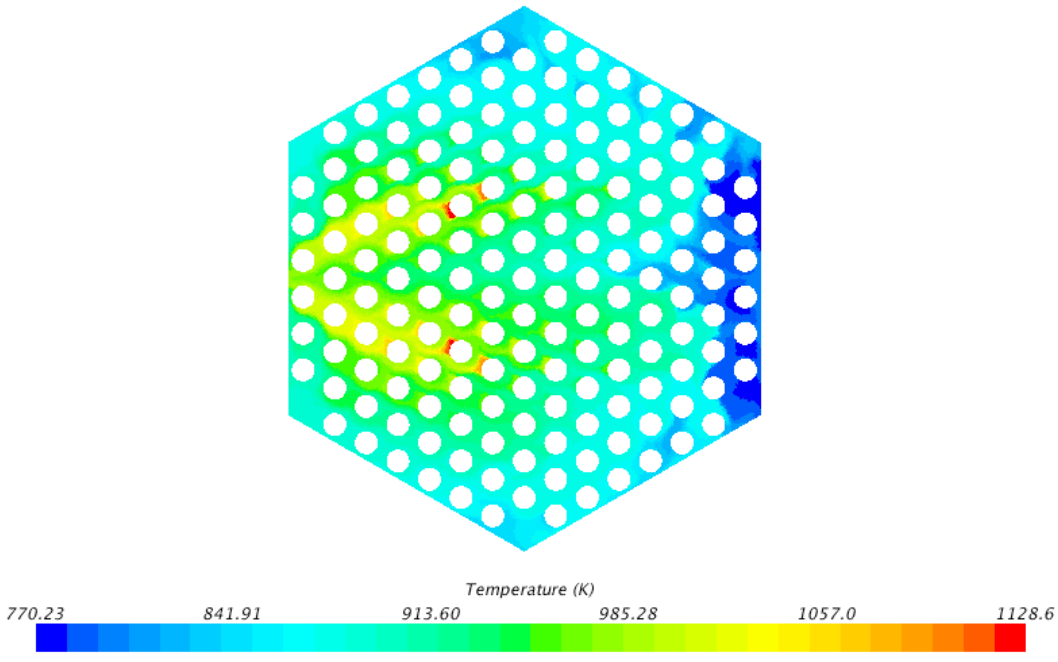

Figure 39 Temperature contour at the lower plenum floor

In Figure 39 it can be also noticed that in the rear part of the lower plenum floor there is a section of almost unmixed gas at 720 K. he other areas of the LP floor is within average gas temperature except four hot spots. In direct vicinity of the support posts facing the outlet, four hot spots are visible at maximum temperature of 1128 K. Two longitudinal areas are formed from the hot spot are toward the LP exit.

The temperature field inside of the gas volume can be observed in Figure 41. The gas volume section is taken at the mid-height of the outlet duct, thus in the upper LP. The temperature profile is similar to the one visible from the surface of the model in Figure 38. The center part of the plenum is filled with high temperature gas whereas the near-wall areas contain gas at the lowest temperatures. It can be seen that gas enters the outlet duct highly stratified with temperature range 836 K – 1228 K.

Four vertical sections have been made to exhibit flow development in the outlet duct. Figure 40 shows the temperature contours at these four sections. The first section is located at the entrance to the duct. High variation in temperatures can be noticed, in the central upper part the temperature varies from 836 K up to 1228 K. The next section, placed 20 cm downstream, exhibits high temperature core surrounded by low temperature gas at the top and moderate temperatures around the surface of the outlet duct. The two remaining sections, display the decrease in the temperature variation in the duct. However, the last section located almost ate the outlet still exhibit temperature gradient of 250 K.

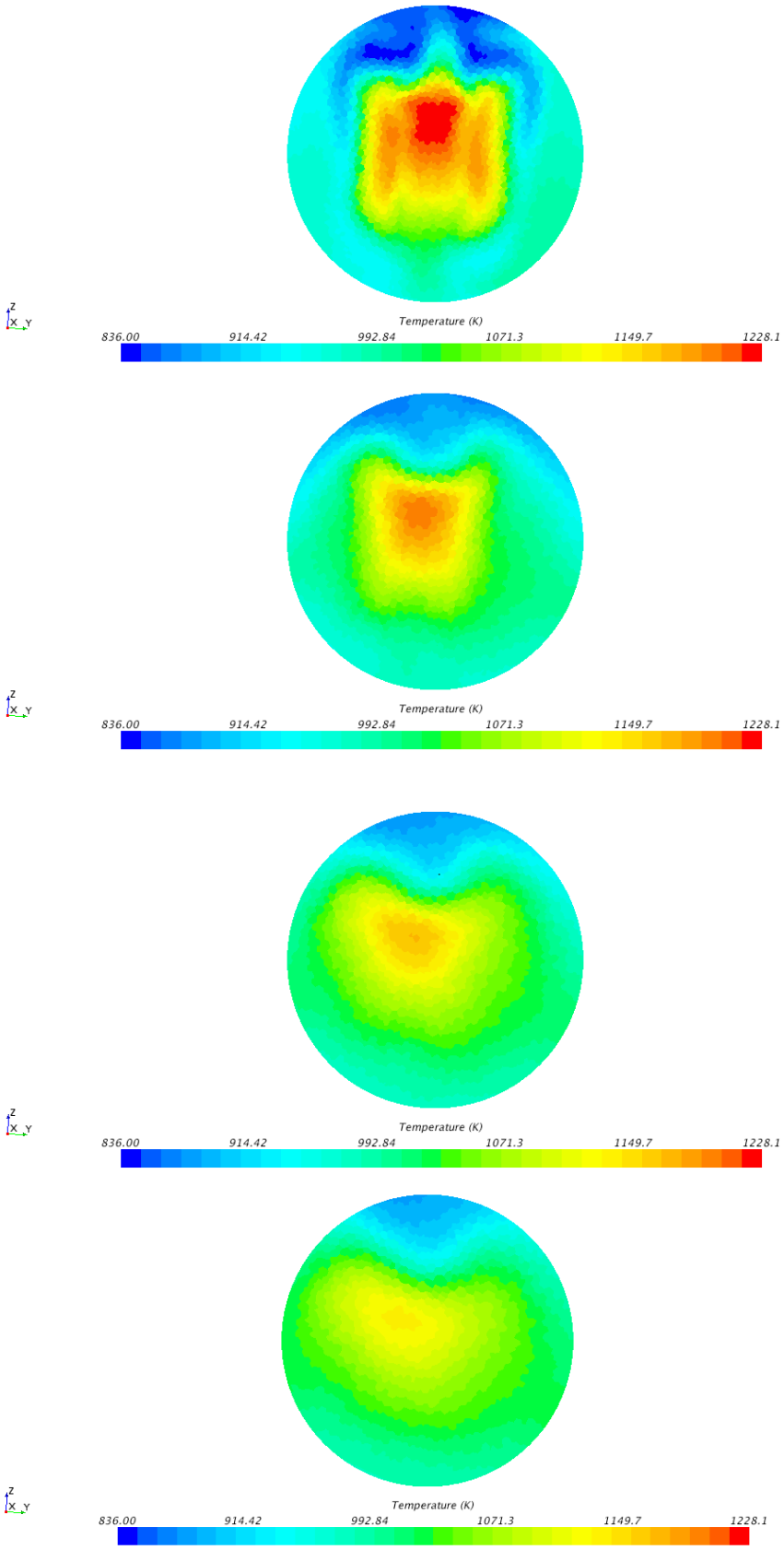

Figure 40 Temperature contour at four planar sections of the outlet duct, from the beginning of the duct, every 20 cm

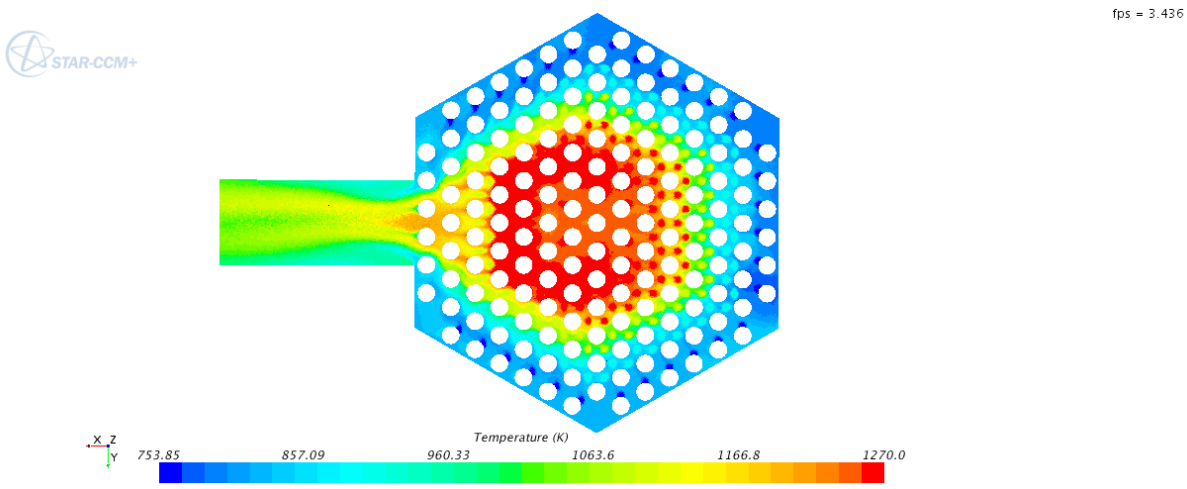

Figure 41 Temperature contour at plane section carried through mid-height of the outlet duct

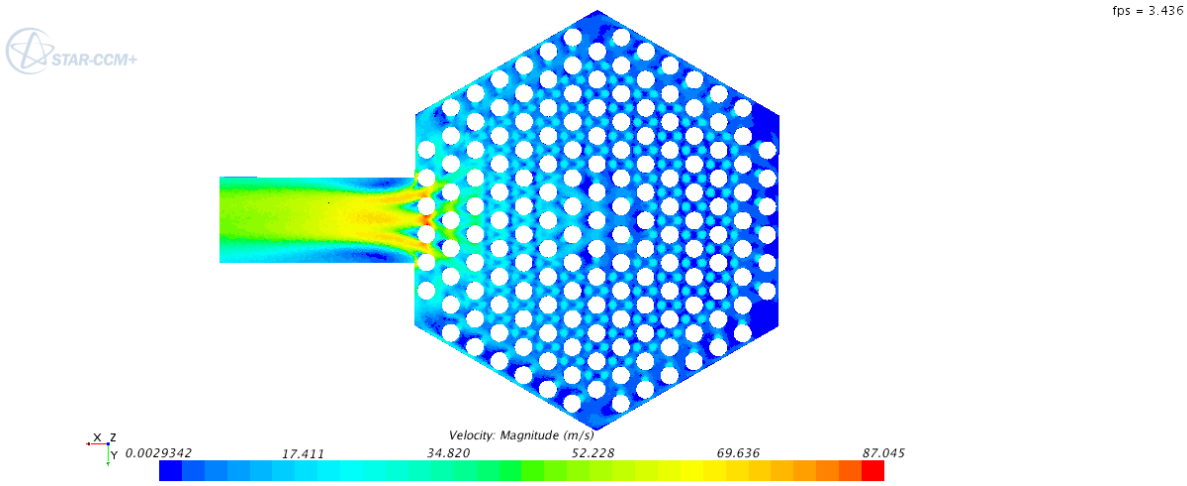

Figure 42 Velocity magnitude contour at plane section carried through mid-height of the outlet duct

Figure 42 exhibits velocity magnitude contour in the same plane as Figure 41. The LP can be characterized as low to moderate velocity flow, with large stagnation area in the rear part of the LP. Closer to the exit, a triangle-shaped area of elevated velocity is formed. This is due to a partially blocked entrance to the outlet duct by the support structure of the core. At the entrance to the outlet duct velocity magnitude is the highest as gas reaches over 80 m/s, forming three streams between the support posts. This high velocity in the center of the plenum causes formation of stagnation zones at the side of the duct, however, only in front area of the duct.

Another cross-section of the model shows the vertical cut through the symmetry plane. Figure 43 shows the temperature profile in the ZX plane. Temperature stratification is easily noticeable, the higher temperature gas flows in the top part of the LP. The low temperature gas from peripheral areas is transported in the vicinity of the LP floor. Figure 44 shows the same section but with velocity contours. The velocity field in the LP ranges from 0 up to 30 m/s depending on the location. The highest velocity is reached behind the support posts at the entrance to the outlet duct. Due to high velocity in the area of the posts the gas is highly turbulent, that is where the turbulent kinetic energy is the largest.

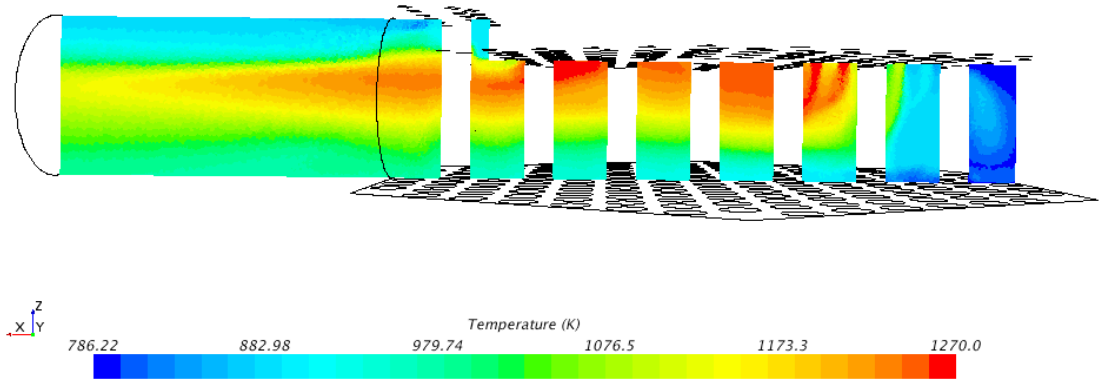

Figure 43 Temperature contour at ZX plane section

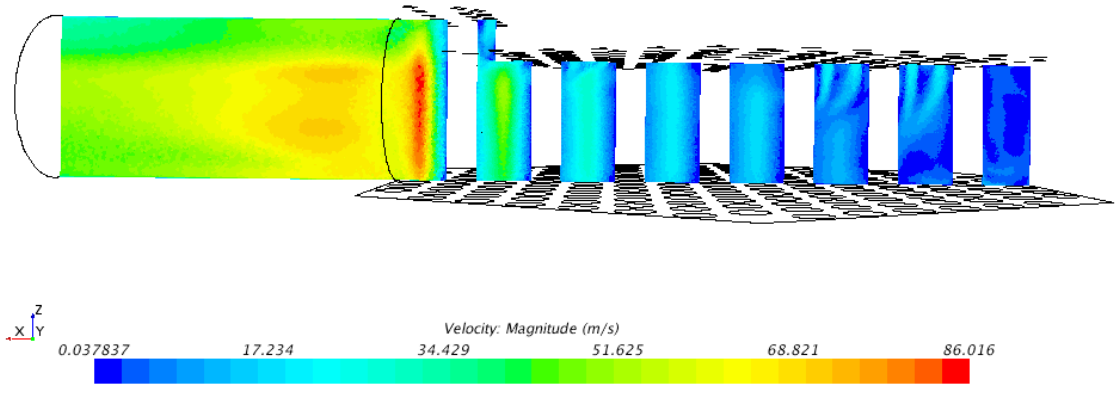

Figure 44 Velocity magnitude contour at ZX plane section

The maximum, minimum and average temperature values at the most significant components have been listed in Figure 45. The temperature gradient at the LP floor, outlet duct and outlet boundary are consequently 360 K, 250 K and 190 K. The value of the temperature gradient thus is too high to be safe and optimal for the use in gas turbine or IHX (if placed indirect vicinity to the outlet boundary).

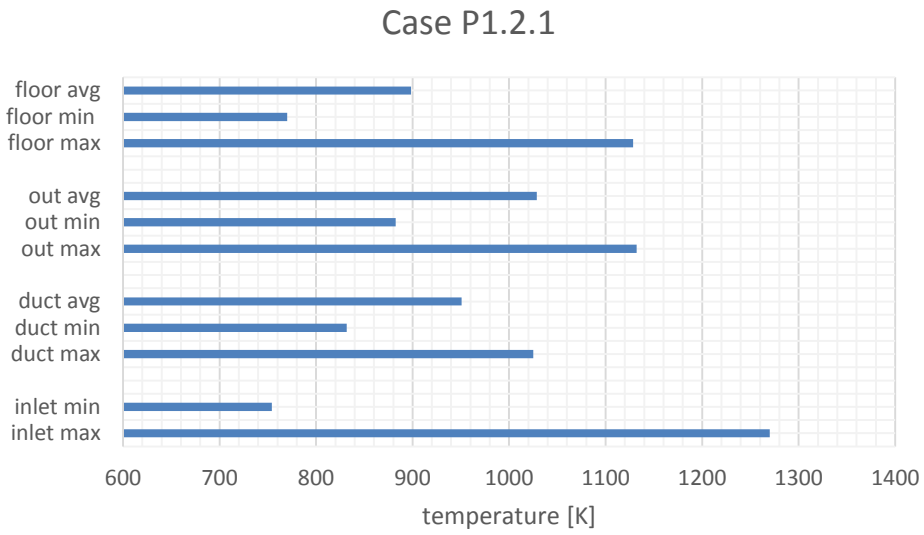

Figure 45 Summary of the temperature maximum, minimum and average values in LP for Case P1.2.1

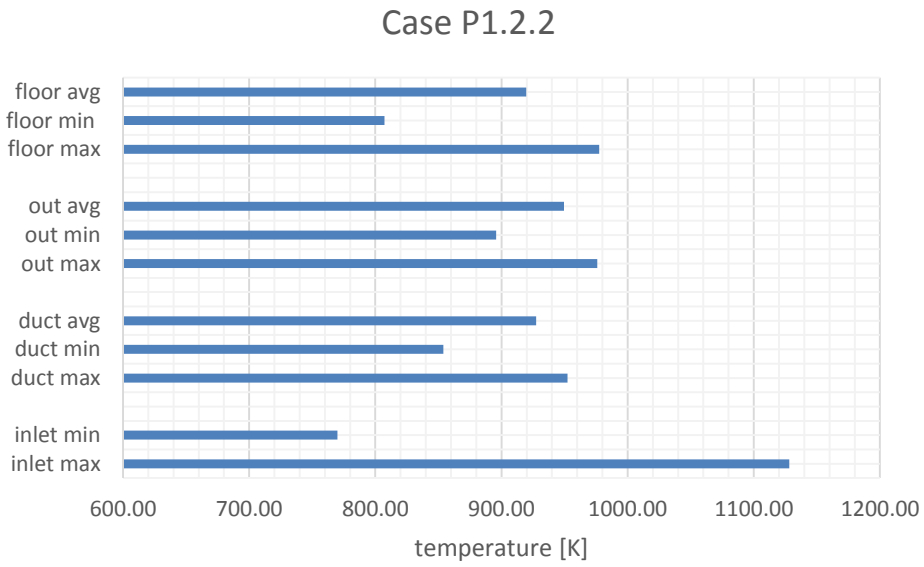

Figure 46 Summary of the temperature maximum, minimum and average values in LP for Case P1.2.2

4.1.4.3 Results – Case P1.2.2

The temperature and velocities field were calculated. Due to selection of the temperature profile approximation the value of mass averaged temperature at the outlet was 10 degrees lower (950 K) than average temperature of operation of the HTTF (960 K). The maximum, minimum and average temperature values at the most significant components have been listed in Figure 46. The temperature gradient at the LP floor, outlet duct and outlet boundary are consequently 170 K, 100 K and 80 K.

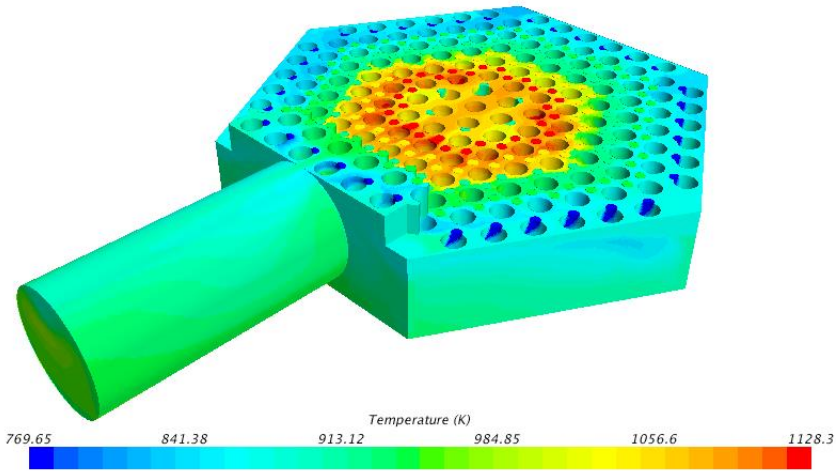

Figure 47 Temperature contours at the inner surface of the model

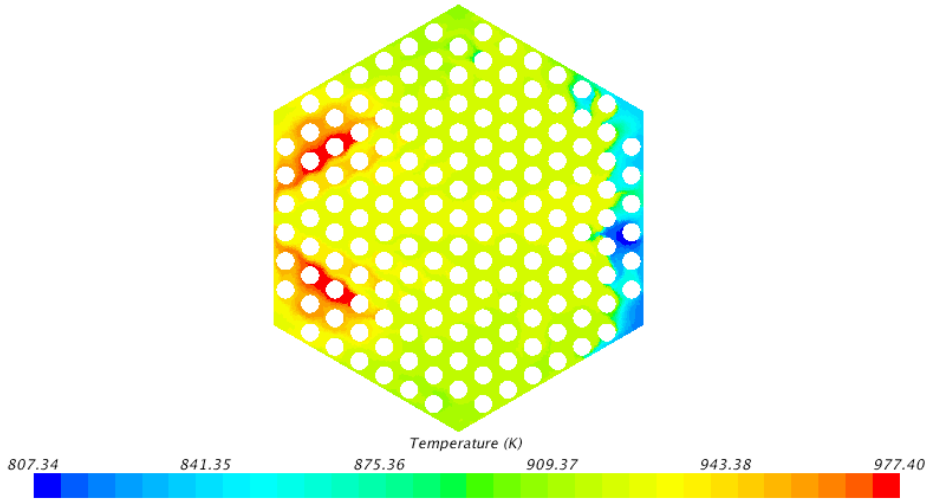

Figure 48 Temperature contour at LP floor

The temperature outline of this simulation can be seen in Figure 47. At the inner surface of the LP, only the central part of the geometry contains gas with very high temperature whereas all peripheral areas are filled with gas at much lower temperatures. The range of the temperatures varies from 770 K up to 1128 K. As in the previous case in the front part (closer to the outlet) of the lower plenum roof, a C-shaped plume of gas at the highest temperature remains unmixed. In contrast to that, gas at the peripheral areas almost never reaches the lowest temperature and some low level of thermal mixing occurs.

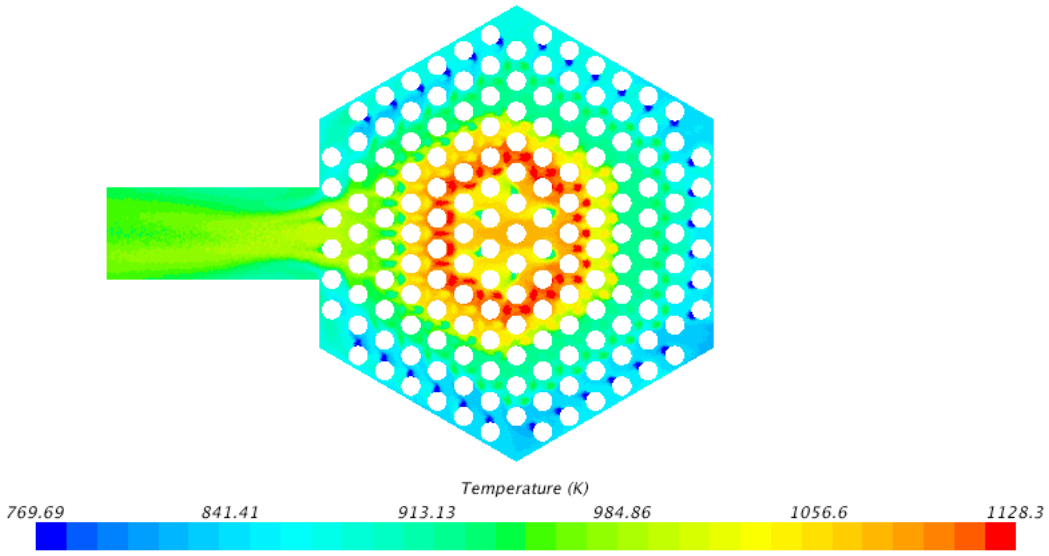

Figure 49 Temperature contour at plane section carried through mid-height of the outlet duct

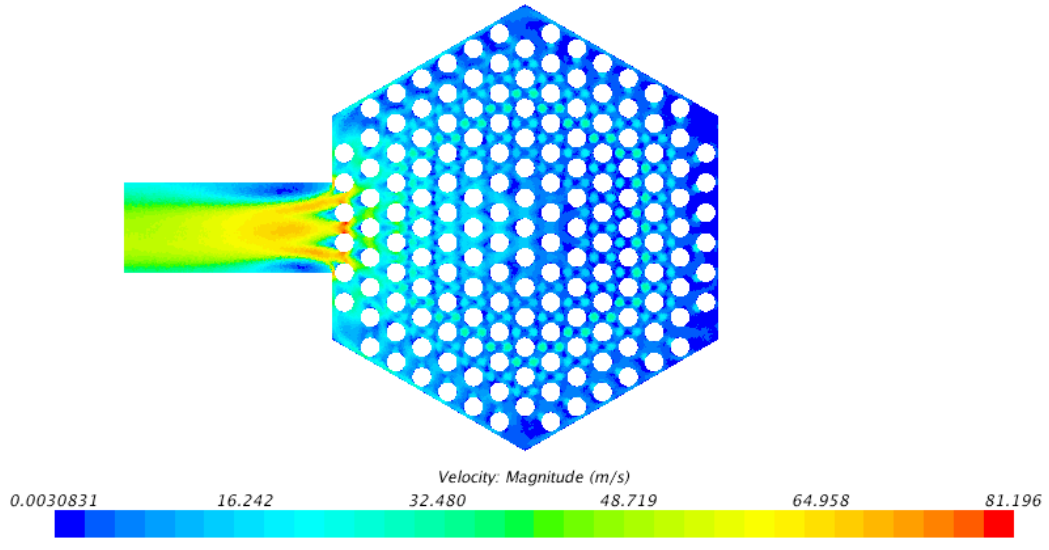

Figure 50 Velocity magnitude contour at plane section carried through mid-height of the outlet duct

Similarly as for previous case in Figure 48 it can be also noticed that in the rear part of the lower plenum floor there is a section of gas at low temperature. However comparing with *the Case P1.2.1* this zone seem smaller. The other areas of the LP floor are within average gas temperature except for two hot spots. In direct vicinity of the support posts facing the outlet, two hot spots are visible at maximum temperature of 977 K, which is much lower than for Case P1.2.1. Two longitudinal areas are formed from the hot spot are toward the LP exit.

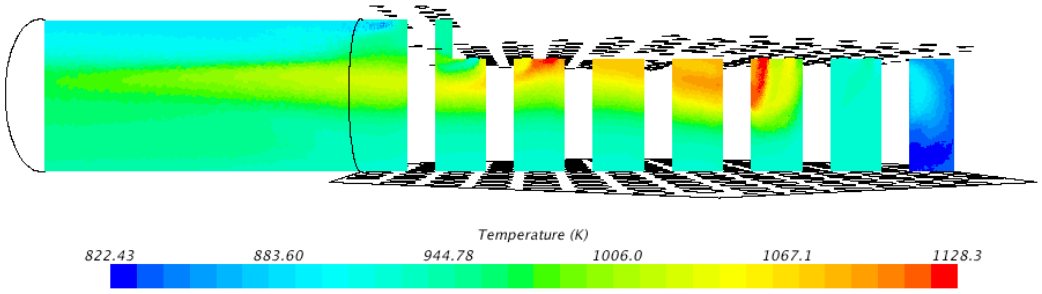

Figure 51 Temperature contour at ZX plane section

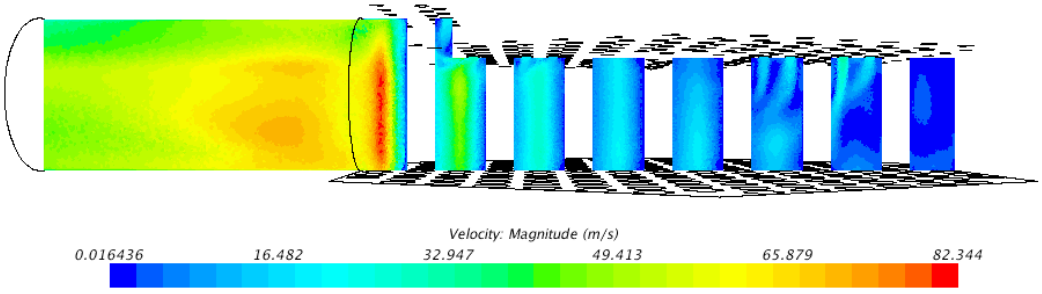

Figure 52 Velocity magnitude contour at ZX plane section

The temperature field inside of the gas volume can be observed in Figure 49. The gas volume section is taken at the mid-height of the outlet duct, thus it is not far from LP roof and inlets rather than in the lower part of the plenum. The temperature profile is similar to the one visible from the surface of the model in Figure 47. The center part of the plenum is filled with high temperature gas whereas the near-wall areas contain gas at the lowest temperatures. The C-shaped hot zone is no longer visible. It can be seen that gas enters the outlet duct highly stratified with temperature range 862 – 1024 K. The lower temperature bound is the same as for previous case but the upper bound temperature is over 200 degrees lower.

Figure 50 exhibits the velocity magnitude contour in the same plane as Figure 49. The LP can be characterized as low to moderate velocity flow, with large stagnation area in the rear part of the LP. Closer to the exit, triangle-shaped area of elevated velocity is formed. This is due to partially blocked entrance to outlet duct by the support structure of the core. At the entrance to the outlet duct velocity magnitude is the highest as gas reaches over 80 m/s, forming three streams between the support posts. This high velocity in the center of the plenum causes formation of stagnation zones at the side of the duct, however, only in front area of the duct. The stagnation/ recirculation zones at each side of the duct are non-symmetrical which suggest non-stationary behavior.

Another cross-section of the model shows the vertical cut through symmetry plane. Figure 51 shows the temperature profile in the ZX plane. Temperature stratification is easily noticeable, the higher temperature gas (1000 – 1100 K) flows in the top part of the LP. The low temperature gas (820 – 1000 K) from peripheral areas is transported in the vicinity of the LP floor. Figure 51 shows the same section colored with velocity contours. The velocity field in the LP ranges from 0 up to 30 m/s depending on the location. The highest velocity is reached behind the support posts at the entrance to the outlet duct. Due to high velocity in the area of the posts the gas is highly turbulent, that is where the turbulent kinetic energy is the largest.

Similarly as in the previous case four vertical sections have been made to exhibit flow development in the outlet duct. Figure 53 shows the temperature contours at this four sections. First section is located at the entrance to the duct. High variation in temperatures can be noticed, in the central upper part the temperature varies from 862 K up to 1024 K. Next section, placed 20 cm downstream, exhibits high temperature core surrounded by low temperature gas at the top and moderate temperatures around the surface of the outlet duct. Two remaining sections, display the decrease in the temperature variation in the duct. However, the last section located almost ate the outlet still exhibit temperature gradient of 80 K.

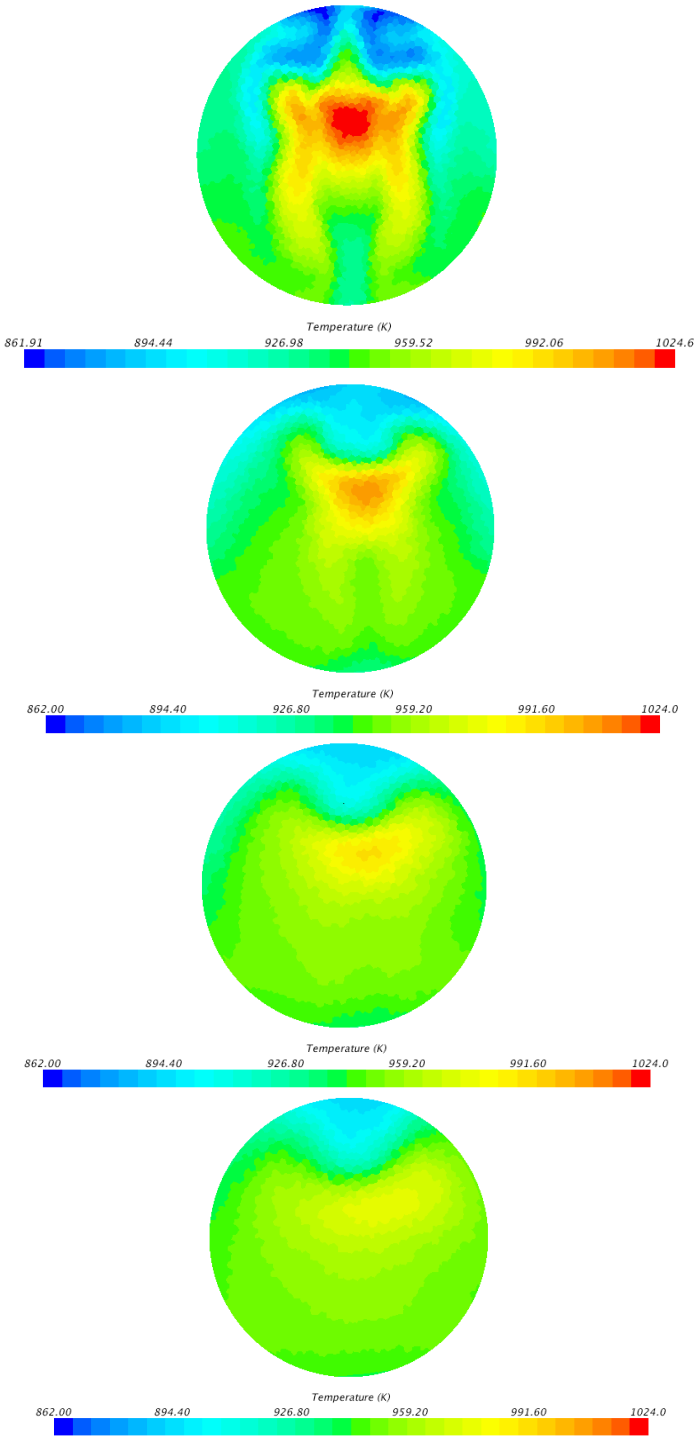

Figure 53 Temperature contour at four planar sections of the outlet duct, from the beginning of the duct, every 20 cm

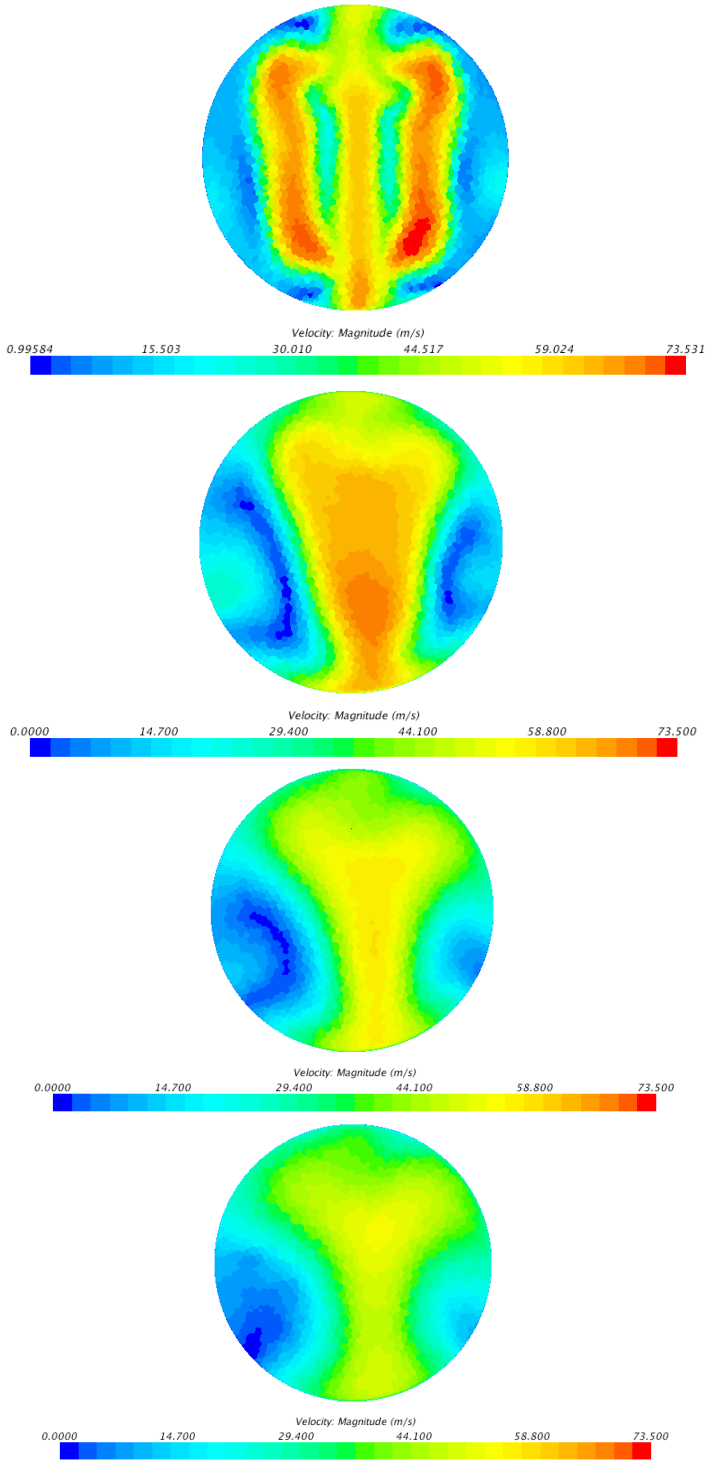

Figure 54 Velocity magnitude contour at four planar sections of the outlet duct, from the beginning of the duct, every 20 cm

4.1.4.4 Conclusions

Two cases of BC (temperature profile) have been calculated. The applied boundary conditions created more realistic temperature profile across the core. Case P1.2.1 resulted with outlet temperature average higher 90 K than the HTTF operating temperature. The other calculated temperature profile – Case P1.2.2 resulted with slightly lower (10 K) temperature than in HTTF. Although the overall average temperature of the gas differ from gas temperature values expected in HTTF the characteristics of the flow should not be changed.

The high variation in temperatures across the core, results in high temperature stratification in the core and then in moderate stratification within the outlet duct. At the outlet duct the temperature variation exceeds 250 K for Case P1.2.1 and 80 K for Case P1.2.2, which in both cases would not be acceptable temperature variation at the inlet to the gas turbine or IHX. In contrast to the "hot channel" case in section 4.1.1 the hottest gas do not reach the surface of the outlet duct. The hot flow is being contained in the central part of the duct surrounded by cooler gas. Still the gradient of temperatures at the outlet duct surface reaches almost 200 K in Case P1.2.1 and 100 K in Case P1.2.2.

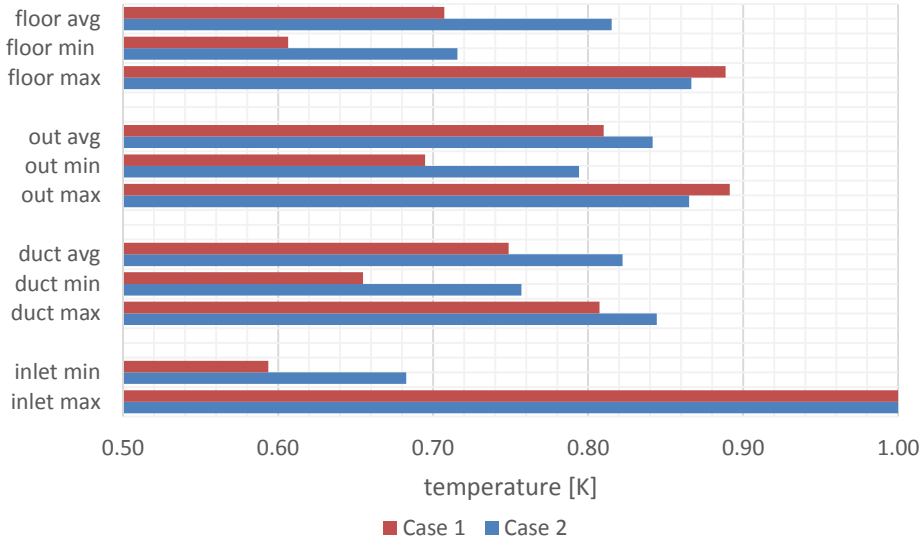

Figure 55 Normalized temperature values t selected locations for Case P1.2.1 and P.1.2.2

The temperature values normalized with maximum inlet temperature at selected locations are presented in Figure 55. Inlet temperature gradient applied through BC was larger for Case P1.2.1. The maximum normalized temperature at LP floor and outlet boundary is higher in Case P1.2.1. However the outlet duct maximum normalized temperature is higher for Case P1.2.2. This may be connected with non-symmetrical flow pattern in outlet duct in Case P1.2.2.

4.2 Part 2 – mixing enhancement methods

The purpose of this study is developing a method for the promotion of gas mixing in the Lower Plenum of High Temperature Test Facility at Oregon State University to reduce risk of thermal stratification phenomena during normal operation. The following aspects were examined: identification of the gas flow behavior in the LP of the HTTF based on CFD simulations, identification of temperature stratification issue in the HTTF LP using CFD tools, a scoping study for available methods for mixing promotion and computational investigation of efficiency of selected method. Investigated methods include modification of the LP geometry in order to induce more turbulence and modification of the LP reflector to enhance helium jet mixing. The flow characteristics are being investigated especially at the LP outlet where temperature stratification has the largest impact. The numerical model of the LP was created using Star-CCM+ software. This study includes a description of the CFD model of the HTTF LP, results of CFD simulation and an evaluation of thermal mixing enhancements using available methods.

Coolant in the prismatic HTGR, in the case of non-uniform power distribution across the core, will exit the core with significantly differentiated temperatures. For some cases due to the annular core geometry and the fuel loading configuration it is anticipated that temperature of some of the cooling channels may be 300°C hotter than the average helium temperature at the core exit (NRC 2008). This value is significantly higher than acceptable temperature variations, which is ±20°C. Moreover it has been shown that helium as a coolant is resistible to the precise thermal mixing what can result in temperature variations on the LP outlet. This may introduce two issues in normal operation of the reactor. First one is thermal stress in the LP chamber

structure caused by hot spots on the LP floor causing accelerated fatigue of the material. The second and more important issue is the temperature-stratified flow entering the heat exchanger (steam generator or gas turbine) may not comply with the operational limitations for temperature variation of those components. Special design features may be needed to enhance good mixing and reduce the thermal streaking in the LP.

A number of simulations were performed in order to quantify the mixing phenomenon in the LP of the prismatic MHTGR (Gradecka and Woods 2014). A numerical model of the LP was built in order to simulate and investigate the gas mixing efficiency and assess probability of "hot spotting" on the LP structure. In this study, the effect of the "hot channel" on the thermal uniformity of the coolant was investigated. It was stated that injection of a gas section with temperature 50 degrees Celsius higher than rest of the jets results with 20 degrees increase of the LP floor temperature. The study concluded with confirmation of flow stratification in the LP and in the hot gas outlet duct.

4.2.1 Vortex generator – single channel

The jet nozzle modification creates opportunity to control and enhance jet mixing. D. E. Parekh performed a study on passive mixing enhancement techniques for axisymmetric jets. This passive technique can be easily applied for HTGR's in the jet inlets to the LP to enhance decay of the axial velocity component and that way promote jet mixing. Detailed description of the vortex generators was presented in Section 2.3.3.

4.2.1.1 CFD model – single model analysis

Numerical calculations have been conducted using the computational fluid dynamics software – STAR-CCM+ 7.04.006 Adapco. The simulation was made for turbulent, compressible gas flow through the geometry described in following subsection.

To investigate options of the mixing improvement in the LP it is necessary to conduct a large number of simulations with high spatial resolution. Only sufficient resolution of the spatial

mesh can accurately model the flow development and mixing progress across the LP geometry. To facilitate this study within an optimal computational cost it was needed to reduce the domain to a single channel connected to the mixing chamber. This adjustment allowed examining several geometrical modifications / vortex generators for their effectiveness in altering the flow and promotion of the uniformity in velocity field. Reduction of the computational domain to a single channel resulted in the removal of the following phenomena from the flow: obstruction caused by multiple jet interactions, impingement of the flow on the structural support posts and 90 degree change in flow direction. All of the mentioned elements would probably introduce distortion of the velocity and temperature field in the LP, thus the simplified geometry will lead to underestimation of the mixing device effect on the flow.

A number of single channel flow simulations were conducted in order to quantify the mixing improvement capability for various designs of the vortex generators. This study investigates flow field distortion with constant temperature in the domain. Thus the vortex generators effectiveness was considered only from the perspective of the mechanical mixing and turbulence of the media and do not include heat transfer as a supporting effect.

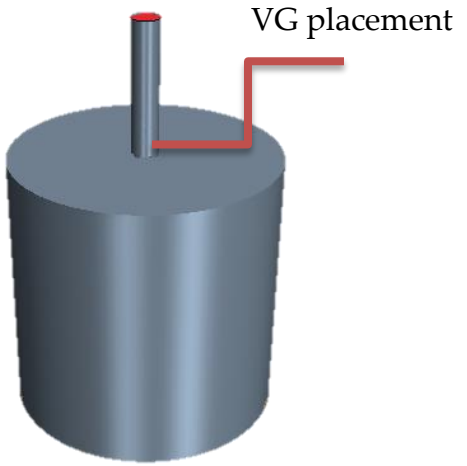

Figure 56 Single channel geometry for the Base case

This method considers the mixing improvement between the gas jets exiting coolant channels only. This study does not include impact of the bypass flow due to vertical and horizontal gaps between prismatic blocks at the flow uniformity. Additional studies should be performed to address this issue.

4.2.1.2 Geometry of the passive vortex generator

Since it may become possible to conduct experimental studies on the effectiveness of various mixing enhancement methods at HTTF facility, a corresponding (MHTGR-like) geometry was used for the CFD modeling in this study.

The geometry (Figure 56, Figure 57) of the model was created using NX 7. Vortex generators geometry was based on work of Carletti (M. Carletti, Rogers, and Parekh 1996), and adjusted for purpose of implementation in the inlet channels of the LP. The geometry for this study is simplified to one channel with dimensions congruent with the channels in the HTTF design connected with cylinder of a large diameter (mixing chamber) as shown in Figure 56. The diameter of second cylinder – mixing chamber was selected arbitrarily. The idea was to create semi - realistic flow conditions like in the LP of the HTTF. However, in this model both the inlet and the outlet are located at horizontal plane, unlike the HTTF LP outlet. This modification has been introduced to separate effect of the vortex generators from flow distortion due to 90º change of flow direction. The inlet channel of ID 0.0254 m and length 0.13 m is connected to mixing chamber of ID 0.254 m and length 0.251 m. The reference geometry is a vertical cylinder with stepwise variable diameter. For modified geometries at the connection of inlet channel and mixing chamber, vortex generator is placed.

Three types of the vortex generators were investigated. The geometry of the vortex generators is shown in Figure 57. For all cases four tabs were placed every 90 degrees. The thickness of the tabs for all vortex generators is 0.002 m, however the rest of dimensions vary from case to case. The comparison of dimensions would be difficult due to various configurations of the tabs, therefore the general parameter describing the vortex generator is blockage. The equation

for blockage is a relation of surface averaged velocities of the flow as follows (M. Carletti, Rogers, and Parekh 1996):

$$B = \frac{\vartheta_{vg} - \vartheta_{reference}}{\vartheta_{reference}} \qquad (1)$$

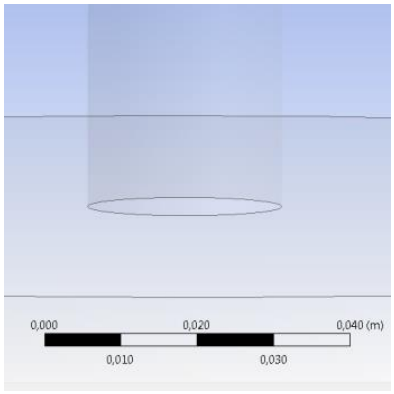

A. REFERENCE

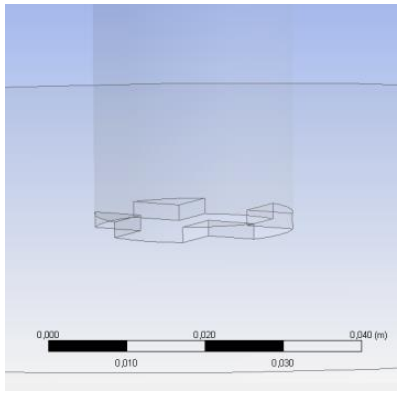

B. DELTA TAB

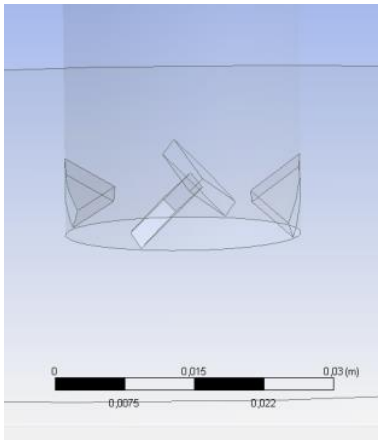

C. DELTA TAB SWIRL

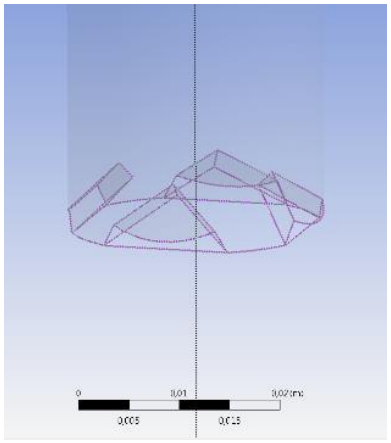

D. DELTA TAB 45⁰

Figure 57 Vortex generator geometry

Where the subscript vg stands for vortex generator model and reference is the case without the vortex generator. The blockage was investigated using average surface velocity at the connection of channel and mixing chamber, below the vortex generator. The investigated vg cases resulted with following values of the blockage: reference – 0%, delta tab – 29.2%, delta tab swirl – 22.9%, delta tab 45° – 2.3%. The preliminary numerical simulation indicated that all of the vortex generators introduce negligible increase in the pressure drop thus if potentially used for LP the

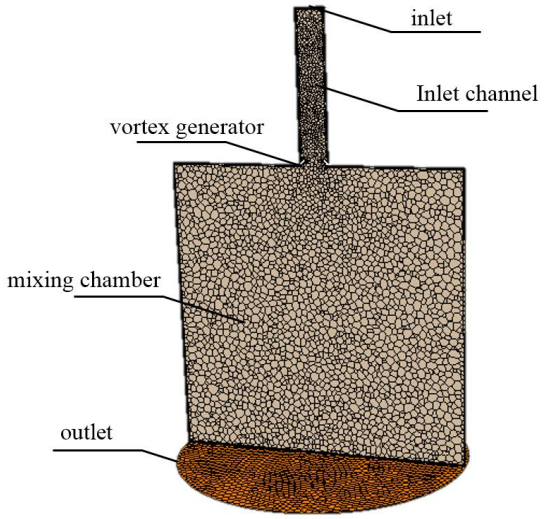

Figure 58 Vertical cross section through computational mesh

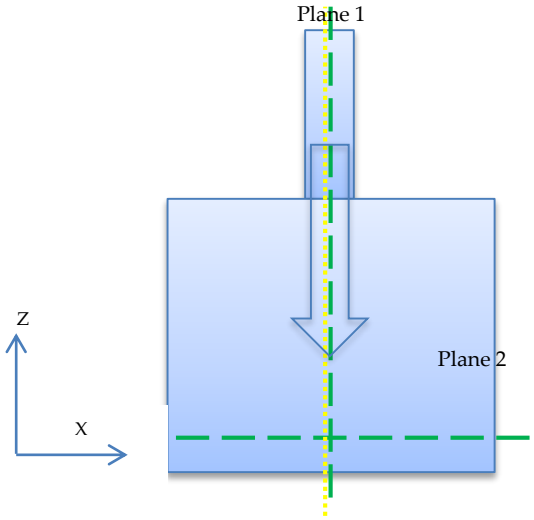

Figure 59 Location of the probe line (yellow) and (green)planes

advantage of mixing will probably outgrow efficiency loss due to pressure drop/pumping power. However this should be furtherly investigated and verified through an experiment.

4.2.1.3 Computational domain – mesh description

An adequate spatial discretization of the computational domain is crucial for the CFD modeling. The proposed mesh consists of 6 million unstructured mesh cells as shown in Figure 58. The base size of 0.005 m was used for creation of the mesh with six optimization cycles to produce mesh which complies with threshold of minimum 80% quality for every cell in the domain. The volume is discretized with the polyhedral cells, however to compute the flow near wall five layers of prisms were applied with specification of the first layer thickness (2.5e-4 m). The mesh in the wall region is sized to achieve dimensionless wall distance $y^+<1$. The geometry for other cases including the vortex generators are meshed using the same setup.

4.2.1.4 Boundary conditions

The flow conditions for this study are uniform as for previous study conducted in this subject (Gradecka and Woods 2014) thus similar to case of the flow in the full LP geometry. Turbulent helium flow is applied at velocity inlet with velocity magnitude 20.8 m/s, temperature

960 K and pressure 0.8 MPa. The outlet boundary is modeled as a pressure outlet. From case to case there is no variation in the boundary conditions and only the geometry was modified.

4.2.1.5 Models, assumptions and solver details

Helium flow was simulated as an ideal, compressible gas. Simulated flow can be classified as turbulent as the Reynolds number at the inlet is equal to 4,700. To solve the turbulent flow realizable k-epsilon turbulence model is used with enhanced wall treatment for low Re numbers. Steady state calculations lead to converged solution (residuals for all solved equations lower than 10-6).

4.2.1.6 Validation considerations

The model presented in this section is a classical representation of a submersed circular jet flow. This subject has been studied thoroughly for decades via experimental research and computational simulation. For simple 2 or 3 dimensional geometry, analytical solution can be presented. The flow pattern development can be divided depending on various criteria but the most recognizable division is presented in Figure 60.

The jet can be divided into two zones, zone of flow establishment and zone of established flow. The first zone is characterized by the length of the jet with intact core velocity. As jet enters the fluid at rest, some of the fluid particles will be entrained with the jet. The cascade of eddies will be created, penetrating deeper and deeper into the jet core. When mixing layers will reach all the way to the jet axis, the centerline velocity will start decaying. The velocity profile in the first zone will be flat and equal to inlet velocity inside of the triangle (2 dimensional geometry) or cone (3 dimensional geometry) created by jet inlet and point of mixing zones meeting. The velocity profile in the second zone can be represented by Gaussian normal probability function presented in Figure 61. The zone division is of course theoretical, as the mixing zones meeting point cannot be specified. In real case some length of transition flow regime will be present between the zones.

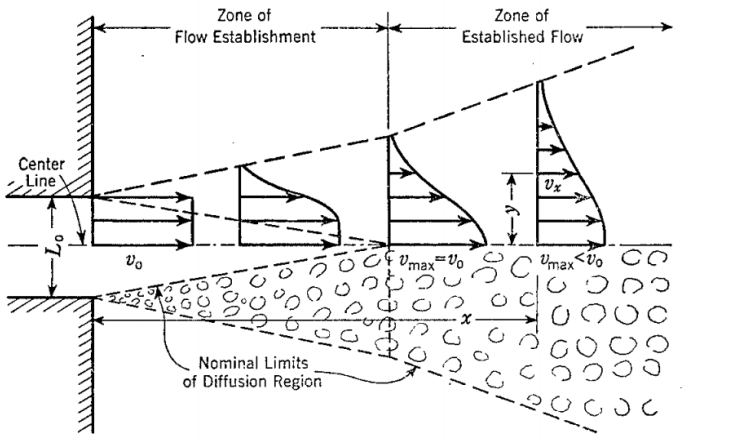

Figure 60 Jet development (Albertson, Jensen, and Rouse n.d.)

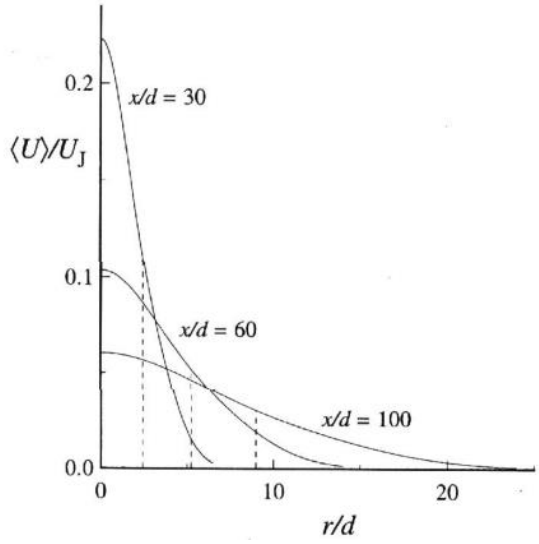

Figure 61 Radial profiles of axial velocity profiles in a circular turbulent jet Re=95500 (Pope 2000)

The model developed for the vortex generator study reassembles the conditions for a submersed jet flow with one exception. The length of the mixing chamber is not sufficient to fully allow jet development and thus the length of the first zone (Zone of Flow Establishment) is shortened. In other words the core velocity of the jet decays sooner than in case of the free jet. The effect of the pressure outlet boundary causes the modification of the flow pattern, however it is introduced with a purpose. The length of the mixing chamber reassembles the length of the HTTF's lower plenum rather imaginary semi finite pool. Thus creating flow conditions similar to the actual target of this study.

In Figure 62 the contours of axial velocity at centered vertical plane are presented. The red arrows bound the area with significant velocity magnitude. It can be seen that the shortened geometry is not affecting the universal spread angle of about 24°. Also the comparison of the velocity profiles presented in Figure 63 and Figure 64 for computed model and theoretical solution confirms the correctness of the selected modeling technique.

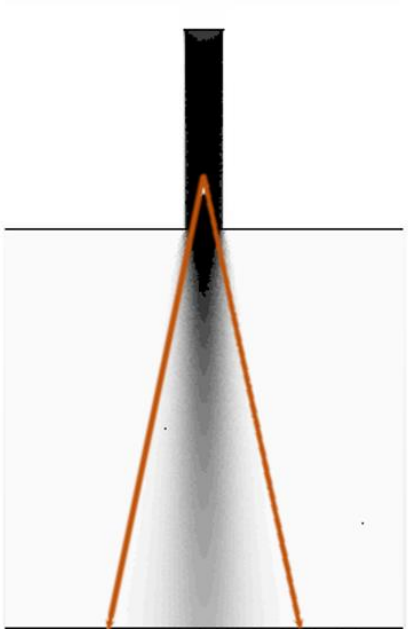

Figure 62 Axial velocity contour presented on a vertical plane of symmetry

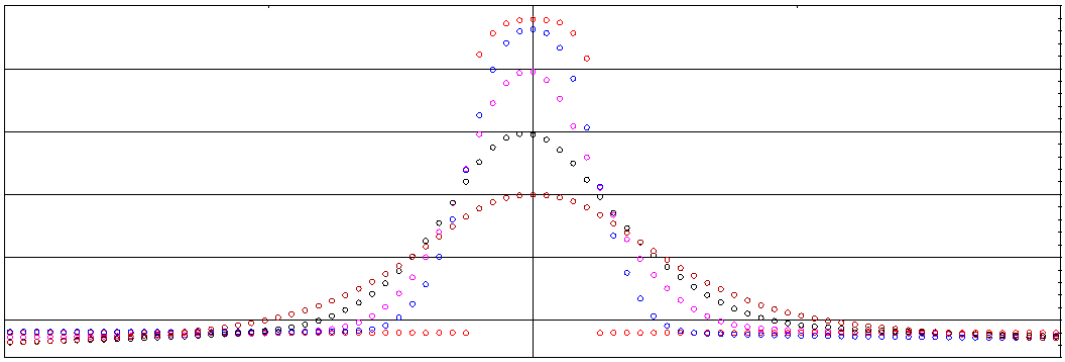

Figure 63 Axial velocity profiles at selected locations computed in Star-ccm+ software

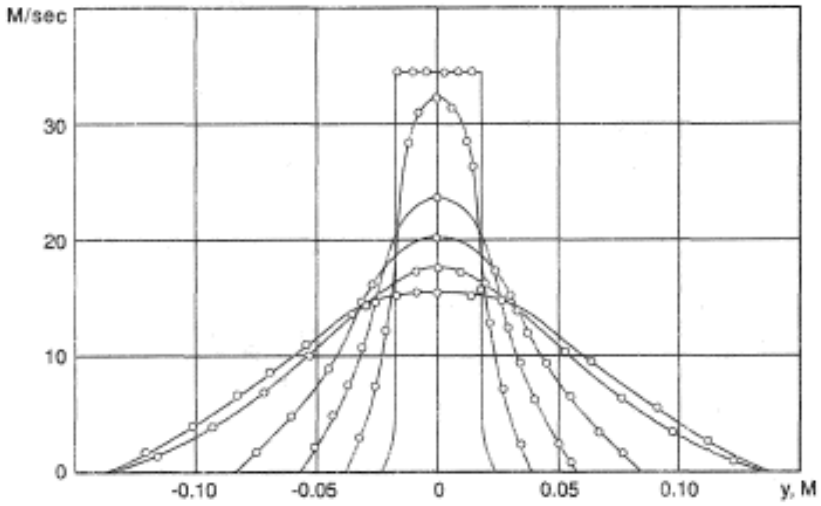

Figure 64 Universal theoretical velocity distribution in various location of circular jet (Beale, 2011)

4.2.1.7 Preliminary results

This section presents the general character of the flow in the modeled geometry. The results are presented in the form of velocity profiles and contours at two strategically located planes as shown in Figure 59. The mixing quality is presented in Figure 68, Figure 69, Figure 70 and

Figure 71. This set of data has been extracted from five vertical planes equally spaced from the placement of VG until the outlet.

The general character of the flow was the primary concern. The horizontal and the vertical planes dissect the domain to thoroughly inspect the influence of the vortex generator on the flow field. The horizontal velocity contour at the plane located at the outlet as shown in Figure 65. It can be seen that application of a vortex generator visibly alters the velocity field in comparison to the reference case. From a graphical representation of the velocity field, it is not obvious which of the vortex generators result in the largest mixing enhancement.

Figure 67 presents contours of the velocity components – X and Z, at the vertical plane. As previously, the difference in velocity contours between reference and remaining models is apparent. Some of the vortex generators (most visible DELTA TAB 45º) cause formation of an acceleration cone at the area of the geometrical insert. This high velocity zone is developed due to high blockage of the channel as described in section 4.2.1.2. This representation of the flow

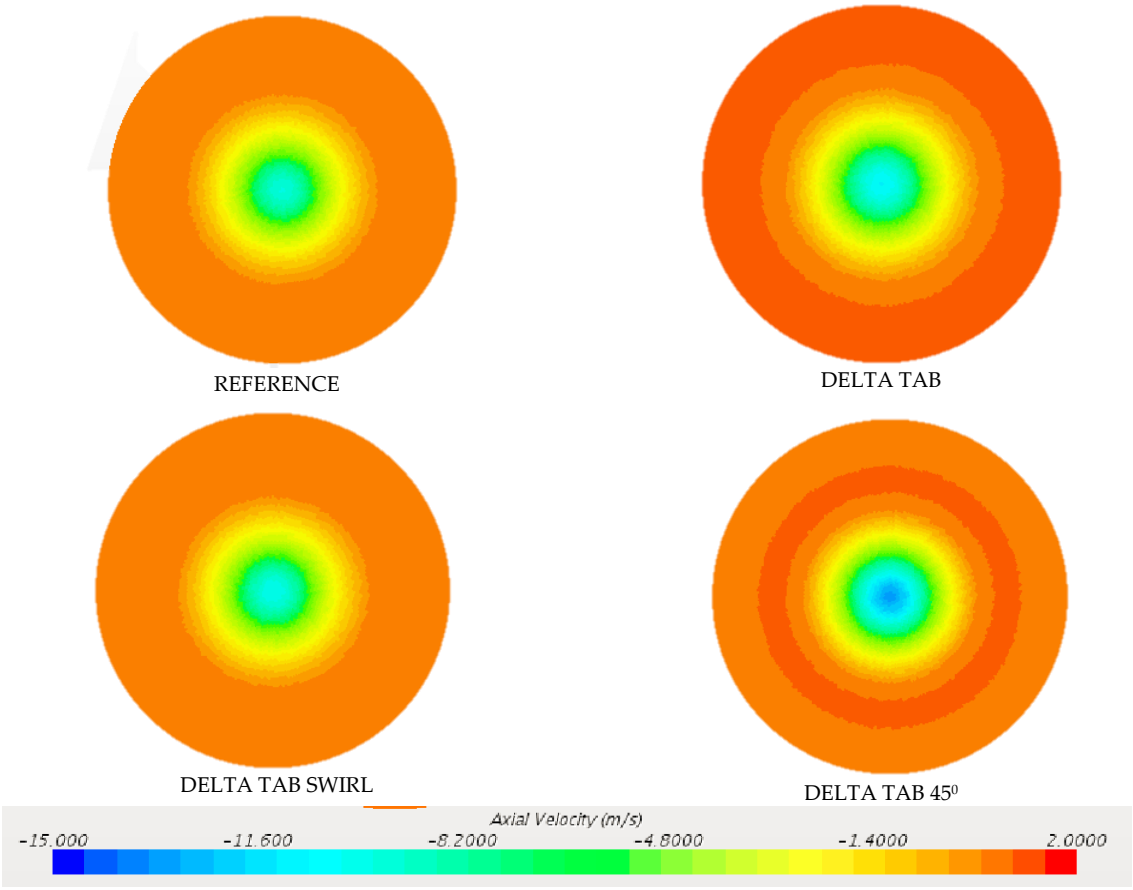

Figure 65 Axial velocity contour at Plane 2 [m/s]

illustrates the influence of the vortex generator in the core of the model and propagation of the mixing enhancement into the peripheries of the domain. In Figure 66 a clear increase in the radial velocity can be seen when the vortex generator is applied. Part of the kinetic energy targeted downward has been redirected into radial movement and turbulence promoting alternative flow behavior.

The velocity profile is shown in Figure 66 using a plot along a probe line, which connects central points of the inlet and the outlet as indicated in Figure 59. The largest increase in velocity

component z can be noted for al VG in the jet inlet to the mixing chamber. However only in case of DELTA TAB 45 the velocity at the centerline remains elevated through whole flow domain. As mentioned before this is an effect of increased blockage of the mixing chamber entrance. This velocity profile alteration does not describe quantitatively the mixing enhancement unambiguously since it exhibits velocity change only on the model centerline.

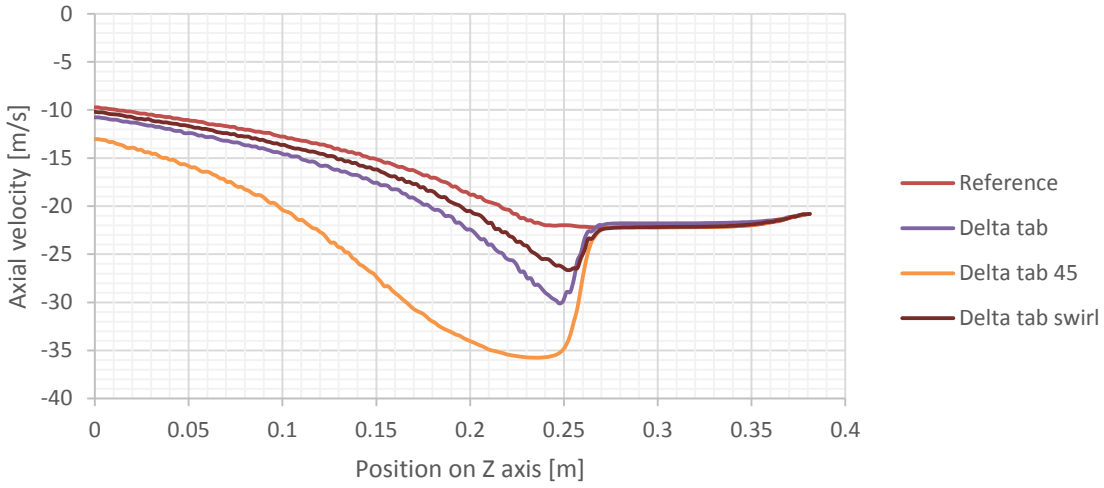

Figure 66 Velocity profile along Probe line 1 - component z [m/s]

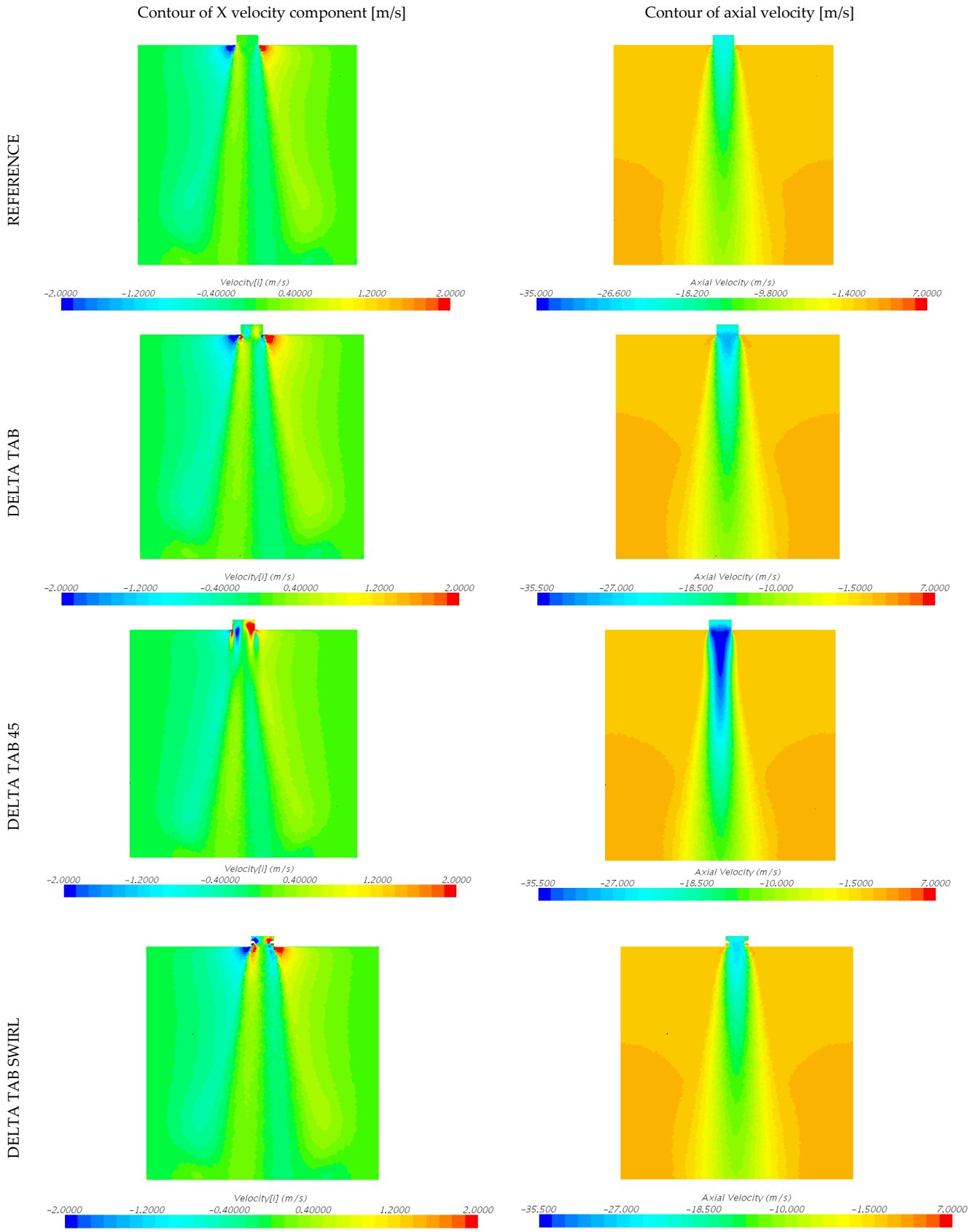

Figure 67 Contour of respectively x and z component of velocity at Plane 1 [m/s]

The mixing enhancement can be reported using number of methods. In this study only few parameters were selected to represent the influence of the vortex generators in the flow pattern, namely a uniformity coefficient of velocity field, standard deviation of velocity field, turbulent kinetic energy and tangential velocity. The uniformity and standard deviation were defined with following formulas (CD-Adapco, 2012):

$$\phi = 1 - \frac{\sum_f |\phi_f - \bar{\phi}| A_f}{2|\bar{\phi}| \sum_f A_f} \quad (2)$$

$$\phi = \sqrt{\frac{\sum_f (\phi_f - \bar{\phi})^2 A_f}{\sum A_f}} \quad (3)$$

Where $\bar{\phi}$ stands for the surface average of ϕ, ϕf is the face value and Af stands for the face area (CD-Adapco, 2012) (extracted at five uniformly spaced horizontal planes located at z=[0.25 m; 0.2 m; 0.15 m, 0.1 m, 0.05 m]). The values of selected parameters were examined at five horizontal planes in the mixing chamber area. The first one is located directly below the vortex generators (z=0.25 m), the subsequent planes are placed every 5 cm downstream up to the outlet face (z=0.0 m). The results for all cases are shown in Figure 68, Figure 69, Figure 70 and Figure 71. In Figure 68 it can be noted that all curves have similar shape, where delta swirl is placed almost exactly at the reference curve. The uniformity coefficient curve for the DELTA TAB and DELTA TAB 45 designs as subsequently placed above and under the reference. From Figure 68 we can see that vortex generators DELTA TAB achieves higher (+2.5% than reference) than reference surface uniformity, whereas DELTA TAB 45 achieve the lowest uniformity coefficient at the outlet boundary (-2.5% than reference). The opposite trend can be seen in the Figure 69 which presents the standard deviation of surface averaged velocity magnitude at preselected locations. All cases result with almost linear curve for decreasing standard deviation as the inlet jet dissolves in the mixing chamber. For this parameter the REFERENCE results with the lowest value of standard deviation at the outlet 1.7 m/s. The improvement of this factor can be noticed for DELTA TAB 45 where the standard deviation in surface averaged velocity increases to 2.17 m/s.

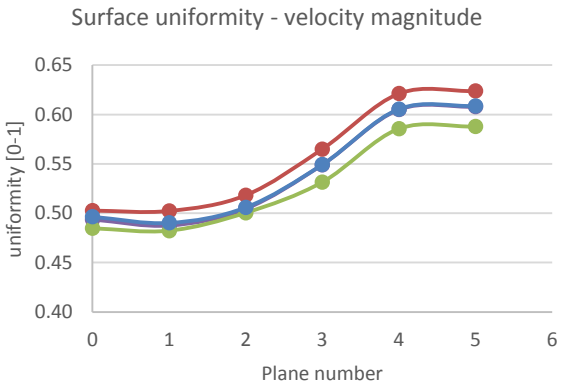

Figure 68 Surface uniformity for velocity magnitude at xy planes located at z=0.0, z=0.05, z=0.1, z=0.15 z=0.2, z=0.25 m

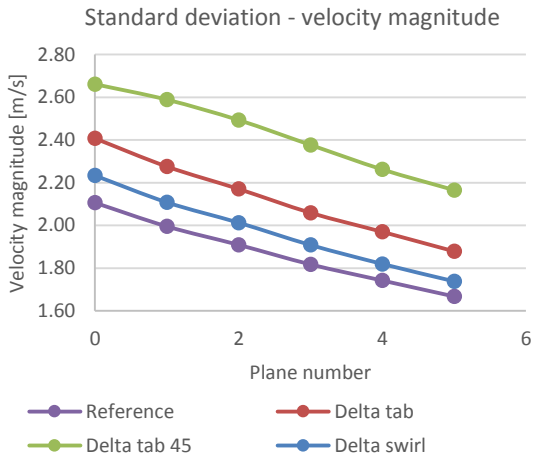

Figure 69 Surface standard deviation for velocity magnitude at xy planes located at z=0.0, z=0.05, z=0.1, z=0.15 z=0.2, z=0.25 m

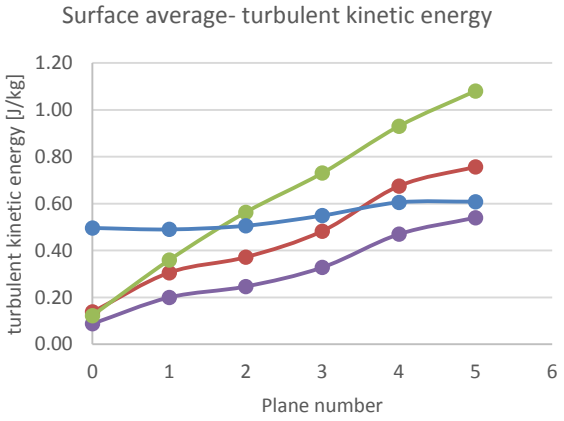

Figure 70 Surface averaged turbulent kinetic energy [J/kg] at xy planes located at z=0.0, z=0.05, z=0.1, z=0.15 z=0.2, z=0.25 m

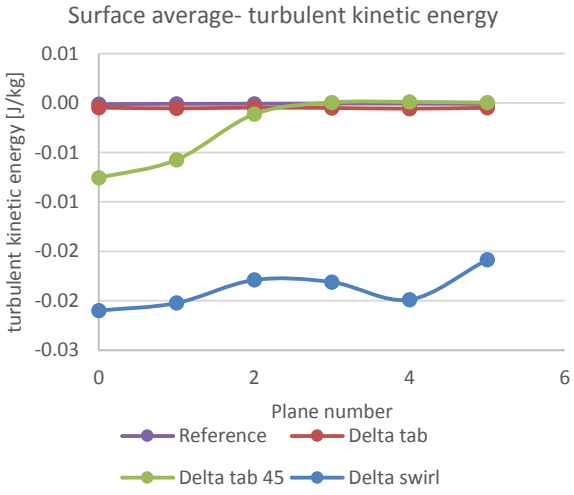

Figure 71 Surface averaged tangential velocity at xy planes located at z=0.0, z=0.05, z=0.1, z=0.15 z=0.2, z=0.25 m

The turbulent kinetic energy is presented in Figure 70. The increment of this parameter ranges from 0.1 to 1 J/kg from vortex generator to the outlet boundary. The reference channel results with the lowest turbulent kinetic energy at the outlet plane. For this factor DELTA TAB 45 results in the highest value of turbulent kinetic energy, equal to 1.08 J/kg at the outlet. Additionally, only in case of the DELTA TAB SWIRL, development of tangential velocity can be

noted as shown in. Figure 71. In this case the vortex generator tabs are slightly twisted, guiding the jet into a rotational movement.

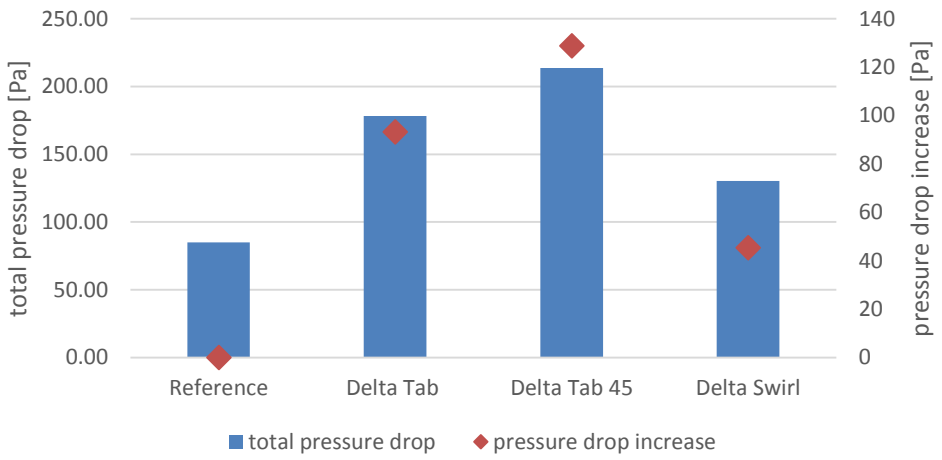

Figure 72 Pressure drop caused by VG's

The pressure drop in connection to the modification of the inlet channel is presented in Figure 72. The largest pressure drop has been created by Delta Tab 45, over 130 Pa increase per channel. Slightly smaller drop was noted by Delta Tab, since both of those designs have quite large blockage coefficient – 20%. The lowest value of pressure drop was achieved by Delta Tab Swirl, only 45 Pa.

4.2.1.8 Conclusions

To investigate the possibility of applying vortex generators (VG) for gas mixing enhancement in the LP of the HTTF, a numerical model of theoretical mixing volume was developed. Three types of vortex generators were introduced into end part of the inlet channel to assess the flow field modification.

As described in the section above, all vortex generators influence different parameters of the flow. Thus it is not obvious which of the vortex generators can be a solution to the stated problem. The achieved mixing enhancement is somewhat lower than expected from reference study, and can be possibly improved by manipulation of the VG dimensions and placement.

The applied modification due to introduction of the VG into the coolant channel did not deliver the expected mixing enhancement. However, the feasibility of this solution should be further examined through modification of the geometry and supplemental CFD analysis of the effects introduced in the scalar mixing for section of the lower plenum.

It is anticipated that the temperature variation need to be incorporated into the future work to determine the most effective solution. It should be noted that in this study an isothermal flow was investigated and the actual effect on the temperature uniformity enhancement could be larger.

4.2.2 Vortex generator – supporting study

Previous section 4.2.1 described investigation of the vortex generators influence on single jet flow via simplified geometry consisted of two cylinders. That approach aimed into exhibition of the VG effect standalone. The results of this study show the mixing effect of the VG was lower than expected due to lack of presence of other factors like relative velocity of the surrounding gas, flow obstruction, multiple jet interactions and change of flow direction. This section will consider VG effectiveness in conditions closer to the flow in LP, thus including mentioned factors.

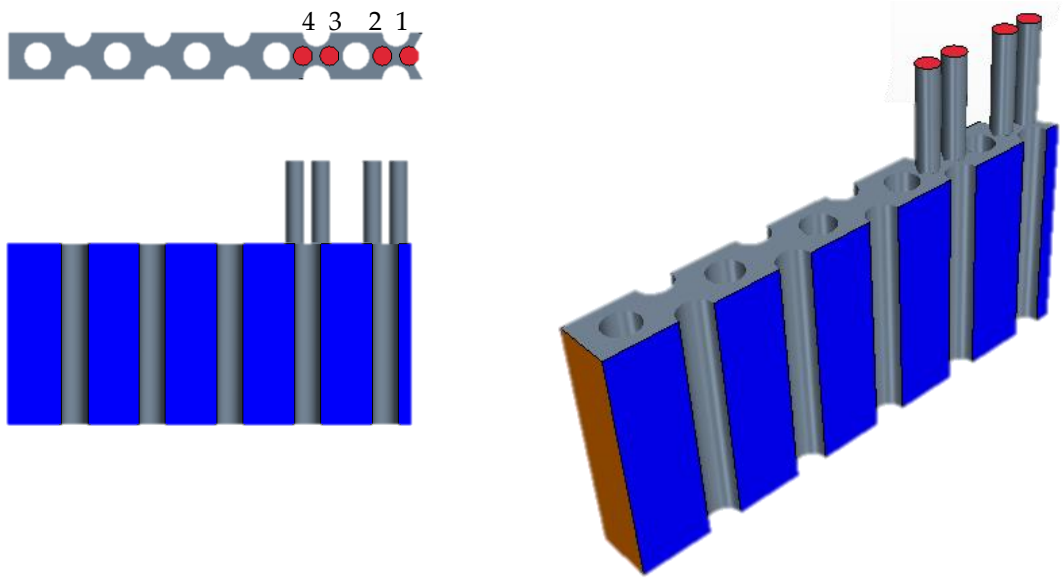

Figure 73 Plenum section - geometry used for the CFD study

To carry this investigation it is necessary to conduct CFD analysis of the model which includes multiple jets, support posts and change in flow direction. This was accomplished using geometrical model developed as an experiment in Idaho National Laboratory (Condie et al. 2005; R. Johnson 2009; H. M. McIlroy, McEligot, and Pink 2010; H. McIlroy and McEligot 2006).

Application of this geometry enables validation of the model as experimental data and other CFD analysis results are available. This introduces theoretical opportunity of evaluating the mixing efficiency of the VG without conducting experimental research.

4.2.2.1 Geometry and mesh

The geometry used for this investigation has been drawn from MIR experiment at INL. The exact dimensions can be found in literature(Condie et al. 2005). The visualization of the geometry is presented in Figure 73. The model is colored according to the boundary conditions applied. The red areas mark four velocity inlets, orange surface marks the pressure outlet boundary and blue surfaces mark the symmetry planes. To ensure lack of influence of the outlet boundary at the flow field additional section was added to the outlet boundary. This box -shaped section was created by extruding (20 cm) outlet face in the Y direction. This "outlet" section is not shown in Figure 73 as the flow field solution from this domain will not be included in the result section. It is added strictly to improve numerical accuracy of the solution.

Two geometries were used in this study. First one reassembles MIR experimental domain, the second one includes VG placed at the connection of the inlet channels and the plenum section as in single channel study. VGs were placed in each of four inlet channels. The mesh has been created using polyhedral cells with prism layer at wall boundaries. The base size of 22 mm was used to build mesh consisted of 3 million elements with cell quality set at 80%.

4.2.2.2 Boundary conditions

Two cases have been considered. The first one resembles the exact setup of the MIR experiment, thus it simulates flow of mineral oil through the mentioned reference geometry. The

purpose of this case was solely validation of the computational setup against MIR experimental results. These conditions were also used to calculate VG performance to serve as possible validation set if MIR experiment would be redone with VG mounted into the inlet channels. The modification of the original BC from the experiment was following: slightly higher temperature (5degrees), hot channel implemented (+50 degrees) in jet number 3.

The other two cases were calculated with hot helium. For both of those cases boundary conditions are the same as in hot channel case from Part 1 and reassemble the conditions in the LP of the HTTF and are as described in Table 11.

Table 11 Case description for Part 2.2

Case number	P2.2.1	P2.2.2	P2.2.3	P2.2.4
Geometry	MIR	MIR+VG	MIR	MIR+VG
Working fluid	Mineral oil		Helium	
Inlet temperature 1,2 and 4	295 K		950 K	
Inlet temperature 3			1000 K	
Inlet velocity	1.7 m/s		20.8 m/s	
Pressure	1 atm		0.8 MPa	

4.2.2.3 Simulation results - mineral oil

These two cases have been created for validation against MIR experimental research. In this case mineral oil was used as medium to match index of refraction. Case P2.2.1 employs unmodified MIR geometry as described previously. The main outcome of this case is the temperature and velocity fields. Both of them are summarized in Figure 74 in form of temperature colored streamlines. The streamlines exhibit undisturbed flow field with visible temperature stratification. The temperature gradient at the model outlet exceeds 19.5 degrees. Clearly jets number 1 and 2 flow almost vertically downward subsequently turn 90 degrees and continue until the outlet in the lower part of the geometry whereas jet 3 and 4 undergo mixing and flow in the upper part of the plenum section. The interaction between jest 1-2 and 3-4 is very limited.

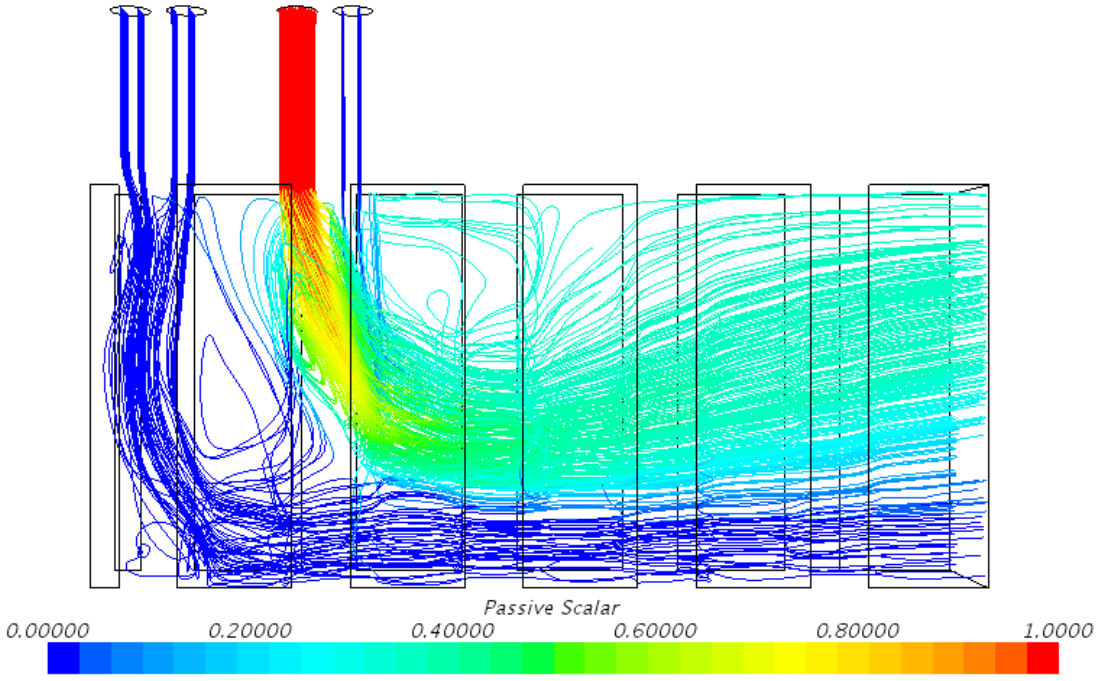

Figure 74 CFD simulation of the MIR experiment with mineral oil

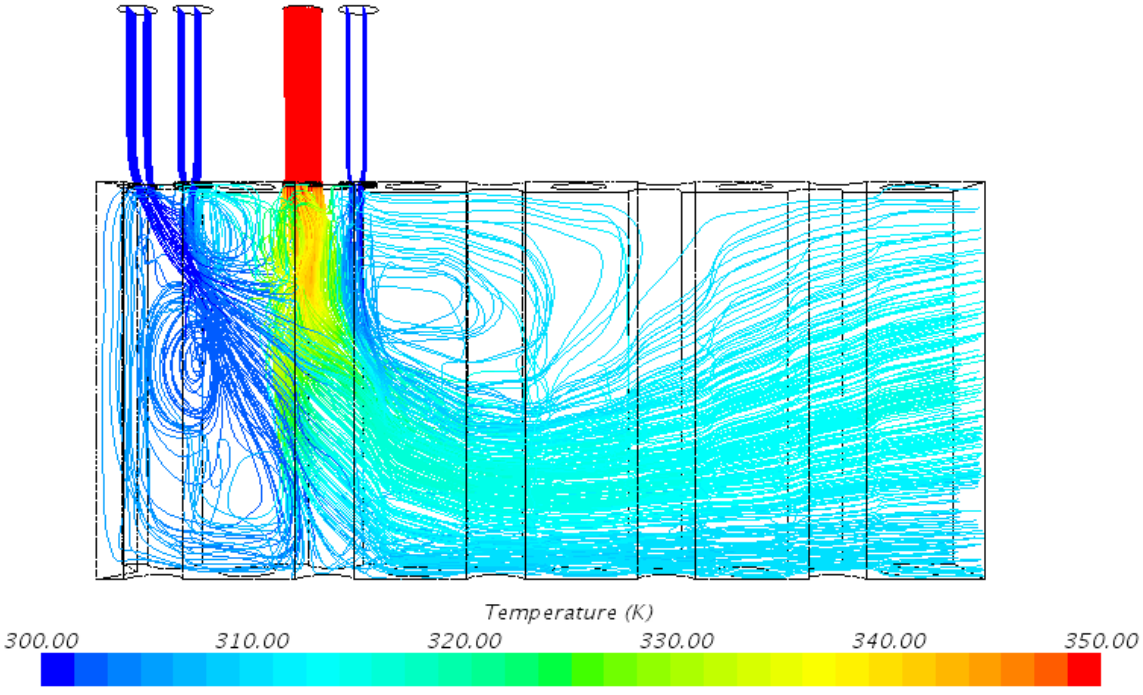

Figure 75 CFD simulation of MIR experiment with VG inserts with mineral oil

Case P2.2.2 is based on MIR geometry with application of vortex generators in the area of connection between inlet channels and LP section. The DELTA TAB design was used for this investigation. The description of the DELTA TAB design can be found in section 4.2.1.2. Each channel contains 4 tabs which gives cumulative number of 16 tabs in the whole model. The results for this case are also presented in form of temperature colored streamlines. The influence of VG can be clearly seen as flow display two large vortexes. The first one, located in left lower corner of the model, causes the shift of the flow path toward the outlet. Shifted flow from jest 1 and 2 intersect with unmixed jest 3 and 4 causing rapid mixing between all of the jets. The second vortex is generated in the upper middle part of the LP section. That is the area where flow changes its main direction from vertical to horizontal. The flow at the outlet is more uniform as temperature gradient is 14.5 degrees. In this case there is no visible separation of the flow between jets 1, 2, 3 and 4.

4.2.2.4 Simulation results – hot helium

Previous section describes effect of the VG (delta tab design) at flow field of mineral oil in LP section. To show the effect of the VG at more realistic conditions another simulation need to be developed, this time using helium as a working fluid. Although the mineral oil and helium have similar Re numbers, it seems beneficial to investigate flow field for the helium option to confirm the VG performance.

The reference geometry with set of four delta tabs is placed in each inlet channel. The passive scalar is used to determine flow path of the gas from channel number 3. This channel also has elevated temperature at the inlet - 50 K. The flow field in reference geometry shown in Figure 76 exhibits vortex in left part of the geometry, however further flow downstream proceeds without disturbances. At the outlet flow is stratified which results with temperature gradient of 16 degrees. The surface uniformity in respect to passive scalar at the outlet boundary is equal to 73%.

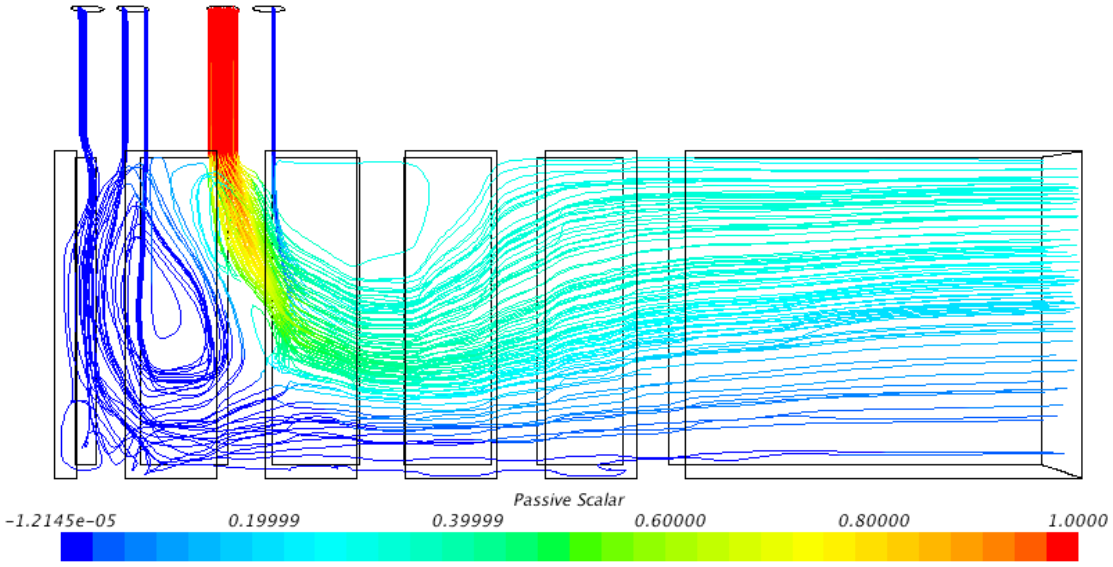

Figure 76 Streamline colored with passive scalar content for reference geometry with helium as a working fluid

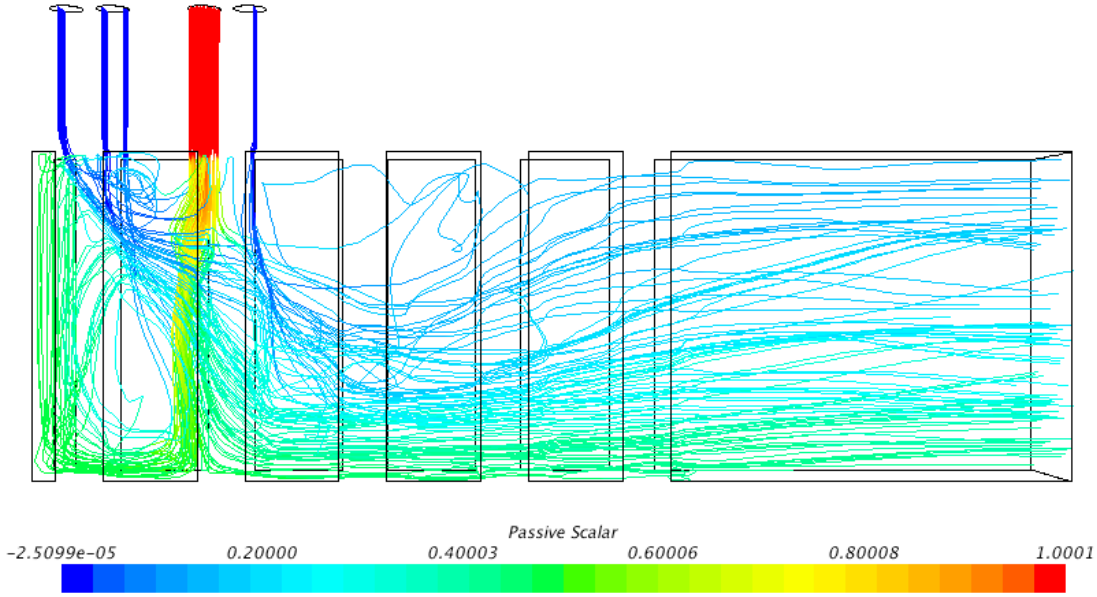

Figure 77 Streamline colored with passive scalar content for geometry modified with Delta Tab, with helium as a working fluid

The results for the geometry with vortex generator implemented are shown in Figure 77. The overall flow field is considerably more chaotic than in previous case. There are multiple vortexes visible and streamlines in the vicinity of the outlet boundary are not parallel to each other. In this case the jet from inlet number 3 reach all the way to the geometry bottom and splits

toward and against the stream. The temperature gradient at the outlet surface is reduced to 14 degrees and the surface uniformity in respect to passive scalar increases to 84%.

4.2.2.5 Conclusions

The experimental geometry was used to investigate thermal mixing improvement when vortex generators are used. In the first step, the simulation mimicking the experiment has been carried out to validate the modeling choices. The next step was investigation of the influence of the VG at the mineral oil flow, as in the experiment. Comparison of those two cases resulted with conclusion that placement of the VG's in the inlet channels increased the thermal mixing. Thermal gradient of 50 K was applied at the inlet boundary. The simulation with original geometry resulted with 19.5 K gradient difference at the outlet boundary, whereas the modified geometry (with VGs) reduced this value to 14.5 K.

Despite similar Reynolds number values at the inlet boundary between mineral oil (room temperature) and helium (HTTF operating conditions) the additional study was performed to confirm this results for gas. The same two geometries were used in simulations with helium as a working fluid.

4.2.3 Screen – outlet duct

The temperature and velocity profiles of the hot gas at the exit of the LP is highly variable. If the outlet duct is empty (not modified), the flow is turbulent, however, the overall temperature profile remains undisturbed. The temperature stratified flow travels through the length of the outlet duct as shown in Figure 78. Then, already in the steam generator, gas travels through 90 degree bend which concludes the hot duct.

The other approach to ensure thorough thermal mixing in the LP is installation of the mixing structure at LP exit. This solution also mixes bypass flow into the main flow which is an additional mixing benefit. Bypass flow is defined as the gas passing between the prismatic blocs in the core and the reflector area. Since bypass flow does not enter the coolant channels it is

anticipated, that it will be significantly colder than gas flowing through an average channel and thus introduce even larger temperature gradient than hot channel-to-average channel.

The outlet duct could be redesigned by installation of a turbulence inducing structure in the LP outlet of the prismatic HTR or at the inlet to the hot leg of the cross duct. This type of modification would cover optimization of not only hot-to-average channel gas mixing but also bypass flow-to-average channel mixing issue. The structure would remain static during all conditions of operation, thus introducing benefits of a passive technology.

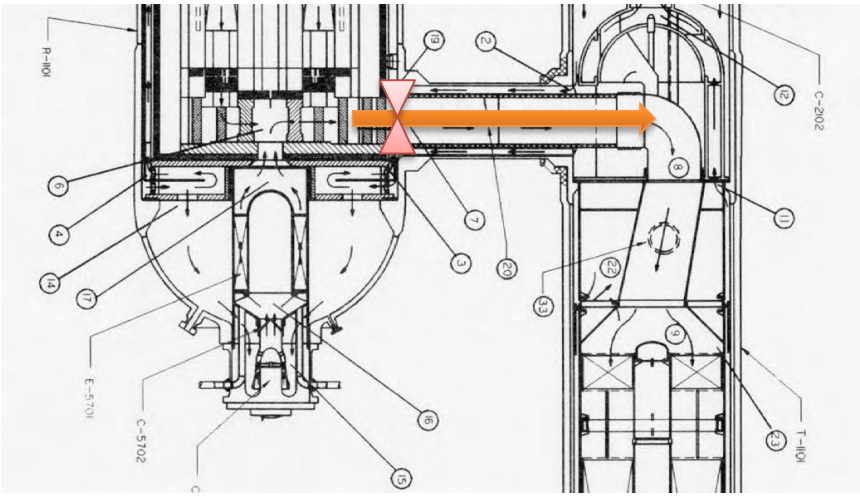

Figure 78 Section of the lower part of MHTGRs lower plenum, hot duct and steam generator (US DOE 1992)

4.2.3.1 Reference study

The reference case utilizes an unmodified geometry of the HTTF's outlet duct. As this section considers modification in outlet duct, simulation of the entire LP is not necessary. Instead temperature and velocity profiles are extracted from case P1.2.2 from corresponding location of connection between the LP and the outlet duct.

The solid model is consisted of a circular straight pipe, known as a hot duct, ended with an elbow-shaped bend. The simulation geometry is shown in Figure 79. The figure includes outlet section which is used only for purpose of increasing accuracy of the simulation and is not

considered for reporting of the results. Horizontally oriented duct starts at the LP exit, as it is shown in Figure 78, and finishes in the steam generator. The length of the straight section of the duct is 69 cm. The duct ends with 90 degree elbow, followed by 30 cm vertical outlet section. The duct has constant inner diameter of 30 cm. The computational mesh consists of $2 \cdot 10^5$ polyhedral cells. The boundary layer is inflated with 5 layers of prismatic cells. The simulation was setup as case P1.1.2 (steady state, 3D, and turbulent flow – Realizable k-epsilon turbulence model with two layer wall treatment).

As mentioned before the inlet boundary conditions were drawn from previously calculated case – P1.2.2. This case concerned the MHTGR design, and normal operation related temperature and velocity non-uniformities across the core. The results of this study conducted in RELAP5-3D were adjusted to be used as cases P1.2.2 inlet boundary conditions. The results of this simulation in Star-CCM+ have been extracted and applied as inlet boundary condition for the outlet duct study.

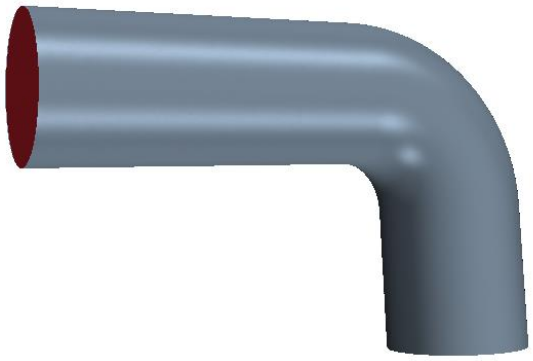

Figure 79 Outlet duct geometry

The results of the simulation are presented in Figure 80, Figure 81, Figure 82. To understand the range of temperatures and velocities in this case it is necessary to refer to Figure 53 which exhibit inlet temperature profile used for this simulation. The inlet velocity contour is shown in Figure 54.

Figure 80 exhibits the temperature contour displayed at the vertical plane located at the symmetry plane of the geometry. The temperature ranges from 880 K to 1024 K. The temperature profile applied at the inlet is transported along the duct without major disturbances. The high temperature (1000 ±20 K) stream located in half height of the duct, decays in terms of temperature but does not disperse. Above the hot stream, low temperature (~890 K) stream is located. It is at the top surface of the hot duct and remain undisturbed in the horizontal part of the duct. As pressure rises at the outer edge of the elbow-bend this low temperature area decays.

The velocity magnitude profile, shown in Figure 81, is moderately homogenous taking into consideration the inlet velocity profile (Figure 54). The velocity magnitude oscillates around 25 – 50 m/s with a maximum of 76 m/s located at the inner edge of the elbow-shaped bend. Downstream from the maximum velocity zone, the recirculation zone appears. This area is relatively small and it is caused by sharp 90 degree turn in the flow direction. It could be removed by increasing the radius of the bend. The last figure (Figure 82) represents absolute pressure contour, which demonstrates the canonical pressure drop in an elbow.

The outlet temperature profiles were plotted at two probe lines to create more accessible form of results. The probe lines are placed on the outlet plane along X and Y axis. The exact position of the probe lines are shown in Table 12. The temperature profiles are shown in Figure 83 and Figure 84.

Table 12 Location of the probe lines X and Y

	Point 1			**Point 2**		
	x	y	z	x	y	z
Probe line X	0.77	1.175	-0.30906	1.1	1.175	-0.30906
Probe line y	0.94	-0.2	-0.30906	0.94	0.2	-0.30906

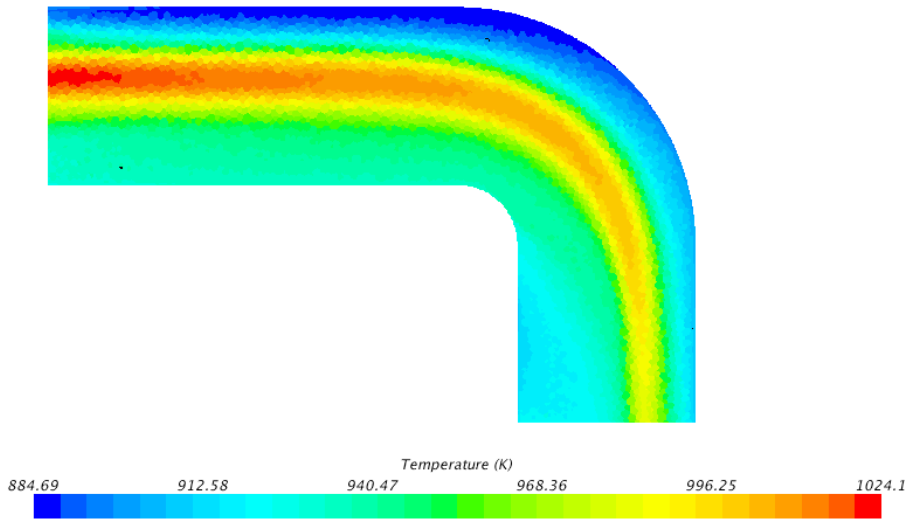

Figure 80 Temperature contour at vertical symmetry plane of the outlet duct model

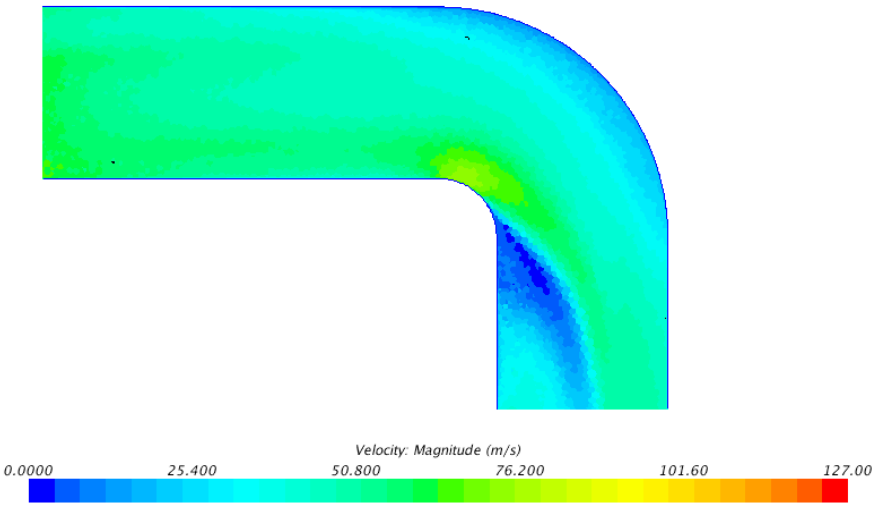

Figure 81 Velocity magnitude contour at vertical symmetry plane of the outlet duct model

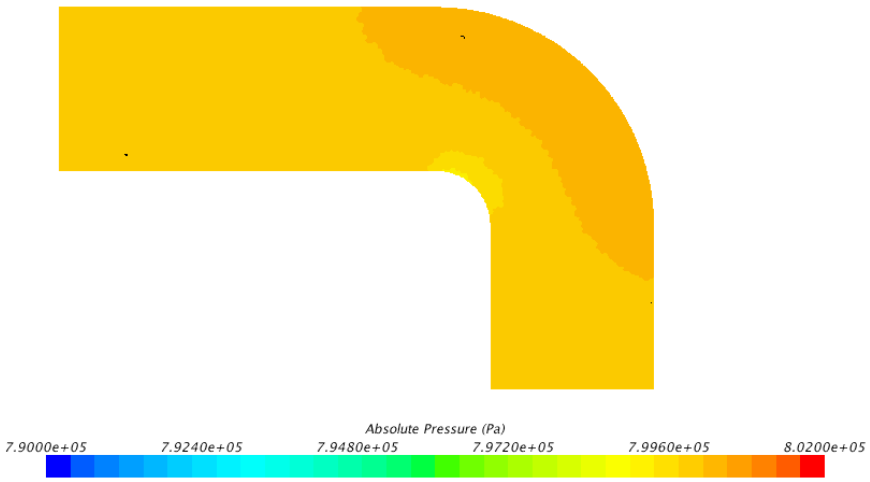

Figure 82 Absolute pressure contour at vertical symmetry plane of the outlet duct model

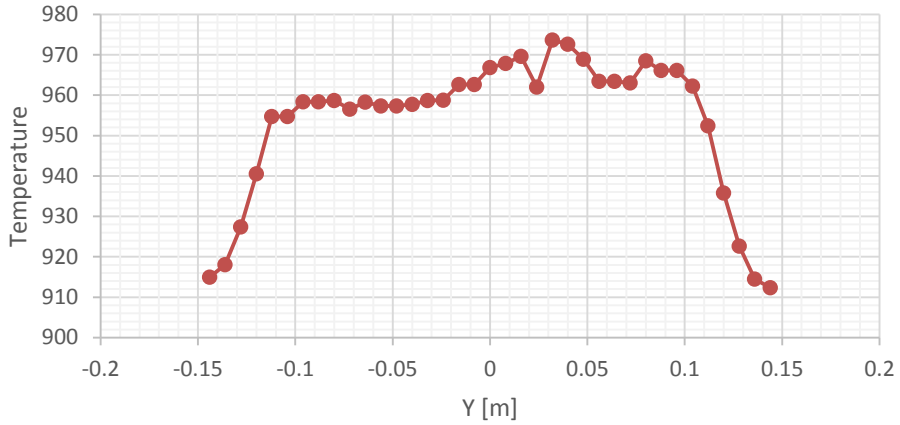

Figure 83 Temperature profile at probe line Y

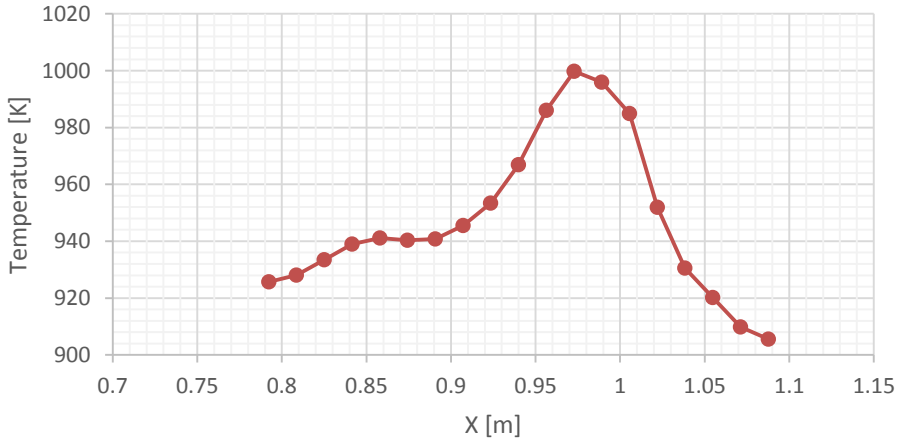

Figure 84 Temperature profile at probe line X

The "take away" result from this reference case is the temperature gradient at the exit from the outlet duct (at the end of the bend but not in the "outlet" section). The temperature range from 903 up to 1000 K, which results in 97 K temperature variation. It should be underlined here that this result was calculated for normal steady state operation of this type of installation.

4.2.3.2 Kwiat

The first choice of design is a simple carved ring placed in the front part of the outlet duct. The geometry of the Kwiat can be seen in Figure 85. The modification is placed 5 cm downstream from the duct inlet boundary. The modification is a 2 cm thick plate with an opening. The opening is symmetrical and was designed arbitrarily. The opening shape consists of four circles with ID

10 cm and a 10 by10 cm square. The boundary conditions and simulation setup are identical as for the reference case. The results are presented in a form of temperature, velocity and pressure fields. In case of turbulence promotion, the induced pressure drop plays very important role. It was determined that described geometry modification introduce pressure drop of 0.8 kPa.

The ring insertion causes rapid contraction of the flow area. The velocity of the flow increases to maintain the constant mass flow through the model. Then rapid expansion of the flow area courses stream dispersion, increasing turbulences and overall mixing level. Additionally the opening is shaped in the way, that pointy elements of the ring penetrate the stream introducing distortion into the core of the flow and vortex cascades behind the structure.

Figure 88 shows temperature profile at the vertical symmetry plane. It can be seen how the insert causes prompt decay of the hot temperature streak. If compared with the reference case, the thermal mixing improvement is significant. At the elbow-bend end the temperature gradient is reduced from 97 K (reference case) to 38 K. This value still exceeds preferable range of temperature variation, which is ±20 K. However it is a major improvement of the thermal mixing in the outlet duct.

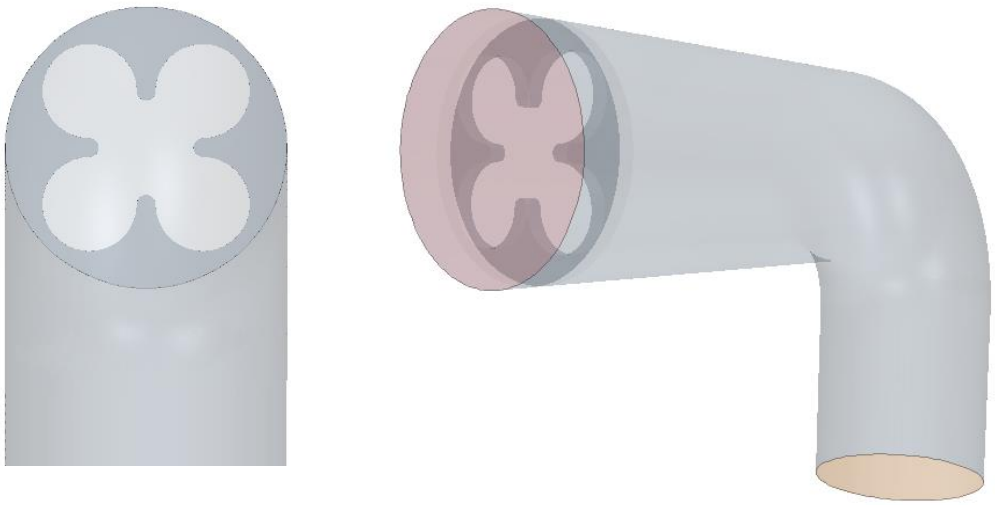

Figure 85 Geometry of the geometry with the modification - kwiat

Figure 89 displays velocity magnitude contours at the symmetry plane. The velocity in this case is much higher due to the ring insertion, where gas in the central part of the insert reaches 100 m/s. The recirculation area downstream from the bend is located closer to the duct surface than in reference case. The velocity profile at the end of the outlet duct is also improved as the standard deviation on the outlet plane is equal to 7.5 m/s in comparison to the reference case – 11.5 m/s.

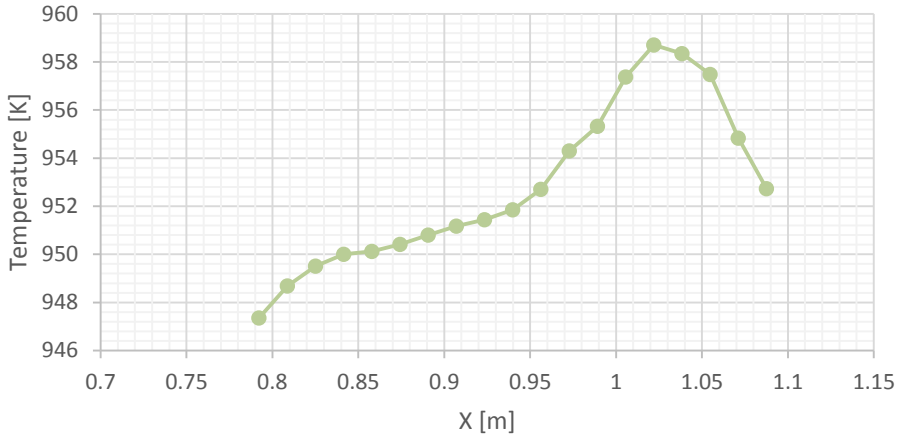

Figure 86 Temperature profile at probe line X

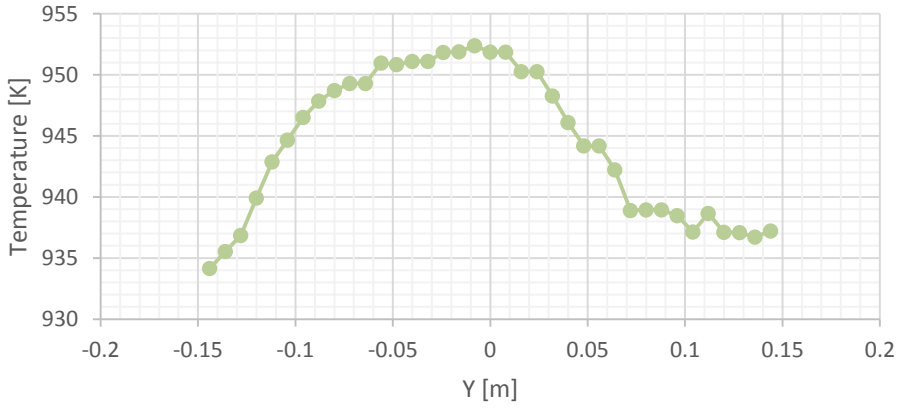

Figure 87 Temperature profile at probe line Y

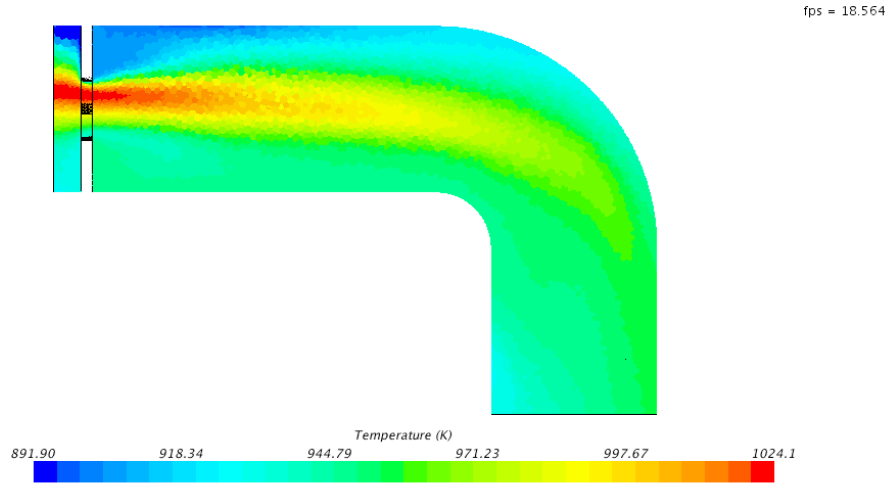

Figure 88 Temperature contour at vertical symmetry plane of the outlet duct model

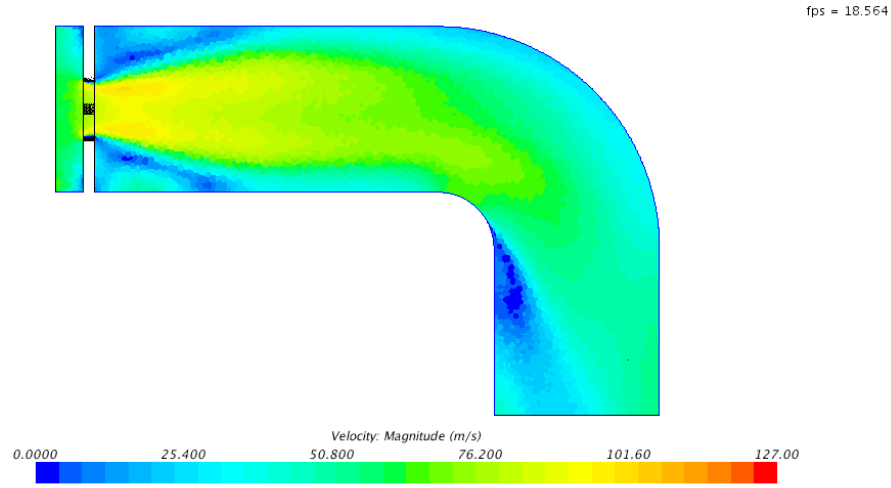

Figure 89 Velocity magnitude contour at vertical symmetry plane of the outlet duct model

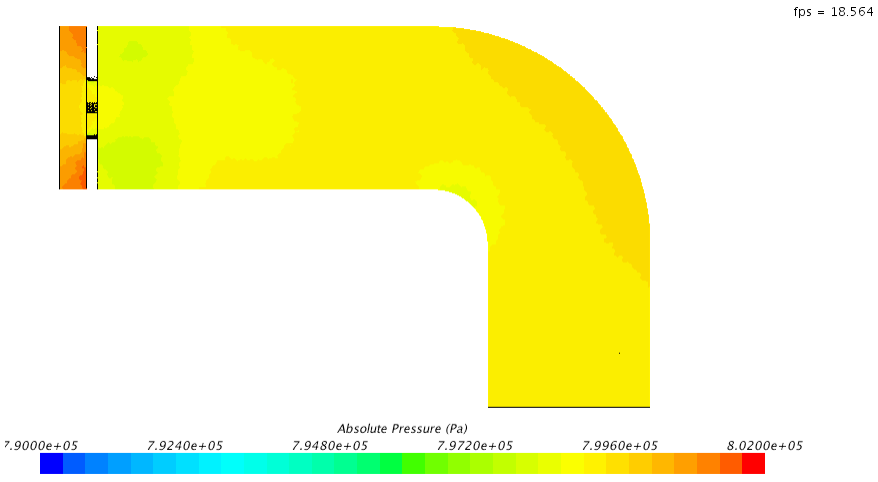

Figure 90 Absolute pressure contour at vertical symmetry plane of the outlet duct model

The pressure contour displayed in Figure 90 differs from the reference case by disturbances introduced by Kwiat. As previously mentioned the additional pressure drop due to Kwiat is ~ 0.8 kPa. The pressure field disturbances decay in the first half of the outlet duct length, the other side of the pressure field is similar to the reference case shown in Figure 82.

As in the reference case the temperature profile was plotted against X and Y axis. Profiles are shown in Figure 86 and Figure 87. Both figures exhibit altered temperature profile, it is clear that temperature range has been reduced.

4.2.3.3 Motionless mixer

Motionless mixers are used in a number of industries, mostly for mixing liquids and gases. They vary in design and can be used for laminar and turbulent flows. This section concerns application of Motionless mixer to the outlet duct of the HTTF to equalize temperature profile at the end of the hot duct. The geometry of the Motionless mixer is shown in Figure 91. The mixer used in the study is designed as two thin 180-degrees twisted blades. Each blade is 1 cm thick and 30 cm long. The blades are rotated 90 degrees with respect to each other. The computational domain was built as for the reference case. Additionally the boundary conditions are identical to two previous cases.

Figure 91 Geometry of the Motionless mixer

The mixing function of this design is based on a double division of the flow. The hot streak, centrally located at the inlet boundary is split vertically at the front of the first mixer. The twist of the blade promotes radial movement of the gas causing outer layer of gas to interact with hot center. The second blade executes secondary flow split this time in horizontal direction, creating four divisions of gas at moderate temperatures. Also the rotation of the second blade is in opposite direction to the first one. This technique should be effective for any temperature distribution, however for large temperature gradient at small area design modifications may be needed (like adding additional mixer or blade length modification). The Motionless mixer causes temperature gradient to drop form 97 K (reference case) to 29 K. The 70% reduction of the temperature gradient at the outlet boundary results with acceptable value of temperature variation which was set to ±20 K.

The other important factor is pressure drop induced by modification of the geometry. In case of double Motionless mixer of this particular design the pressure drop induced by Motionless mixer structure is 0.9 kPa.

As for Reference and Kwiat cases the temperature profiles were plotted against X and Y axis, profiles are shown in Figure 95 and Figure 96. In this case temperature range is similar to the Kwiat case, however the profile shape are different.

Four variations of the Motionless mixer design were considered. The first examined blades were extended and subsequently shortened by 5 cm to investigate the change in the pressure drop and the temperature gradient. Also a design with three short blades was investigated. The resulting temperature gradients and pressure drop are summarized in Figure 97. The shortened blades resulted with higher pressure drop and slightly lower mixing capability than the original design. The opposite effect was observed in case of the elongated blades. The case with a triple blade resulted with similar mixing capability as short blades, however with a higher pressure drop. This indicates the best mixing result can be achieved for the long double blade mixer.

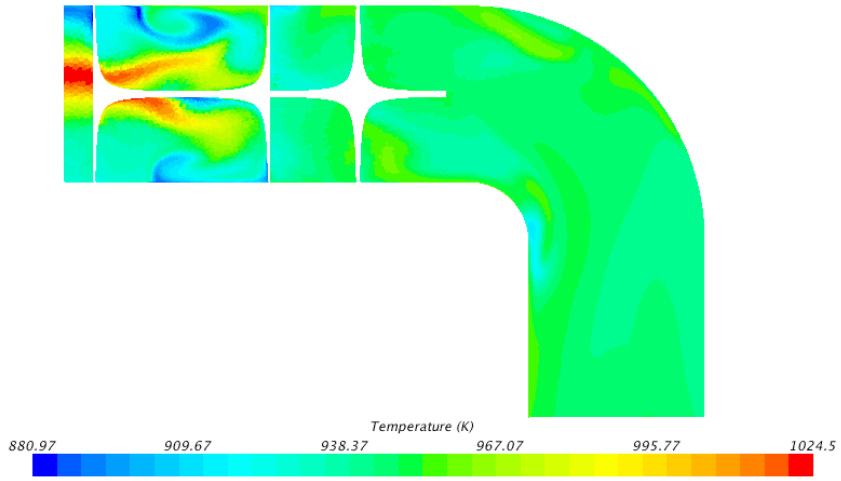

Figure 92 Temperature contour at vertical symmetry plane of the outlet duct model

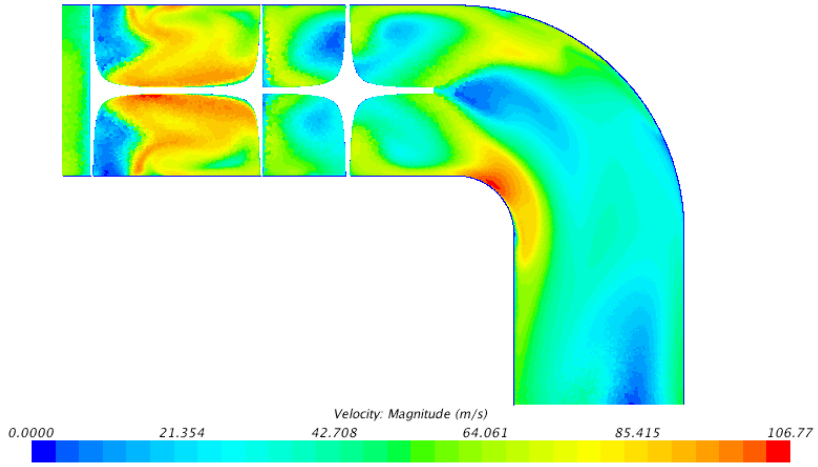

Figure 93 Velocity magnitude contour at vertical symmetry plane of the outlet duct model

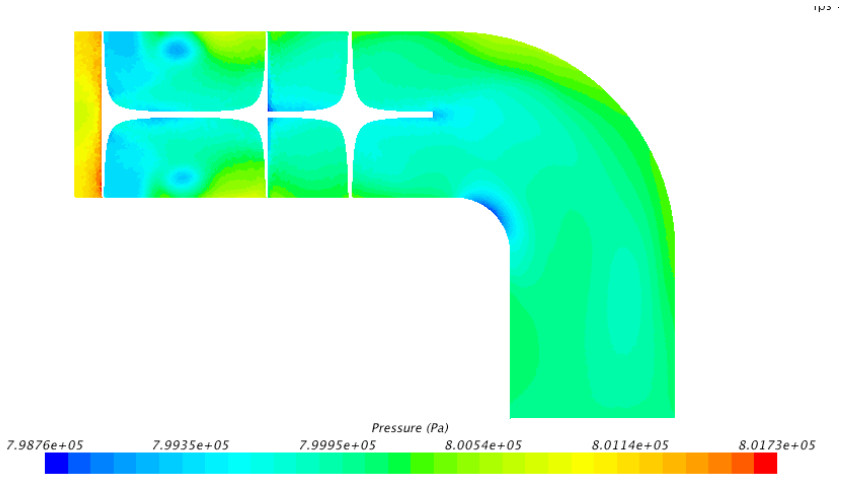

Figure 94 Pressure contour at vertical symmetry plane of the outlet duct model

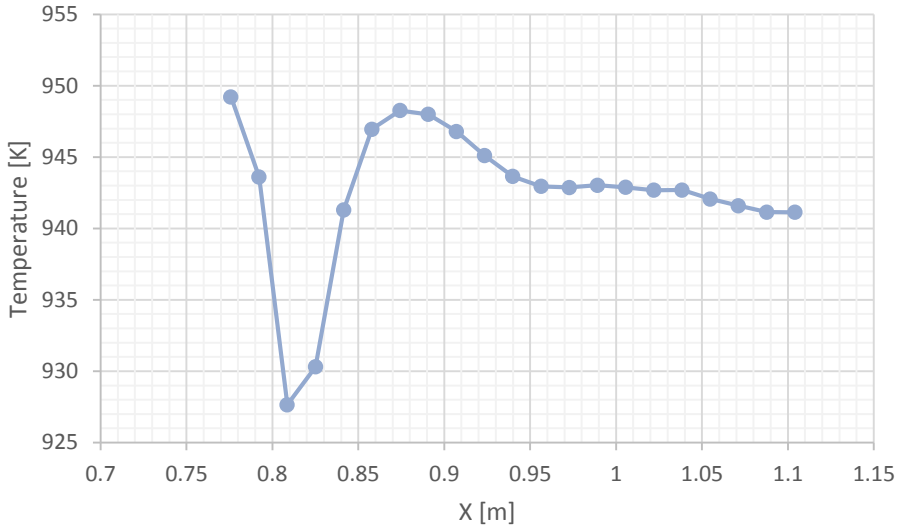

Figure 95 Temperature profile at probe line X

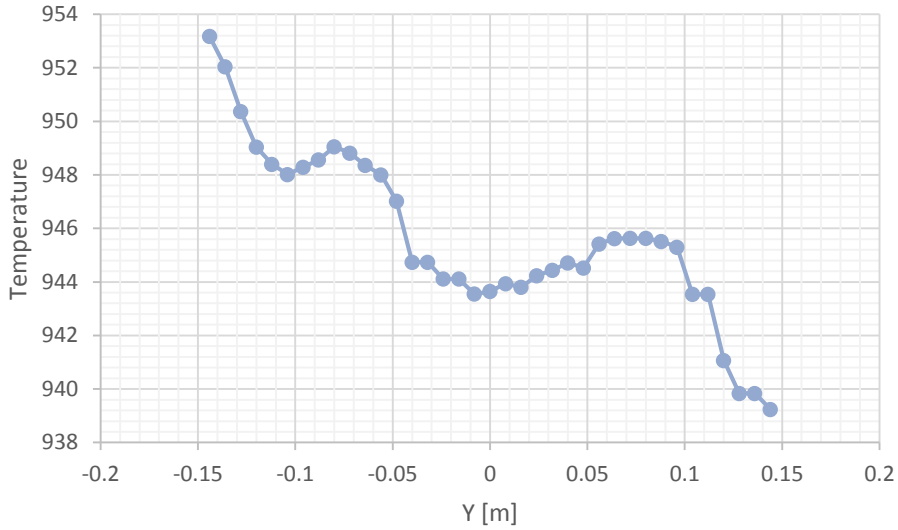

Figure 96 Temperature profile at probe line Y

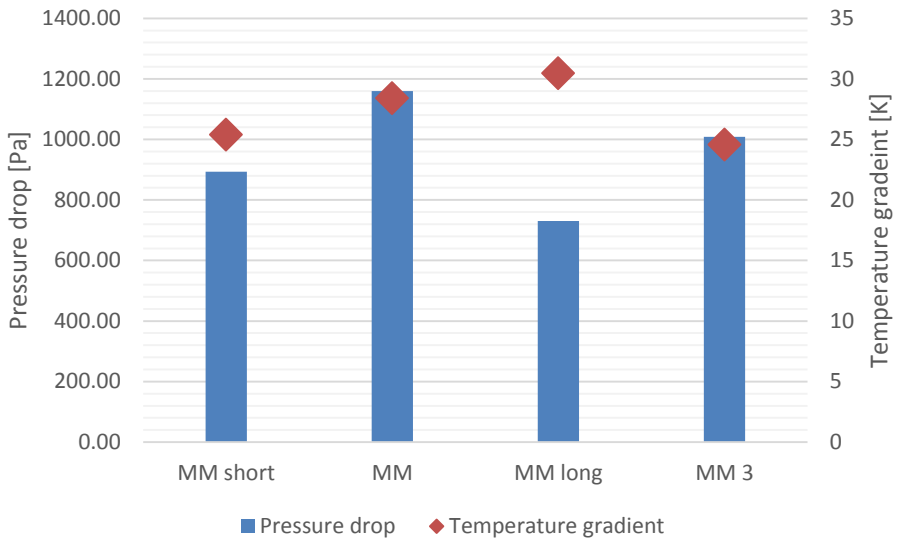

Figure 97 Motionless mixer design exploration

4.2.3.4 Conclusions

This section described investigation on thermal mixing enhancement in the outlet duct of the HTTF LP. Tree cases were simulated:

- P2.3.1 Reference - which resembles the outlet duct,
- P2.3.2 Kwiat – the reference geometry was modified with carved ring placed in the front part of the outlet duct,
- P2.3.3 Motionless mixer – the reference geometry was modified with inserting two twisted blades directly into the channel.

The simulation was carried out with inlet BC imported form case P1.2.2, the velocity and temperature profiles were extracted from the corresponding location in LP geometry. As a result of that, all of P.2.3 cases resembles realistic flow conditions as simulated in the HTTF's LP.

The resulting temperature profiles show that if high temperature streak appears at the inlet of the outlet duct, it will remain, for the most part, undisturbed and will be transported into the steam generator. The resulting temperature gradient at the outlet plane from the duct reached

~100 K. This temperature variation is excessive and should be reduced to ±20 K for effective and safe long term operation of a steam generator (or gas turbine).

To accommodate this threshold the geometry of the outlet duct has been modified. Two separate cases of modification have been examined. The first case – P2.3.2 Kwiat was arbitrary designed carved ring. Kwiat's purpose was to disturb the main flow, causing propagation of turbulent mixing at the whole diameter of the flow. This resulted in ~0.8 kPa pressure drop in the outlet duct and reduction of the outlet temperature gradient to 40% of the original value.

The second modification was the motionless mixer. This type of device is commonly used in industrial mixing tasks. The Motionless mixer in this case was designed as two blades with 180 degrees twist. Blades were placed one behind another in the straight part of the outlet duct and occupy almost all its length. The blades divide the flow first horizontally and then vertically, while promoting radial movement of the gas. The application of the Motionless mixer resulted with pressure drop of ~0.9 kPa and reduction of the outlet temperature gradient to 29% of the original value.

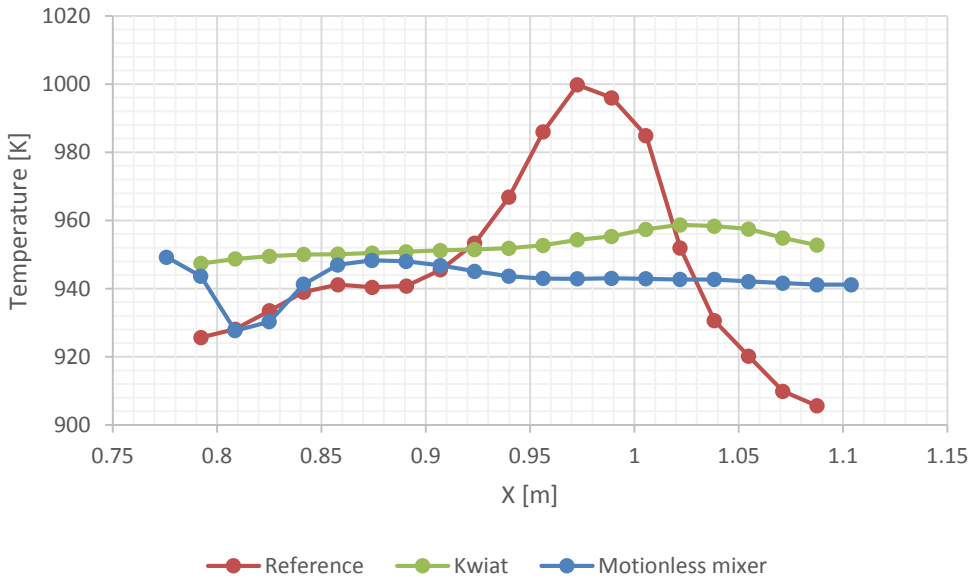

Figure 98 Comparison of the temperature profiles at probe line X for Reference, Kwiat and Motionless mixer case

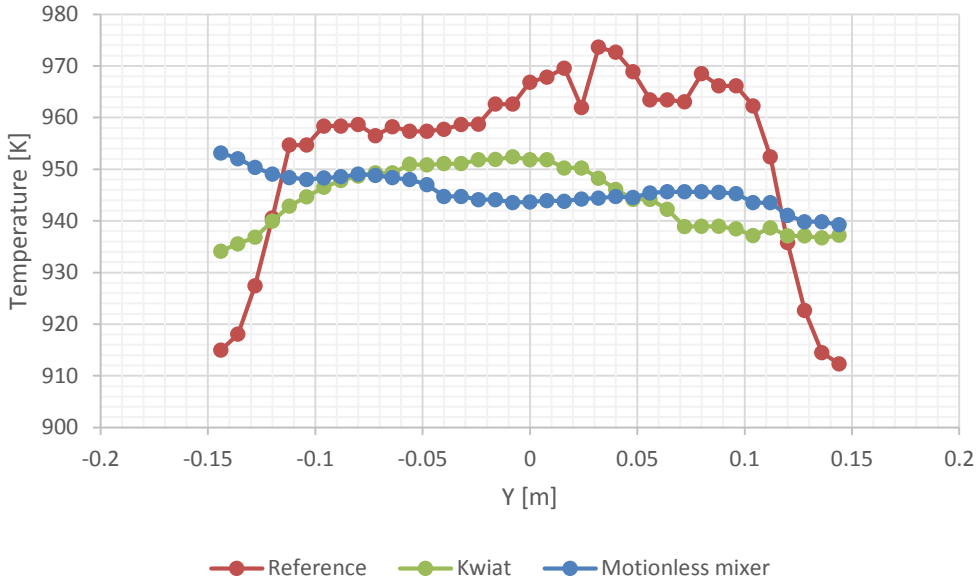

Figure 99 Comparison of the temperature profiles at probe line Y for Reference, Kwiat and Motionless mixer case

Figure 98 and Figure 99 summarize the temperature profiles for all the cases considered. Figure 98 shows that the central high temperature streak has been diminished in both cases, as well as cold streak located by the wall (right side of the plot). In Figure 99 temperature for the reference case has been low at the wall and high in central part of the duct. This non-equality was flattened for both Kwiat and Motionless mixer cases.

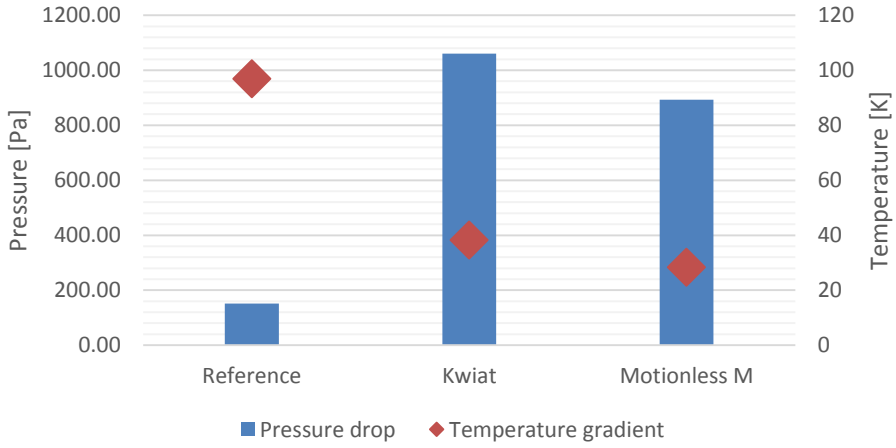

Figure 100 Pressure drop vs temperature gradient for cases

The original threshold of ±20 K has been met, thus the presented modifications pose realistic solution to this problem if appropriately designed (to maximize mixing while minimizing

the pressure drop). The question of applicability of this solution depends on the magnitude of the pressure drop that can be introduced without jeopardizing the economics. Also additional study should be developed to select material suitable for this application.

4.3 Part 3 – modified LP

Sections 4.1 and 4.2 described the flow conditions in the LP at normal operation conditions and scoped selected methods for mixing enhancement. This section investigates final mixing improvement when one of the considered methods is applied. To execute this objective the results from Part 1 and Part 2 are blended to build last part of this study - Part 3.

4.3.1 Simulation setup

The boundary conditions were designed to demonstrate the mixing enhancement and challenge its effectiveness. The set of the BC's was drawn from "approximate temperature profile" case (P1.3.2) described in Table 10. This case accommodates realistic temperature and mass flow profile in the LP. This BC's set was applied to exhibit probable mixing enhancement achievable due to application of a mixing structure.

Section 4.2.3 introduced an alternative method to mixing enhancement by placement device altering flow of the gas in a outlet duct. Two designs were presented: Kwiat and Motionless mixer. Both designs have similar characteristics, the pressure drop and temperature gradient reduction caused by structures were comparable. However, the Motionless mixer produced slightly better temperature uniformity.

In section 4.2.3 only outlet duct was included as a computational domain. This section presents analogous study performed with whole LP domain and the outlet duct, finished with an elbow shaped bend. The LP's geometry form Part 1 of the study has been extended by elbow-shaped 90 degree bend at the end of the outlet duct. This element is taken from the original MHTGR design and scaled accordingly. In HTTF facility the duct is extended and leads upward as steam generator is placed higher than the outlet from the reactor pressure vessel. This

modification has been introduced only due to limited space in the building, and thus there is no need to model it in that manner. The geometry is shown in Figure 101. At the end of elbow-bend an outlet section has been added to ensure no backflow from the outlet boundary. The computational mesh was prepared as case P1.2.2 resulting in 6 million polyhedral cells and 5 prismatic layers.

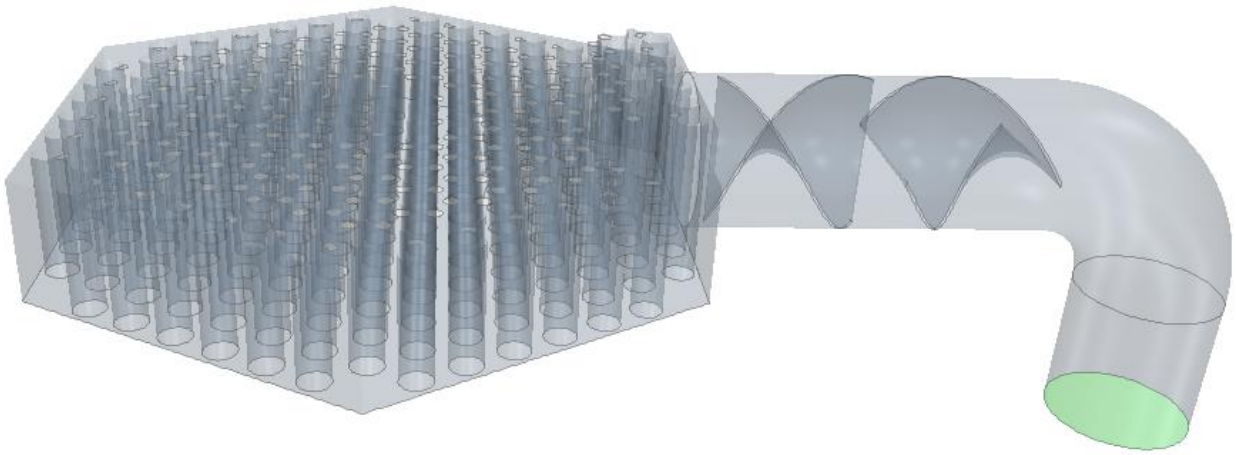

Figure 101 Geometry of LP with Motionless mixer

4.3.2 Results

The results of the simulation can be seen in Figure 103, Figure 104 and Figure 105. The maximum and minimum temperature values were extracted from a plane before the elbow bend. This way the values can be compared with results from section 4.1.3 without a modification.

The temperature contour presented in Figure 103 displays the effect of the Motionless mixer placed in the front part of the outlet duct. The hot streak flows from the plenum to the outlet duct, it is visible that the streak is dispersed at the first mixer. After both mixers gas temperature varies from 938 K up to 961 K which gives 23 K spread. After the elbow bend the temperature gradient decreases to 16.5 K. This result can be compared with the same BC set investigated in

simulation P1.2.2 (without mixer). No-mixer case resulted with 80 K temperature spread, the application of the mixer reduced this value to 23 K.

The velocity contour at the symmetry plane of the model is shown in Figure 104. The flow velocity range is similar as for no-mixer case. It can be seen that the velocity contours in the outlet duct are different from "duct-only" study – P2.3.3. In this case the flow field at the entrance to the outlet duct is altered by presence of the Motionless mixer placed downstream.

4.3.3 Economic argument

In any case of implementation of a mixing enhancement device the pressure drop in the loop will be elevated. It is necessary to weight the thermal mixing gain against the pressure drop caused by the mixing device. An optimal balance need to be obtained when the thermal mixing reaches satisfactory level without jeopardizing the effectiveness of the plant by excessive consumption of the pumping power. Considering design of the HTTF, the total pressure drop can reach up to 12 kPa. This value was obtained through scaling of the total pressure drop in MHTGR. The added pressure drop due to the Motionless mixer (standard, two blades) was calculated to be 0.73 kPa, thus it adds 6% of the total pressure drop (in terms of added pumping power – 2.15 kW). This results in increase from 1.5% to ~1.62%.in ratio of the pumping power to the rated thermal power of the HTTF.

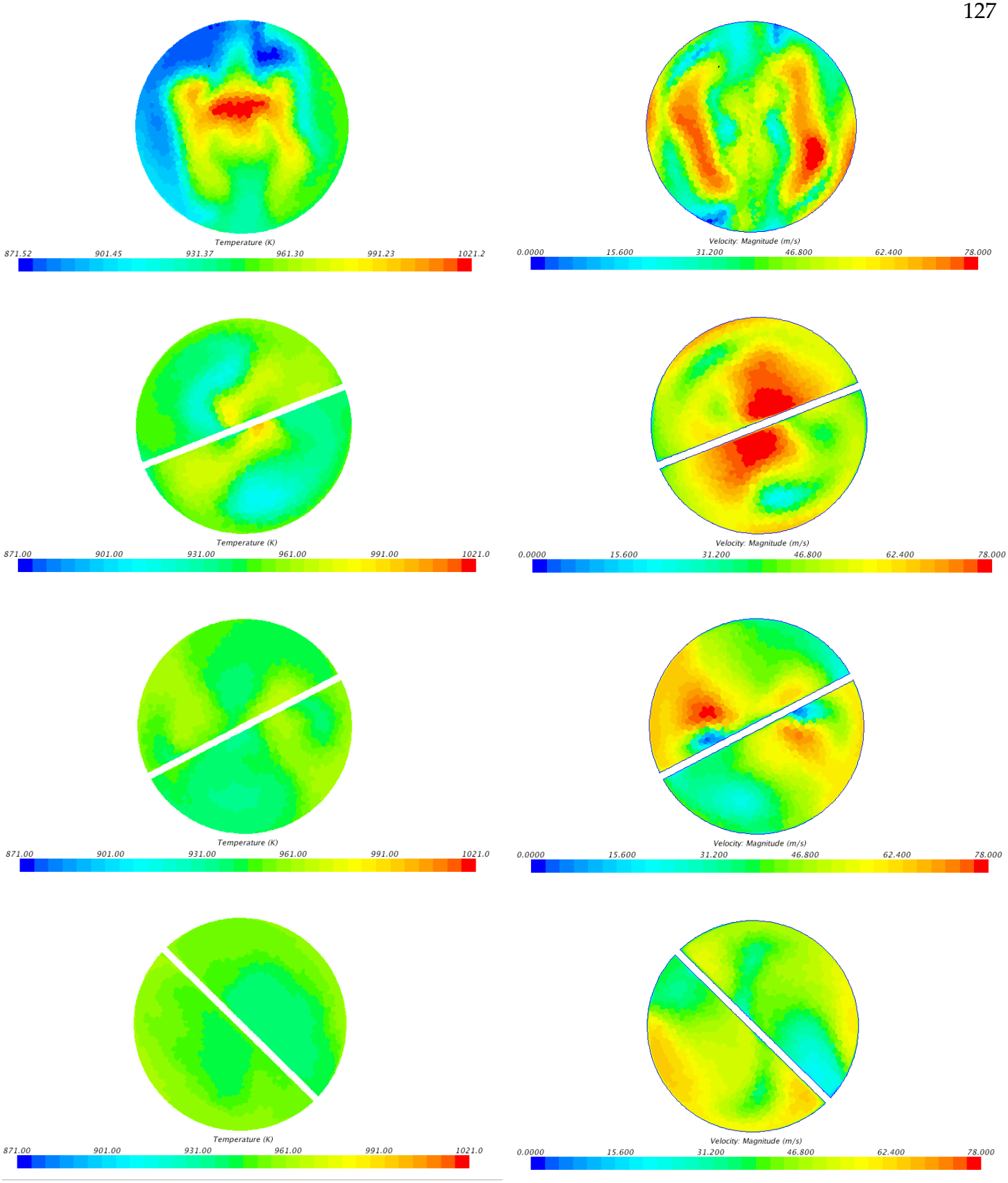

Figure 102 Temperature (left column) and velocity magnitude (right column) contours at four planes spaced equally from the outlet duct entrance toward the outlet.

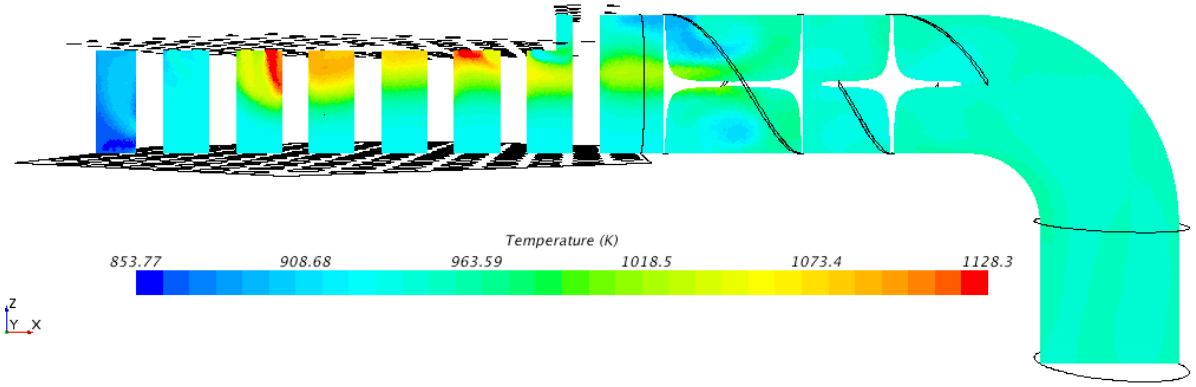

Figure 103 Temperature contour at ZX plane

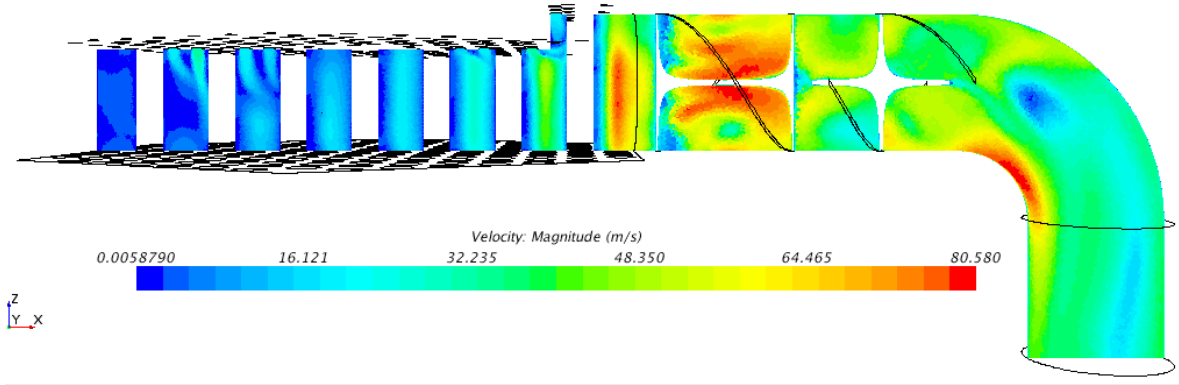

Figure 104 Velocity contour at ZX plane

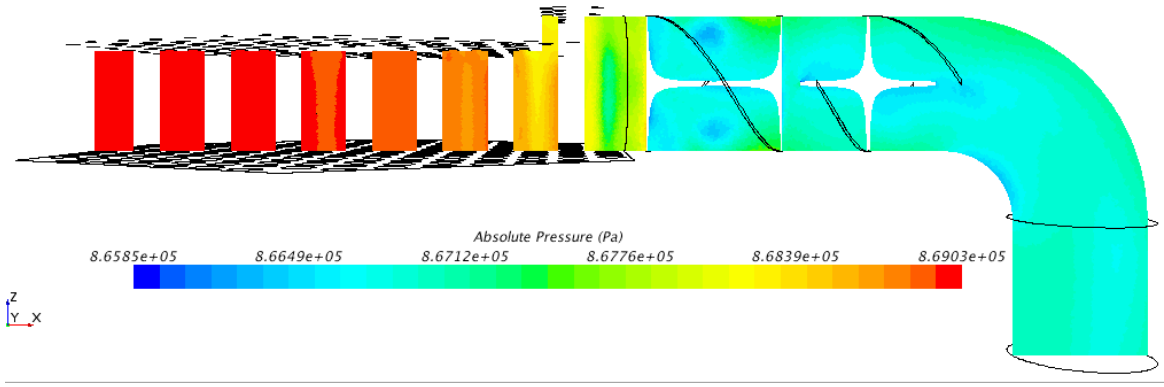

Figure 105 Absolute pressure contour at ZX plane

4.3.4 Conclusions

One structural modifications have been selected for final stage of evaluation of the mixing enhancement method. The structure modification was done through placement of the Motionless mixer in the front part of the outlet duct. The structure placed in the outlet duct increased the hot duct pressure drop significantly. However if the pressure drop is considered for the whole loop (for the HTTF) the increase seems to be within reasonable boundaries. Additionally if the pumping power increase is considered the solution appear not to jeopardize the efficiency of the hypothetical plant. The advantage of this approach is mixing enhancement not only between the gas jets exiting the core but also the gas from the reflector section and the bypass flow. The Motionless mixer after optimization can reduce the temperature gradient up to 80% at the outlet boundary (the temperature gradient ~18 K for the long blade Motionless mixer). The visualization of the mixing is shown in Figure 106 Additionally installation of the Motionless mixer in the hot duct of the MHTGR appear to be manageable from engineering point of view (after selection of the material with appropriate structural properties).

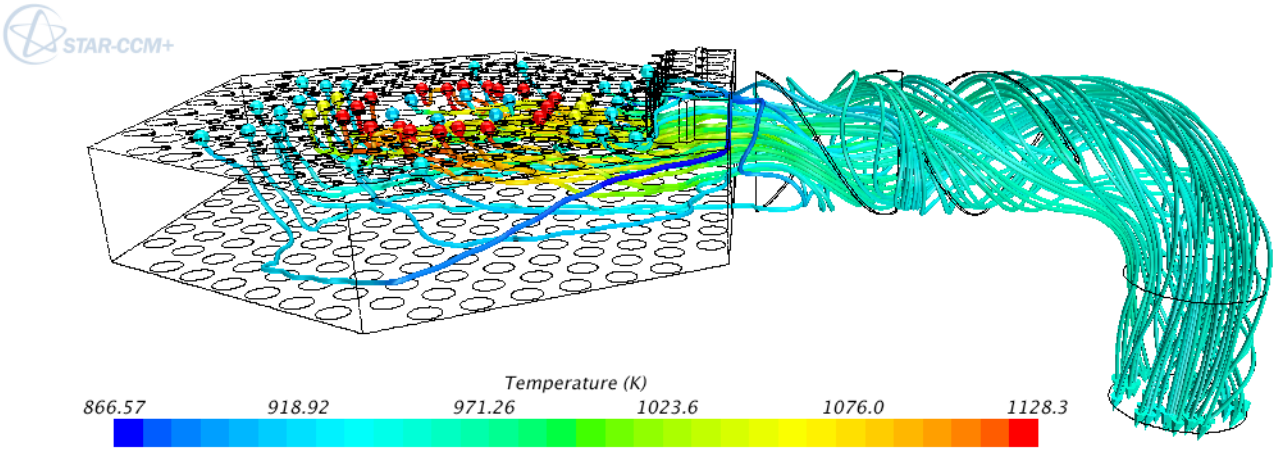

Figure 106 temperature colored streamlines in modified geometry of the LP and outlet duct

4.4 Summary

This study concerns the mixing of the hot helium in the lower plenum of the HTTF. As shown in section 4.1 the thermal mixing of the gas may be insufficient and allowable temperature variation for the heat exchanger can be exceeded. This value for a steam generator is postulated in the literature to be ±20 K. Section 4.1.4 describes CFD studies of the LP's mixing using two sets of boundary conditions. Both of the studies result with the temperature variation of 80 K and 180 K, respectively, exceeding allowed limit.

To provide satisfactory mixing technique for the LP, a few geometrical modifications were considered. In section 4.2 two sets of structure were examined in terms of a possible mixing improvement. The first structure (Vortex Generators) involved enhancement of the coolant jet dispersion after gas leaves the reactor core to allow more effective mixing in the LP's volume. Three designs of the vortex generators were proposed and investigated using reduced flow domain in CFD analysis. The applied modification due to introduction of the VGs into the coolant channel did not deliver the expected mixing enhancement. However, the feasibility of this solution should be further examined through modification of the geometry and supplemental CFD analysis of the effects introduced in the scalar mixing for section of the lower plenum.

The first solution (VGs) generates relatively small pressure drop per channel. However, the mixing effectiveness of this solution can be ranked as moderate or small. Additionally this solution will not involve the coolest gas (originating from bypass flow/ crossflow) into the mixing process. The VG's tabs are small and installation of such structure in large number of inlet channels can pose a challenge (also from mechanical stresses point of view). If vortex generators are to be placed only in certain location the pressure drop in selected channels will increase thus decreasing the mass flow through the channel. This will cause adverse "jet heating" effect which was not accounted for in this study.

The second technique was applied after hot gas jets initially premix in the LP volume. The mixing structure was placed in the front part of the outlet duct, forcing gas to mix and decrease

the residual temperature variation. Two types of geometries were developed, Kwiat and Motionless Mixer, both are described in section 4.2.3. The CFD simulations were carried out with inlet BC's imported form case P1.2.2, the velocity and temperature profiles were extracted from the corresponding location in LP's geometry to reassemble realistic flow conditions in the HTTF. In the first case– P2.3.2, the structure "Kwiat" was arbitrary designed carved ring. Kwiat's purpose was to disturb the main flow, causing propagation of the turbulent mixing at the whole diameter of the flow. This resulted in ~1 kPa pressure drop in the outlet duct and reduction of the outlet temperature range to 40% of the original value.

The second modification was Motionless Mixer. This type of devices are commonly used in industrial mixing tasks. The Motionless mixer in this case was designed as two blades with 180 degrees twist. Blades were placed one behind another in the straight part of the outlet duct and occupy almost all its length. The blades divide the flow first horizontally and then vertically, while promoting radial movement of the gas. The application of the Motionless mixer resulted with pressure drop of ~0.9 kPa and reduction of the outlet temperature gradient to 29% of the original value.

The temperature threshold of ±20 K has been met. The presented modifications pose realistic solutions to this problem if appropriately designed (to maximize mixing while minimizing the pressure drop). The question of applicability of this solution depends on the magnitude of the pressure drop that can be introduced without jeopardizing the efficiency of the plant thus influencing economic feasibility.

4.5 Future work

The experiments which will be performed in the future at the HTTF (not included in this dissertation) will concern temperature distribution across the LP and will provide validation capabilities to examine accuracy of CFD simulation performed in this document. The results will determine the reliability of this study's computational model and this reliability can be extended

to evaluate influence of the LP geometry modification at mixing process occurring in the HTTF's LP.

Two structures, Kwiat and Motionless mixer, are promising in terms of mixing promotion and should be further investigated and design optimization should be carried out to achieve maximum thermal mixing gain and minimal pressure drop.

Additionally, if possible, mixing methods developed for the outlet duct could be examined during an experiment at the HTTF. The experiment would require replacement of the element of the duct and addition of matrix of the thermocouples downstream from the mixing structure.

A future work complementary to this dissertation should include evaluation of feasibility of manufacturing and implementation of the developed mixing methods including material study and stress analysis.

5 Bibliography

Beale, S. (2011, March 16). *Thermopedia.* Retrieved from http://www.thermopedia.com/content/1211/

Blevins, R. D. (1990). Flow Induced Vibration. *Van Nostrand Reinhold Co.*, 2nd Edn.

CD-Adapco. (2012). User's guide STAR-CCM+ Version 7.04.006.

CFD Online. (2014, June 19). Retrieved from http://www.cfd-online.com/

HTR2014 Conference. (2014, October 23). Retrieved from http://www.htr2014.cn/?type=common&action=index

IAEA-TECDOC. (May 2014). *Industrial Applications of Nuclear Energy.* IAEA-TECDOC in preparation.

JAEA. (2014, May 6). *High Temperature engineering Test Reactor*. Retrieved from http://httr.jaea.go.jp/eng/index.html

Lebenhaft, J. R. (2001). *MCNP Modeling of Pebble Bed Reactors.* MIT, Engineer's Degree Thesis.

NC2I. (2014, July 2). *Nuclear Cogeneration Industrial Initiative*. Retrieved from http://www.nc2i.eu/

O. Simonin, M. B. (1988). 4th International Symposium on Applications of Laser Anemometry to Fluid Mechanics. *Measurements and prediction of turbulent flow entering a staggered tube bundle*, (p. paper. Vol. 5. 1988.). Lisbon.

Schlünder, E. U. (1983). *Heat Exchanger Design Handbook.* Washington: Hemisphere Pub. Corp.

US Department of Energy. (2014, January 4). Retrieved from http://energy.gov/

Ahuja, K. K., and W. H. Brown. 1989. "Shear Flow Control by Mechanical Tabs." *AIAA, 2nd Shear Flow Conference* -1. http://adsabs.harvard.edu/abs/1989shfl.confQ....A (March 1, 2015).

Albertson, M. L., R. A. Jensen, and Hunter Rouse. "Diffusion of Submerged Jets." *American Society of Civil Engineers*. ftp://ftp.wargamer.com/pub/TechSpec/Underwater Protection/US Diffusion of Submerged Jets 1950.pdf (March 25, 2015).

Anderson, Nolan Alan. 2006. "COUPLING RELAP5-3D © AND FLUENT TO ANALYZE A VERY HIGH TEMPERATURE REACTOR (VHTR) OUTLET PLENUM."

Bradbury, L. J. S., and A. H. Khadem. 2006. "The Distortion of a Jet by Tabs." *Journal of Fluid Mechanics* 70(04): 801. http://journals.cambridge.org/abstract_S0022112075002352 (March 1, 2015).

Carletti, Mark J, and C B Rogers. 1994. "The Effect of Streamwise Vorticity on Jet Behavior." *ASME-PUBLICATIONS-FED* 193: 19.

Carletti, MJ, CB Rogers, and DE Parekh. 1996. "Parametric Study of Jet Mixing Enhancement by Vortex Generators, Tabs, and Deflector Plates." *ASME-PUBLICATIONS-FED*. http://www.tuftl.tufts.edu/Users2/TUFTL/htmlpages/Articles/pdf_folder/ASME_SanDiego.pdf (March 1, 2015).

Condie, Keith G, Glenn E Mccreery, Hugh M Mcilroy, and Donald M Mceligot. 2005. "Development of an Experiment for Measuring Flow Phenomena Occurring in a Lower Plenum for VHTR CFD Assessment." *Inl* DOE(September).

European Commission. 2013. *EU Energy in Figures - Statistical Pocketbook 2013*. http://ec.europa.eu/energy/sites/ener/files/documents/2013_pocketbook.pdf (March 1, 2015).

Gradecka, Malwina J, and Brian Woods. 2014. "RANS Simulation of the Thermal Mixing in HTTF LP during Normal Operation Conditions – High Temperature Test Facility at Oregon State University." In *HTR2014*, Weihai.

Ha, Jung Hoon, Jin Ki Ham, Min-hwan Ki, and Won Jae Lee. 2014. "Numerical Study on the Helium Flow Characteristics for Steam Generator Subsystem of HTR."

"High Temperature Gas Reactors: Assessment of Applicable Codes and Standards." http://www.pnnl.gov/main/publications/external/technical_reports/PNNL-20869.pdf (January 11, 2015).

Iwaki, C., K. H. Cheong, H. Monji, and G. Matsui. 2004. "PIV Measurement of the Vertical Cross-Flow Structure over Tube Bundles." *Experiments in Fluids* 37(3): 350–63. http://link.springer.com/10.1007/s00348-004-0823-1 (January 9, 2015).

Johnson, Richard W, and Richard R Schultz. 2004. "Bounding Estimates For The 'Hot' Channel Coolant Temperature And Preliminary Calculation Of Mixing In The Lower Plenum For The NGNP Point Design Using CFD." *Idaho National Engineering and Environmental Laboratory* Idaho 8341(December).

Johnson, RW. 2005. *Validation Studies for Numerical Simulations of Flow Phenomena Expected in the Lower Plenum of a Prismatic VHTR Reference Design*. http://www.inl.gov/technicalpublications/documents/3634248.pdf (March 1, 2015).

———. 2009. “CFD Investigation of Experimental Data Proposed to Be a Validation Data Set.” *17th International Conference on ….* http://proceedings.asmedigitalcollection.asme.org/proceeding.aspx?articleid=1630137 (February 26, 2015).

Johnson, RW, DP Guillen, and Tara Gallaway. 2006. *Investigations of the Application of CFD to Flow Expected in the Lower Plenum of the Prismatic VHTR*. http://www.inl.gov/technicalpublications/Documents/3600907.pdf (February 26, 2015).

Johnson, RW, and RR Schultz. 2009. “Computational Fluid Dynamic Analysis of the VHTR Lower Plenum Standard Problem.” *Idaho National Laboratory*. http://www.inl.gov/technicalpublications/Documents/4310608.pdf (February 26, 2015).

Karaismail, Ertan, and Ismail Celik. 2010. “Numerical and Modeling Issues in Application of CFD to Flow in a Simplified Plenum Relevant to a Prismatic VHTR.” *Nuclear Engineering and Design* 240(8): 2011–22. http://linkinghub.elsevier.com/retrieve/pii/S0029549310001366 (January 9, 2015).

Kresta, Suzanne M, and Robert S Brodkey. 2004. “Turbulence in Mixing Applications.” In *Handbook of Industrial Mixing*, , 19–87. http://dx.doi.org/10.1002/0471451452.ch2.

Lyles, L, LA Disrud, and RK Krauss. 1971. “Turbulence Intensity as Influenced by Surface Roughness and Mean Velocity in a Wind-Tunnel Boundary Layer.” *Trans. ASAE* 14(2). http://afrsweb.usda.gov/SP2UserFiles/Place/54300520/1116 Turbulence intensity as influenced by surface roughness and mean velocity in a wind tunnel boundary laye.pdf (February 26, 2015).

Mccreery, Glenn E, Keith G Condie, and Richard R Schultz. 2007. “Scaled Experimental Modeling of VHTR Plenum Flows.”

Mceligot, D M, and G E Mccreery. 2004. “Scaling Studies And Conceptual Experiment Designs For NGNP CFD Assessment.” (November).

McIlroy, HM, and DM McEligot. 2006. “PIV Experiments to Measure Flow Phenomena in a Scaled Model of a VHTR Lower Plenum.” *… Laboratory Report INL/ …* DOE(September). http://www.inl.gov/technicalpublications/documents/4156455.pdf (February 26, 2015).

McIlroy, Hugh M., Donald M. McEligot, and Robert J. Pink. 2010. “Measurement of Turbulent Flow Phenomena for the Lower Plenum of a Prismatic Gas-Cooled Reactor.” *Nuclear Engineering and Design* 240(2): 416–28.

Next Generation Nuclear Plant:A Report to Congress. 2010. http://www.energy.gov/sites/prod/files/4.4_NGNP_ReporttoCongress_2010.pdf (March 1, 2015).

NRC. 2008. *Next Generation Nuclear Plant Phenomena Identification and Ranking Tables (PIRTs)*. NUREG/CR-6944.

Paul D. D. 1976. "FLODIS: A Computer Model to Determine the Flow Distribution and Thermal Response of the Fort St. Vrain Reactor."

Paul, Edward L., Victor A. Atiemo-Obeng, and Suzanne M. Kresta. 2004. *Handbook of Industrial Mixing: Science and Practice*. http://site.ebrary.com.ezproxy.proxy.library.oregonstate.edu/lib/oregonstate/reader.action?docID=10114017 (April 7, 2015).

Pope, S B. 2000. 1 Book *Turbulent Flows*.

"Review of DOE's Nuclear Energy Research and Development Program." http://www.nap.edu/openbook.php?record_id=11998&page=R1 (March 1, 2015).

Roache, P. J. 1997. "Quantification of Uncertainty in Computational Fluid Dynamics." *Annual Review of Fluid Mechanics* 29(1): 123–60.

Rodriguez, Sal B, and Mohamed S El-genk. 2011. "Recent Advances in Modeling Axisymmetric Swirl and Applications for Enhanced Heat Transfer and Flow Mixing." (1).

Rodriguez, Sal B., and Mohamed S. El-Genk. 2010. "Numerical Investigation of Potential Elimination of 'Hot Streaking' and Stratification in the VHTR Lower Plenum Using Helicoid Inserts." *Nuclear Engineering and Design* 240(5): 995–1004. http://linkinghub.elsevier.com/retrieve/pii/S0029549310000221 (January 9, 2015).

Rodriguez, SB. 2011. "Swirling Jets for the Mitigation of Hot Spots and Thermal Stratification in the VHTR Lower Plenum." *… 7474, Sandia National Laboratories (available at …*. https://repository.unm.edu/handle/1928/12873 (February 26, 2015).

Rodriguez, SB, and MS El-Genk. 2011. "Coupled Computational Fluid Dynamics and Heat Transfer Analysis of the VHTR Lower Plenum." https://inis.iaea.org/search/search.aspx?orig_q=RN:44092987 (March 1, 2015).

S, Naga Sarada, Kalyani K Radha, and A V S Raju. 2009. "EXPERIMENTAL INVESTIGATIONS IN A CIRCULAR TUBE TO ENHANCE TURBULENT HEAT TRANSFER." 4(5): 53–60.

Samimy, M., M. F. Reeder, and K. B. M. Q. Zaman. 1991. “Supersonic Jet Mixing Enhancement by Vortex Generators.” http://ntrs.nasa.gov/search.jsp?R=19910057115 (March 1, 2015).

Shah, Ramesh K., and Dusan P. Sekulic. 2003. *Fundamentals of Heat Exchanger Design*. John Wiley & Sons. https://books.google.com/books?id=beSXNAZblWQC&pgis=1 (April 7, 2015).

Surks, P, C B Rogers, and D E Parekh. 1994. “The Effect of Enhanced Streamwise on the Mixing and Acoustic Characteristics of an Air Jet.” *AIAA Journal October*.

Thome, John R. 2004. “Engineering Data Book III.” *Wolverine Tube Inc*.

US DOE. 1992. 1 *PRELIMINARY SAFETY INFORMATION DOCUMENT FOR THE STANDARD MHTGR*.

Versteeg, Henk Kaarle, and Weeratunge Malalasekera. 2007. *An Introduction to Computational Fluid Dynamics: The Finite Volume Method*. Pearson Education.

Williamson, C. H. K. 1988. “Defining a Universal and Continuous Strouhal–Reynolds Number Relationship for the Laminar Vortex Shedding of a Circular Cylinder.” *Physics of Fluids* 31(10): 2742. http://scitation.aip.org/content/aip/journal/pof1/31/10/10.1063/1.866978 (March 1, 2015).

Yan, Yizhou, and Rizwan-uddin. 2011. “COUPLED CFD—SYSTEM-CODE SIMULATION OF A GAS COOLED REACTOR.” *International Conference on Mathematics and Computational Methods Applied to Nuclear Science and Engineering (M&C 2011)*. http://mathematicsandcomputation.cowhosting.net/MC11/_pdf/mc03_127_paper.pdf (February 26, 2015).

Zaman, K. B. M. Q., M. F. Reeder, and M. Samimy. 1994. “Control of an Axisymmetric Jet Using Vortex Generators.” *Physics of Fluids* 6(2): 778. http://scitation.aip.org/content/aip/journal/pof2/6/2/10.1063/1.868316 (March 1, 2015).

Zaman, K.B.M.Q. 1993. “Streamwise Vorticity Generation and Mixing Enhancement in Free Jets by ‘Delta-Tabs.’” In *Shear Flow Conference*, http://arc.aiaa.org/doi/abs/10.2514/6.1993-3253 (March 1, 2015).

Ziada, Samir. 2006. “Vorticity Shedding and Acoustic Resonance in Tube Bundles.” XXVIII(2).

Zukauskas, A. 1987. *ADVANCES IN HEAT TRANSFER, Tom 18*. https://www.google.pl/books?hl=pl&lr=&id=Vs6SCRjaAYYC&pgis=1 (March 1, 2015).

This work of this dissertation was supported by the INSPE Project: Innovative Nuclear and Sustainable Power Engineering. INSPE project has been co-financed by the European Social Fund.